



**UNIVERSIDADE FEDERAL DE PERNAMBUCO-UFPE
CENTRO DE TECNOLOGIA E GEOCIÊNCIAS-CTG
DEPARTAMENTO DE OCEANOGRAPHIA-DOCEAN
PROGRAMA DE PÓS-GRADUAÇÃO EM
OCEANOGRAPHIA**

**Seasonal and intraseasonal variability of the
western boundary regime off the Eastern Brazilian
Coast**

DÓRIS R. A. VELEDA

**Recife/Brasil
2008**

DÓRIS R. A. VELEDA

**Seasonal and intraseasonal variability of the
western boundary regime off the Eastern Brazilian
Coast**

Tese apresentada ao Programa de
Pós-graduação em Oceanografia da
Universidade Federal de Pernambuco como
requisito parcial para obtenção do título de
Doutor em Ciências, na área de
Oceanografia Física

Orientador: Dr. Moacyr Araújo

Co-orientador: Dr. Raul Montagne

**Recife/Brasil
2008**

V436s

Veleda, Dóris R. A.

Seasonal and intraseasonal variability of the western boundary regime off the Eastern Brazilian Coast / Dóris R. A. Veleda. - Recife: O Autor, 2008.

xxii, 127 folhas, il : figs., tabs.

Tese (Doutorado) – Universidade Federal de Pernambuco. CTG. Programa de Pós-Graduação em Oceanografia, 2008.

Inclui bibliografia.

1. Oceanografia. 2. Variabilidade Sazonal. 3. Cisalhamento Eólico.
I. Título.

UFPE

551.46

CDD (22. ed.)

BCTG/2008-230

DÓRIS R. A. VELEDA

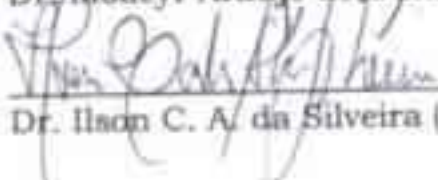
**Seasonal and intraseasonal variability of the western
boundary regime of the South Atlantic**

Tese apresentada pela seguinte banca examinadora em
11/09/2008.

Titulares:



Dr. Moacyr Araújo de Cunha Filho (DOCEAN/UFPE)




Dr. Ilson C. A. da Silveira (IO/USP, São Paulo)

Dr. Jacques Servain (IRD, Brest)



Dr. Paulo Roberto Maciel Lyra (DEMEC/UFPE)



Dr. Paulo E. P. Ferreira Travassos (Depto. Eng. Pesca/UFRPE)

Suplentes:

Dr. Alex Costa da Silva (UECE)

Dr. Monica Ferreira Costa (DOCEAN/UFPE)

**Aos meus pais,
Eloy e José e a minha filha
Alessandra pelo amor e apoio que
recebo ao longo da vida.**

Acknowledgments

Aos meus pais e minha filha Alessandra Aires Veleda pelo companheirismo e amor que me dedicaram neste período.

Ao professor e amigo Dr. Moacyr Araújo pela sua orientação e principalmente pela sua confiança e incentivo. Agradeço também ao Prof. Raul Montagne pelas valiosas discussões e orientação.

À Profa. Carmem, à Profa. Tereza, à Profa. Mônica, ao Prof. Mario pelo carinho e estímulo durante este curso e a todos os professores do Departamento de Oceanografia da UFPE.

A CAPES e ao DAAD, pela concessão de Bolsa de Pesquisa aqui no Brasil e na Alemanha durante a realização do Estágio de Doutorado, modalidade “Sandwich”, realizado no Leibniz-Institut für Meereswissenschaften an der Universität Kiel - IFM-GEOMAR, Kiel, Alemanha.

I thank the colleagues from IfM-GEOMAR for giving free access to the K1-K5 mooring data of the “German Climate Variability and Predictability (CLIVAR)” Project. I am also grateful to Dr. Lothar Stramma for his orientation, to Prof. Peter Brandt and to Dr. Rainer Zantopp, who cooperated to my work in IFM-GEOMAR. Thanks also to the Captain and crew of the R/V METEOR, for their assistance during the two Cruises in 2004 (M62/2) e 2006 (M68/2).

Agradeço aos meus amigos do LOFEC, Marcus, Ana Regina, Marcelo, Patrícia, Fabiana, Rodolfo, Isaac e Márcio, pela amizade e companheirismo.

Agradeço à Christina, Jaqueline, Sheila, Juliana, Tiago, Neves, Adilma e a todos os amigos e colegas do Departamento de Oceanografia.

A todos os funcionários do DOCEAN, pela amizade e simpatia.

Ich möchte gerne bei allen brasilianischen und deutschen Freunden in Kiel bedanken, die mich während im meines Aufenthalts in Kiel mit Zuneigung empfangen haben, herzlich bedanken. Ganz besonders bedanken möchte ich mich bei Sabine, Siegmund und Mathias Semling, Fabiana, Holger, Eliane, Eliene, Daniele, Tim und Olaf Hohlfs.

Finalmente agradeço a todos aqueles que, de uma forma ou outra, contribuíram para a realização deste trabalho.

Resumo

A circulação da fronteira oeste do Oceano Atlântico Sul tropical exerce um importante papel no controle climático através da troca inter-hemisférica de massa e calor. Nesta região, o ramo sul da Corrente Sul Equatorial (sCSE) se bifurca dando origem a Sub-corrente Norte do Brasil (SCNB), para o norte, e a Corrente do Brasil (CB), para o sul. Nesta tese, foi investigada a variabilidade desta parte do oceano utilizando-se medidas de correntes oriundas de uma seção normal à costa brasileira em 11°S, composta de 5 fundeios (K1-K5). Os fundeios foram instalados durante os cruzeiros (2000-2004) realizados no âmbito da contribuição alemã ao Programa CLIVAR (Climate Variability and Predictability Program). A seção a 11°S abrange a estrutura da SCNB e o núcleo da Corrente de Contorno Oeste Profunda (CCP), que fazem parte dos ramos superior e inferior da Célula Meridional Termohalina do Oceano Atlântico, respectivamente. Aplicando a técnica de decomposição em Funções Ortogonais Empíricas (FOE) e de análise espectral, identificaram-se tanto modos de variabilidade sazonal como intra-sazonal nos dados de corrente. A dinâmica da sCSE, bem como as principais estruturas tri-dimensionais na fronteira oeste foram também investigadas utilizando um modelo regional climatológico com 1/12° de resolução horizontal (ROMS – Regional Ocean Model System). Os resultados da simulação confirmaram a variabilidade sazonal na estrutura de correntes a 11°S. Médias mensais de 47 anos de re-análise da base SODA (Simple Ocean Data Assimilation) confirmaram a variabilidade sazonal encontrada nos resultados numéricos. A simulação da divergência da sCSE mostra que esta desloca-se para sul conforme aumenta a profundidade do oceano, variando de 8°S em 100 m de profundidade até 20°S em 500 m. Nas simulações do modelo ROMS a bifurcação da sCSE atinge sua posição mais ao norte no verão austral e sua posição mais ao sul no inverno austral. Isto corresponde a um mais fraco e a um mais intenso transporte da SCNB, respectivamente. Em 200 m de profundidade a sCSE bifurca-se a 13°S no verão austral e a 19°S no inverno austral. A 500 m de profundidade a bifurcação da sCSE é em torno de 20°S, durante todo o ano com fraca variabilidade meridional. A bifurcação das sCSE nos resultados da base SODA são sincronizados com a linha zero do rotacional do cisalhamento eólico, assim como com os resultados da simulação do ROMS. Nos resultados SODA, em 200 m, a sCSE bifurca-se em 15°S no verão austral e em 18°S no inverno austral. A Análise de Componentes Principais dos dados medidos a 11°S mostra que a temperatura é fortemente acoplada à velocidade das correntes no núcleo da CCP, com uma periodicidade de dois meses. A intensidade de acoplamento entre as velocidades tangenciais à costa e a temperatura é de 60%, indicando que as correntes no núcleo da Água Profunda do Atlântico Norte (APAN) são responsáveis, nesta proporção, pela troca de calor inter-hemisférico. A simulação do modelo ROMS indica que a CCP reproduz estruturas anticiclônicas da mesma ordem de magnitude das escalas dos vórtices encontrados nos dados dos fundeios (K1-K5) a 11°S. Os resultados numéricos indicaram ainda a presença de uma contracorrente na borda leste da SCNB, que reduz o transporte de água para o norte. Em escala intra-sazonal, sinais energéticos em alta frequência foram detectados como um

modo de variabilidade dominante na extremidade oeste da SCNB, os quais decaem com a distância da costa. Todavia, não foram encontrados mecanismos locais que expliquem estas variabilidades. De fato, os valores de corrente a 11°S são bem correlacionados com dados remotos de cisalhamento eólico meridional, próximos à costa brasileira entre 22°S- 36°S. Os mais altos valores de correlação foram verificados no inverno e primavera austral, com defasagens em torno de 8 a 10 dias. Estes sinais propagam-se para o equador com velocidade de $285 \pm 63 \text{ km.dia}^{-1}$, típica de uma onda costeira, forçada remotamente por influências meteorológicas. Estes últimos resultados apóiam a existência de *Coastally Trapped Waves* (CTW) como um mecanismo apropriado para explicar a nítida correlação entre a componente meridional do cisalhamento eólico e a componente da corrente tangencial à costa. Sugere-se, como futuro trabalho, um estudo mais abrangente deste fenômeno através da análise de ondeletas e de técnicas de modelagem numérica para confirmar as hipóteses aqui evidenciadas.

Palavras chave: correntes de contorno oeste, limite oeste do Oceano Atlântico Sul, cisalhamento eólico, Modelo Oceânico ROMS.

Abstract

The circulation of the western tropical South Atlantic Ocean plays an important role in controlling climate through the inter-hemispheric change of mass and heat. In this region, the southern branch of the South Equatorial Current (sSEC) bifurcates, resulting in the North Brazil Undercurrent (NBUC) to the north and in the Brazil Current (BC) to the south. The present work investigated the variability of this part of the ocean, using current measurements of a normal section of the Brazilian coast at 11° S, composed by 5 moorings (K1-K5). The moorings were installed during the cruises (2000-2004) under the German contribution to the CLIVAR Program (Climate Variability and Predictability Program). The section at 11° S covers the NBUC structure and the core of the Deep Western Boundary Current (DWBC), that are part of the upper and lower branches of the South Atlantic thermohaline cell, respectively. Applying Empirical Orthogonal Functions (EOF) technique and spectral analysis, two modes of seasonal and intraseasonal variability were identified. The dynamics of sSEC and the main three-dimensional structures at the western boundary were also investigated using a climatological regional model of $1/12^{\circ}$ horizontal resolution (ROMS - Regional Ocean Model System). The simulation results confirmed the seasonal variability in the current structure at 11° S. Monthly averages of 47 years of SODA reanalysis (Simple Ocean Data Assimilation) confirmed the seasonal variability found in numerical results. The simulation of the sSEC divergence shifts southward as ocean depth increases, ranging from 8° S at 100 m depth up to 20° S at 500 m. In simulations of the model ROMS the sSEC bifurcation reaches its northernmost position during the austral summer and its southernmost position during the austral winter. It corresponds to the weaker and the stronger transport of NBUC, respectively. In 200 m depth the sSEC bifurcates up to 13° S in the austral summer and 19° S in the austral winter. At 500 m depth of the sSEC bifurcation is about 20° S, during whole year with low meridional variability. The sSEC bifurcation from SODA reanalysis is synchronized with the zero line of the wind stress curl, and with the ROMS simulation. In the SODA results, at 200 m, the sSEC bifurcation is at 15° S during the austral summer and at 18° S during the austral winter. The Principal Components Analysis of the measurements at 11° S section shows that the water temperature was strongly coupled to the currents in the core of the DWBC, with a periodicity of two months. The intensity of coupling between alongshore currents and the temperature is 60%, indicating that the currents in the core of the North Atlantic Deep Water (NADW) are responsible, in the same proportion, to the change of inter-hemispheric heat. The simulation of the ROMS model indicates that the DWBC breaks into anticyclonic structures with the same magnitude of eddy scales found on moorings (K1-K5) at 11° S. The numerical results also indicated the presence of a counterflow of the NBUC, which reduces the northward water transport. Concerning intraseasonal scales, a dominant mode of variability at high frequencies, at the western flank of the NBUC, which decay with the distance from the coast, was detected. However, there are no local mechanisms that explain these variabilities. In fact, the current values to 11° S are well correlated with the remote wind stress, near

the Brazilian coast between 22° S-36° S. The highest values of correlation were found during austral winter and spring, with lags of 8 to 10 days. These signals propagate equatorward with a speed of $285 \pm 63 \text{ km.day}^{-1}$, typical of a coastal wave forced remotely by weather influences. These results support Coastally Trapped Waves (CTW) as a suitable mechanism for explaining the clear correlation between the meridional wind stress and alongshore current. It is suggested, as future work, a more comprehensive study of this phenomenon through the wavelet analysis and numerical modeling techniques to confirm the hypothesis here highlighted.

Keywords: western boundary currents, western boundary of the South Atlantic Ocean, wind stress, ROMS Ocean Model.

Figure List

Figure 3.1. (left) Chart of study area with domain limited by 10°N-40°S and 20°E-60°W and location of the K1-K5 moorings along the offshore normal transect about 11°S. Schematic representation of mean zonal and meridional currents are indicated: The upper ocean northward NBUC flow (red solid line), and the deepest southward transport by the DWBC (blue dashed line). The sSEC bifurcation at 100m depth (solid line); between 200m and 500m depth (dashed line); between 500m and 1200m depth (pointed line), according with Stramma and England (1999). The three sea level Stations are indicated (green points). Dashed dark rectangle is the modeled area. (Right) On top the crossshore mooring array position. Bottom the depth measurements at the mooring array.	19
Figure 4.1. Mean currents: (a) crossshore component, (b) standard deviation of crossshore, (c) alongshore component (Adapted from Schott et al., 2005), (d) standard deviation of alongshore. Instrument depths are marked with a black dot.....	28
Figure 4.2 a. Combined vector time series of 40-hour low-passed current anomalies from March 2000 to August 2004 of the mooring K1. The time series are rotated 36° parallel to the coast (adapted from von Schuckmann, 2006). .	29
Figure 4.2 b. Combined vector time series of 40-hour low-passed current anomalies from March 2000 to August 2004 of the mooring K2. The time series are rotated 36° parallel to the coast (adapted from von Schuckmann, 2006). .	30
Figure 4.2 c. Combined vector time series of 40-hour low-passed current anomalies from March 2000 to August 2004 of the mooring K3. The time series are rotated 36° parallel to the coast (adapted from von Schuckmann, 2006). .	31
Figure 4.2 d. Combined vector time series of 40-hour low-passed current anomalies from March 2000 to August 2004 of the mooring K4. The time series are rotated 36° parallel to the coast (adapted from von Schuckmann, 2006). .	32
Figure 4.2 e. Combined vector time series of 40-hour low-passed current anomalies from March 2000 to August 2004 of the mooring K5. The time series are rotated 36° parallel to the coast (adapted from von Schuckmann, 2006). .	33
Figure 4.3. Seasonal alongshore current: (a, c, e, g) mean component, (b, d, f,	

h) standard deviation.....	34
Figure 4.4. Variance preserving spectrum of kinetic energy [$\text{cm}^2 \text{s}^{-2}$] (solid line), for moorings K1-K4, at 50 to 300 m depth, from March 2000 to August 2004, with the respective 95% confidence interval (dashed line).	36
Figure 4.5. Variance preserving spectrum of the first Principal Component for current in the: a) K1, b) K2, c) K3, d) K4 and e) K5 stations.	40
Figure 5.1. Mean (Dec/ 2001-Feb/ 2005): (a) zonal component, (c) meridional component and (e) curl of wind stress; (b), (d) and (f) respective standard deviations.....	47
Figure 5.2. Seasonal mean for December, January and February: (a) zonal component, (c) meridional component and (e) curl of wind stress. (b), (d) and (f) respective standard deviation.	48
Figure 5.3. Seasonal mean for March, April and May: (a) zonal component, (c) meridional component and (e) curl of wind stress. (b), (d) and (f) respective standard deviation.	49
Figure 5.4. Seasonal mean for June, July and August: (a) zonal component, (c) meridional component and (e) curl of wind stress. (b), (d) and (f) respective standard deviation.	50
Figure 5.5. Seasonal mean for September, October and November: (a) zonal component, (c) meridional component and (e) curl of wind stress; (b), (d) and (f) respective standard deviation.	51
Figure 5.6. Variance preserving spectrum of kinetic energy on 10-30 days band, calculated using 3 year records of wind stress [$\text{m}^2 \cdot \text{s}^{-2}$] along the western boundary of the South Atlantic.....	52
Figure 6.1. Monthly mean distribution of SST obtained from the last year of the climatological ROMS simulation.	56
Figure 6.2. Monthly mean horizontal current ($\text{m} \cdot \text{s}^{-1}$) fields at 200 m depth obtained from last year of the climatological ROMS simulation. Red points represent the location of the sSEC bifurcation.	58
Figure 6.2. (Continuation) Monthly mean horizontal current ($\text{m} \cdot \text{s}^{-1}$) fields at 200 m depth obtained from last year of the climatological ROMS simulation. Red points represent the location of the sSEC bifurcation.	59
Figure 6.3. Seasonal averaged (three months) meridional velocity ($\text{m} \cdot \text{s}^{-1}$)	

obtained from last year of the climatological ROMS simulation. The velocities are averaged within a 1° longitude band off the Brazilian coast. The dark line is the contour of zero velocity that represents the bifurcation of the sSEC. The white areas represent Vitoria-Trindade Ridge and Abrolhos Bank.	61
Figure 6.4. Annual averaged meridional velocity (m.s^{-1}) obtained from last year of the climatological ROMS simulation. The velocities are averaged within a 1° longitude band off the Brazilian coast. The dark line is the contour of zero velocity that represents the bifurcation of the sSEC. The white areas represent Vitoria-Trindade Ridge and Abrolhos Bank.	62
Figure 6.5. Hovmoeller of the meridional component of velocity (m.s^{-1}) at 200 m depth. Results from the last 5 year of simulation of ROMS model. The alongshore component is a mean of 1° longitude from the coast. The white line represents the locations where the western boundary currents are reversed. Extreme positions are indicated by red points.	63
Figure 6.6. NBUC transport anomalies at 11°S (German CLIVAR data) and the superposition of annual and semiannual harmonics (dashed line). Adapted from von Schuckmann (2006).	64
Figure 6.7. Meridional transport obtained from ROMS simulation at 11°S : November. Positive values are indicated by solid lines corresponding to northward currents, while negative southward transport is represented by dashed sections. Horizontal dashed lines indicate the boundaries between different water masses.	65
Figure 6.8. Meridional transport obtained from ROMS simulation at 11°S : July. Positive values are indicated by solid lines corresponding to northward currents, while negative southward transport is represented by dashed sections. Horizontal dashed lines indicate the boundaries between different water masses.	66
Figure 6.9. NBUC transport at 11°S for the last year of the climatological ROMS simulation.	68
Figure 6.10. Alongshore monthly mean velocities obtained from last year of the ROMS simulation Section at 11°S . Positive values are indicated by solid lines corresponding to northward currents, while southward flow is indicated by dashed sections.	70

Figure 6.11. Horizontal current fields obtained in ROMS simulations at 1900 m depth: August.	71
Figure 6.12. Horizontal current fields obtained in ROMS simulations at 1900 m depth: February.	72
Figure 6.13. Monthly mean horizontal current fields at 200 m depth obtained from 47 years of the SODA reanalysis. Black points are the sites where the alongshore component of the zero velocity reaches the coast.....	75
Figure 6.14. Monthly mean horizontal current fields at 500 m depth obtained from 47 years of the SODA reanalysis. Black points are the sites where the alongshore component of the zero velocity reaches the coast.....	76
Figure 6.15. Hovmoeller of the meridional component of velocity ($m.s^{-1}$) at 200 m depth. Results from the last 5 year of simulation of ROMS model and climatological SODA reanalysis. The alongshore component is a mean of one degree of longitude from the coast. The white line represents the site where the western boundary currents are reversed in ROMS simulations. Red points represent the location of the sSEC bifurcation from ROMS model, and black points are the sites where the alongshore component of the zero velocity reaches the coast in SODA reanalysis.	79
Figure 7.1. The variance preserving spectra of sea level data [$cm^2 s^{-2}$] for Ponta da Armação, Cananéia, and Imbituba Stations. The 95% confidence interval is shaded.....	89
Figure 7.2. Cross-correlation between local meridional wind stress and sea level. The 95% confidence level is ± 0.0604 for Ponta da Armação, ± 0.0750 for Cananéia, and ± 0.0662 for Imbituba Station.	90
Figure 7.3. Cross-correlation for sea level and alongshore current at 100m depth in K2 mooring. The 95% confidence level is ± 0.0604 for Ponta da Armação, ± 0.0750 for Cananéia, and ± 0.0662 for Imbituba Station.	92
Figure 7.4. Cross-correlation between wind stress and currents at 100 m depth in K1 mooring, March/2002 to January/2003. The upper left panel shows cross-correlation between zonal wind stress and alongshore current; the upper right panel shows cross-correlation between meridional wind stress and alongshore current. Just below are the lags for zonal and meridional wind stress, respectively. At center, the variance spectrums for both wind stress	

components (left) and alongshore current (right). The 95% confidence interval is ± 0.076 (dashed lines). At lower 2 panels, the 10-30 days bandpass filter data for zonal wind stress lagged 6 days with the alongshore current and, the 10-30 days bandpass filter data for meridional wind stress lagged 6.5 days with alongshore current.....95

Figure 7.5. Cross-correlation between wind stress and currents at 100 m depth in K1 mooring, June/2003 to August/2004. The upper left panel shows cross-correlation between zonal wind stress and alongshore current; the upper right panel cross-correlation between meridional wind stress and alongshore current. Just below are the lags for zonal and meridional wind stress, respectively. At center, the variance spectrums for both wind stress components (left) and alongshore current (right). The 95% confidence interval is ± 0.067 (dashed lines). At lower 2 panels, the 10-30 days bandpass filter data for zonal wind stress lagged 6 days with the alongshore current and, the 10-30 days bandpass filter data for meridional wind stress lagged 10 days with alongshore current.....96

Figure 7.6. Cross-correlation between wind stress and currents at 100 m depth in K2 mooring, March/2002 to May/2004. The upper left panel shows cross-correlation between zonal wind stress and alongshore current; the upper right panel cross-correlation between meridional wind stress and alongshore current. Just below are the lags for zonal and meridional wind stress, respectively. At center, the variance spectrums for both wind stress components (left) and alongshore current (right). The 95% confidence interval is ± 0.05 (dashed lines). At lower 2 panels, the 10-30 days bandpass filter data for zonal wind stress lagged 10 days with the alongshore current and, the 10-30 days bandpass filter data for meridional wind stress lagged 9 days with alongshore current.....98

Figure 7.7. Cross-correlation between wind stress and currents at 100 m depth in K3 mooring, June/2003 to August/2004. The upper left panel shows cross-correlation between zonal wind stress and alongshore current; the upper right panel cross-correlation between meridional wind stress and alongshore current. Just below are the lags for zonal and meridional wind stress, respectively. At center, the variance spectrums for both wind stress

components (left) and alongshore current (right). At lower 2 panels, the 10-30 days bandpass filter data for zonal wind stress lagged 5.5 days with the alongshore current and at last the meridional wind stress lagged 7 days with alongshore current. The 95% confidence interval is ± 0.065 100

Figure 7.8. Cross-correlation between wind stress and currents at 100 m depth in K4 mooring, March/2002 to August/2004. The upper left panel shows cross-correlation between zonal wind stress and alongshore current; the upper right panel cross-correlation between meridional wind stress and alongshore current. Just below are the lags for zonal and meridional wind stress, respectively. At center, the variance spectrums for both wind stress components (left) and alongshore current (right). The 95% confidence interval is ± 0.046 (dashed lines). At lower 2 panels, the 10-30 days bandpass filter data for zonal wind stress lagged 9.5 days with the alongshore current and at last the meridional wind stress lagged 9.5 days with alongshore current. 102

Figure 7.9. Cross-correlation between wind stress curl and currents at 100 m depth in K1 mooring, June/2003 to August/2004. The upper left panel shows cross-correlation between wind stress curl and crossshore current; the upper right panel is the cross-correlation between wind stress curl and alongshore current. Just below are the lags between curl and the crossshore and alongshore currents, respectively. At center, the variance spectrums for wind stress curl (left) and alongshore current (right). The 95% confidence interval is ± 0.067 (dashed lines). At lower 2 panels, the 10-30 days bandpass filter data for wind stress curl lagged 6.5 days with the crossshore current and the wind stress curl lagged 2 days with alongshore current. 105

Figure 7.11. a) Time series of chlorophyll (mg m^{-3}) and wind stress curl (N m^{-3}) for 2003-2004; b) variance preserving spectrum of chlorophyll and wind stress curl; c) cross-correlations for wind stress curl and chlorophyll (full line) and for alongshore wind stress and chlorophyll (point line); d) 10-30 days bandpass for alongshore wind stress and chlorophyll; e) 10-30 days bandpass for wind stress curl and chlorophyll. 107

Figure 7.12. Cross-correlation at 11° S between: a) zonal wind stress and crossshore current, b) meridional wind stress and crossshore current, c) curl and crossshore current, g) zonal wind stress and alongshore current, h)

meridional wind stress and alongshore current, i) curl and alongshore current.
Lag (days) between: d) zonal wind stress and crossshore current, e)
meridional wind stress and crossshore current, f) curl and crossshore current,
j) zonal wind stress and alongshore current, k) meridional wind stress and
alongshore current, l) curl and alongshore current..... 109

Table List

<i>Table 3.1. Mooring time records, positions, instruments and current-meter depth. For K3 and K4 stations there are temperature measurements for the same time interval and depths.....</i>	<i>20</i>
<i>Table 4.1. EOF analysis applied to the alongshore component of the current at 11°S. The SFC is Squared Fraction Covariance for each mode in alongshore velocity of current from mooring data. The column “Period (days)” shows the periodicity of the maximum variance for each mode in single field analysis...39</i>	<i>39</i>
<i>Table 4.2. EOF analyses applied to the (coupled field) alongshore current-temperature along transect 11°S. CC is the correlation coefficient, which quantifies the strength of the coupling.</i>	<i>42</i>
<i>Table 6.1. Comparison between this work and related works.</i>	<i>82</i>
<i>Table 7.1. Cross-correlation between meridional wind stress and alongshore currents for moorings K1 to K4. The coordinates of the oceanic regions where the maxima cross-correlations occur are shown, as well as the corresponding distances (in km) and lag periods (in days) between these regions to 11°S and the respective wind and current signals.....</i>	<i>103</i>

List of Abbreviations

AABW	Atlantic Antarctic Bottom Water
AAIW	Atlantic Antarctic Intermediate Water
AC	Agulhas Current
ACC	Antarctic Circumpolar Current
ACM	Acoustic Current Meter
ADCP	Acoustic Doppler Current Profile
AMSR-E	Advanced Microwave Scanning Radiometer
BC	Brazil Current
Brazilian CHM	Brazilian Navy Hydrographic Center
CC	Coefficient of Correlation
CLIVAR	Climate Variability and Predictability Program
COADS	Comprehensive Ocean-Atmosphere Data Set
cSEC	central band of the South Equatorial Current
CTW	Coastal Trapped Wave
CW	Central Water
DMSP	Defense Meteorological Satellites Program
DWBC	Deep Western Boundary Current
EOF	Empirical Orthogonal Functions
ERA-40	Reanalysis of the Global Atmosphere for 45 years
ERS	European Remote Sensing Satellite
ETOPO-2	Digital Terrain Data with 2'' resolution
EUC	Equatorial Undercurrent
Guinea C.	Guinea Current
GC	Gulf Current
GEOSAT	Geodetic Satellite
GFDL	Geophysical Fluid Dynamics Laboratory
GLOSS/IOC	Global Sea Level Observing System
GOES	Geostationary Operational Environmental Satellites
HDF-EOS	Hierarchical Data Format - Earth Observing System
IBGE	Brazilian Institute of Geography and Statistics
IO/USP	Institute of Oceanography of São Paulo University

ISV	Intraseasonal Variability
ITCZ	Intertropical Convergence Zone
IWBC	Intermediate Western Boundary Current
MOC	Meridional Overturning Cell
MODIS	Moderate-resolution Imaging Spectroradiometer
MOM	Modular Ocean Model
MSLA	Mean Sea Level Anomaly
NADW	North Atlantic Deep Water
NBC	North Brazil Current
NBUC	North Brazil Undercurrent
NCAR	National Center for Atmospheric Research
NCEP	National Centers for Environmental Prediction
NEC	North Equatorial Current
nSEC	northern band of the South Equatorial Current
NOAA	National Oceanic and Atmospheric Administration
OCCAM	Ocean Circulation and Climate Advanced Modeling Project
PCA	Principal Component Analysis
POD	Proper Orthogonal Decomposition
POP	Parallel Ocean Program
QuickSCAT	Quick Scatterometer
RCM	Recording Current Meter
RMPG	Geodetic Permanent Tide Gauge Network
ROMS	Regional Ocean Modeling System
SAC	South Atlantic Current
SACW	South Atlantic Central Water
SACZ	South Atlantic Convergence Zone
SASH	South Atlantic Subtropical High
SBB	Southeast Brazil Bight
SCF	Squared Covariance Fraction
SEC	South Equatorial Current
SEUC	South Equatorial Undercurrent
SICC	Southern Intermediate Countercurrent

SMW	Salinity Maximum Water
SODA	Simple Ocean Data Assimilation
sSEC	southern band of the South Equatorial Current
SSM/I	Special Sensor Microwave
SST	Sea Surface Temperature
STC	Subtropical Cell
Sv	Sverdrup
SVD	Singular Value Decomposition
TMI	Microwave Imager
TOGA-TAO	Tropical Ocean Global Atmosphere - Tropical Atmosphere Ocean
TRMM	Tropical Rainfall Measuring Mission
TSW	Tropical Surface Water
TW	Tropical Water
uCDW	upper Circumpolar Deep Water
WOA	World Ocean Atlas
ZCAS	Convergence Zone of the South Atlantic

List of Symbols

τ^x	zonal wind stress
τ^y	meridional wind stress
σ_\square	potential density surface
V_s	velocity estimated with satellite-scaled values
V_m	velocity estimated with NRA-2 model values
r	slope parameter

Contents

ACKNOWLEDGMENTS.....	III
RESUMO.....	IV
ABSTRACT.....	VI
FIGURE LIST.....	VIII
TABLE LIST.....	XV
LIST OF ABBREVIATIONS.....	XVI
LIST OF SYMBOLS	XIX
CONTENTS	XX
CHAPTER 1.....	1
1. MOTIVATION AND OBJECTIVE.....	1
CHAPTER 2.....	6
2. OCEAN-ATMOSPHERE DYNAMICS IN THE SOUTHWESTERN ATLANTIC	6
2.1. The meteorological forcing	6
2.2. The mean circulation.....	9
2.3. The water masses.....	13
CHAPTER 3.....	17
3. THE STUDY AREA AND DATA.....	17
3.1. The study area.....	17
3.2. Moored array observations at 11°S	18
3.3. Wind stress data.....	21
3.4. Sea level gauge.....	22

3.5. Chlorophyll data	23
3.6. The Regional Ocean Modeling System - ROMS	23
3.7. Simple Ocean Data Assimilation – SODA reanalysis data.....	25
CHAPTER 4.....	26
4. THE WESTERN BOUNDARY VARIABILITY OF THE SOUTH ATLANTIC AT 11°S.....	26
4.1. The mean boundary current structure at 11°S cross section.....	26
4.2. Seasonal and intraseasonal variability.....	28
4.3. Principal Component Analysis – PCA.....	36
CHAPTER 5.....	44
5. WIND STRESS VARIABILITY IN THE SOUTH ATLANTIC.....	44
5.1. Wind-forced motions	45
CHAPTER 6.....	54
6. ROMS RESULTS AND SODA REANALYSIS.....	54
6.1. Meridional variability and depth dependence.....	54
6.2. Current structure and transport variability at 11°S	64
6.2.1. <i>Northward NBUC transport</i>	64
6.2.2. <i>Southward DWBC transport</i>	69
6.3. Climatology of the SODA reanalysis.....	72
6.4. Summary.....	77
6.4.1. <i>The bifurcation of the southern branch of the SEC</i>	77
6.4.2. <i>The eddies at NADW core</i>	80
6.4.3. <i>The counterflow offshore the NBUC</i>	80
CHAPTER 7.....	83
7. INTRASEASONAL VARIABILITY ON THE NORTH BRAZIL UNDERCURRENT FORCED BY REMOTE WINDS.....	83
7.1. Coastal trapped waves.....	83
7.2. Cross-correlation method.....	87

7.3. Cross-correlation analysis between wind stress, sea surface height gauge and currents.....	88
7.4. Cross-correlation between wind stress and currents.....	93
7.5. Cross-correlation between wind stress curl and crossshore and alongshore currents.....	103
7.6. Cross-correlation between wind stress curl and Chlorophyll concentration.....	106
7.7. Discussion.....	108
7.8. Summary.....	111
CHAPTER 8.....	114
8. SUMMARY AND PERSPECTIVES.....	114
REFERENCES	119

Chapter 1

1. Motivation and objective

The South Equatorial Current (SEC) is the major pathway by which water of South Atlantic origin is imported into the tropical Atlantic Ocean (Stramma et al., 2005). Climatic signals from the subtropical South Atlantic contained in the water masses are transported toward the western boundary of the South Tropical Atlantic by the South Equatorial Current (Malanotte-Rizzoli et al., 2000; Stramma et al., 2003; Lumpkin and Garzoli, 2005).

Furthermore, the western boundary regime of the tropical South Atlantic Ocean is an important crossroad of inter-hemispheric transfer of warm and cold water masses (Bourlès et al., 1999; Schott et al., 2005). The Deep Western Boundary Current (DWBC) transports cold North Atlantic Deep Water (NADW) toward the southern hemisphere, while the North Brazil Undercurrent (NBUC) transports warm upper waters northward to close the thermohaline overturning cell (Gordon, 1986; Schmitz, 1995). The pathway that runs into the western boundary regime is a limb of the near surface wind-driven anticyclonic Subtropical gyre (Peterson and Stramma, 1991; Stramma and England, 1999). The circulation near the surface is dominated

by this gyre, which is formed by four different parts. Westward, the southern band of the South Equatorial Current (sSEC) at north, southward the Brazil Current (BC) at west, eastward the South Atlantic Current (SAC) at south and northward the Benguela Current at east (Stramma and England, 1999). The southern limit of this gyre corresponds to the South Atlantic Subtropical Front or Convergence zone. Southern of the Subtropical Convergence, along the western side of the basin, the Falkland Current flows equatorward carrying water from the Antarctic Circumpolar Current. In this area, the Brazil and Falkland Currents converge and the Tropical Surface Water (TSW) and the high-salinity Central Waters (SACW) are formed in the South Atlantic. This confluence creates a strong thermohaline front with high temperature gradients, also called the Confluence Front, which is connected to the South Atlantic Current and recirculates within the southern subtropical gyre and finally, into the sSEC toward the Brazilian shelf (Stramma and England, 1999).

Towards the north, the northern limb of the sSEC termination forms the North Brazil Undercurrent-North Brazil Current (NBUC-NBC) system, one of the most powerful western boundary current in the world. The southern limb of sSEC forms the Brazil Current (BC) propagating southward along the coast of Brazil and meeting at about 35°S the Falkland Current (Gordon and Greengrove, 1986).

Despite of the importance of the NBUC for the large and mesoscale ocean circulation, knowledge of its current field, from a moored boundary array, deployed during 2000-04 close to Brazilian coast at 11°S, suggests that intraseasonal signals are evident in the western boundary tropical Atlantic, which are presumed to play a role in the coupled ocean-atmosphere system.

Von Schuckmann (2006) indicates that the dominant mode of variability at 11°S in the NBUC domain ranges from 50 to 100 days periods. This author also found strong coherence on the anomalies of NBUC transport and the gradient of the mean sea level in a 60-70 days range. It implies that 50-100 days intraseasonal variability of the NBUC is associated with fluctuations in the altimeter measurements. But the high-frequency

fluctuations (<1 month) could not be compared with altimeter measurements, since the Mean Sea Level Anomalies (MSLA) data have a temporal resolution of 7 days. However, at the western flank of the NBUC, biweekly signals are the dominant modes of variability.

Theoretically, intraseasonal fluctuations in the upper-ocean circulation can be excited through several dynamic processes such as direct wind forcing, wind forcing in remote areas via waveguide dynamics, mean flow instability, and resonance due to coastline geometry. In this thesis the currents measurements indicate considerable variability at the NBUC at periods of 10-30 days range. Wind stress data reveal also variability within the same intraseasonal band at the western boundary of the South Atlantic, suggesting that the ocean intraseasonal variability could be wind forced.

Although some above mentioned evidences, it is not obvious how these high-frequency fluctuations are generated. These features open several questions, as: What is the physical mechanism responsible for these signals ? Could they result from coastal inhibition ? Are they consequence of wave's periods ? Or are they forced by the local or remote winds ? If remote influences are important, where are their origins and through which physical processes do they exert influences on the Southwestern tropical Atlantic Ocean ? A prospective mechanism to be pointed out as an answer for some of these questions is the Coastally Trapped Waves (CTW). These signals are located at coastal zone, which is an energetic environment, with pronounced variations of currents. The motion of the oceanic waters over the continental shelf and slope is influenced by the earth's rotation, the density stratification, the offshore current regime, the sloping bottom topography and the presence of a coastline (Allen, 1980). In order to have CTW, two main properties are important. The first property is the sloping bottom topography of the continental margin which, in the absence of stratification, can support barotropic continental shelf waves. The other property is the density stratification which, with the presence of a vertical boundary and a flat bottom can support baroclinic Kelvin waves. These waves depend on the depth variations of the shelf and slope for their restoring mechanism.

Supported by the above ideas, the goal of this work is to investigate the seasonal and intraseasonal variability of the western boundary regime of the South Atlantic. I will conduct this research walking through the following pathways:

- (a) The analysis of the structure of the currents at 11°S close to Brazilian coast, linking with the seasonal and intraseasonal variability of the North Brazil Undercurrent;
- (b) The use of a climatological oceanic modelling and an ocean reanalysis database as tools to confirm the theories about the dynamic of the western boundary regime in the South Atlantic. As suggested by recent literature, it was found that the seasonal variability of the NBUC is coupled to large scale mechanism such as the seasonal migration of the sSEC bifurcation along the eastern Brazilian edge;
- (c) The investigation of the wind stress variability as an important forcing for the intraseasonal variability of the western boundary regime at 11°S. The higher frequencies are studied and linked to its main forcing, the wind stress, with the purpose of explaining coastal wave theories.

The manuscript is organized as follows: the next chapter brings an overview of the main meteorological forcing, features of the mean circulation and water masses at the Southwestern Atlantic Ocean. In the Chapter 3, the study area, the used datasets, and the modeling approach are described. Seasonal and intraseasonal analyses of the variability of the mean flow field at 11°S section are made in the Chapter 4. The spectral analysis is used to identify the signals of the currents and the atmosphere. Additionally, statistical methods such as the Empirical Orthogonal Functions (EOF) are used to evaluate the main patterns of variability found in the NBUC at 11°S. The Chapter 5 describes the spatial and temporal characteristics of the wind stress datasets. It is especially important to establish the winds as being representative of the atmospheric seasonal oscillation, prior to demonstrate its connection to the current signals. In the Chapter 6, a high-resolution Regional Ocean Modeling System (ROMS) approach is used for evaluating

the seasonal variability of the southern branch of the SEC divergence off Brazil, and to investigate the circulation structures in the western Atlantic Ocean boundary (5°S-25°S and 20°W-47°W). Model results are once more compared to field measurements obtained from the current-array moored along the cross-Brazilian-shore transect situated at 11°S. Another contribution of this chapter is an analysis of the current fields for tropical South Atlantic using results from the Simple Ocean Data Assimilation (SODA) version 2.0.2. The Chapter 7 extends the search for energy, correlation and forcing to the Southwestern Atlantic, in order to investigate whether the oceanic oscillation is related to its atmospheric counterpart and if so, where and in what way. Finally, the last chapter presents the conclusion and perspectives.

Chapter 2

2. Ocean-atmosphere dynamics in the Southwestern Atlantic

2.1. The meteorological forcing

The dynamics of both ocean and atmosphere systems are coupled via exchange processes through their common interface. Consequently, to understand climate variability is vital to study the common variability of both systems and its relation to the exchange processes.

The prevailing surface winds over the tropical ocean are the trade winds that blow persistently from the northeast in the Northern Hemisphere and from the southeast in the Southern Hemisphere. Trade winds drive both North and South Equatorial Currents westward, thus transporting warm ocean-surface waters in that direction. Equatorial counter-currents and equatorial undercurrents return some warm waters eastward. Counter-currents flow along the surface whereas under currents flow at greater depths below the surface.

The trade winds of the two hemispheres converge in a narrow east-west zone located near the equator, an area of low pressure, known as the Intertropical Convergence Zone (ITCZ). The ITCZ is an important component of the planetary-scale atmospheric circulation that is particularly well defined over the tropical ocean. Warm and humid air ascending in the ITCZ provides a large source of diabatic heat to the troposphere and is associated with a band of convective clouds giving rise to a band of heavy precipitation around the globe providing freshwater to the ocean. The latitudinal position of the ITCZ in the Atlantic varies from a minimum close to the equator in austral fall (March-May) in the west to a maximum extension of 10°-15°N in late austral winter (August) in the east. Consequently, the eastward-flowing Equatorial Counter Current, separating the surface current systems of the two hemispheres, also lies mostly just north of the equator.

The dynamics controlling the intensity of the trade wind systems in the tropical Atlantic and the ITCZ is a result of complex processes in which continental convection and influences from other basins play an important part as well as the seasonally and interannually varying SST of the Atlantic Ocean. The ITCZ has a meridional seasonal migration with SST about 28°C. Also interannual variability of fluctuations in the meridional gradient of SST gives rise to fluctuations in the southernmost position of the ITCZ with severe implications for the climate of the northeastern region of Brazil. Seasonal changes in surface wind speed and cloud cover give rise to strong seasonal variations in surface latent heat release and net solar heating, which are important terms in the heat balance of the oceanic mixed layer in the tropical Atlantic (Grotsky and Carton, 2003).

The Brazilian coast, mostly in its southern portion, is often under the influence of synoptic and mesoscale meteorological systems, which induce significant disturbances in the ocean, such as mean sea level changes, generations of surface waves and drive currents. The frontal systems are among the most important atmospheric responsible for precipitation and change of temperatures in Brazil, being the South region the most affected. The frontal systems originated from atmospheric baroclinic waves of mean

latitudes immersed in winds from west. The baroclinic waves are deriving from the Pacific Ocean and interact with the atmospheric circulation above the South America. These systems have propagation typical from southwest to northeast along the coast of South America and are more frequent between 20°S and 35°S.

In South America, the frontal systems from the Pacific moving eastwards and, after crossing the Andes regularly acquire a component toward the equator. These systems can move over the continent or move to the Atlantic Ocean (Cavalcanti and Kousky, 2003; Satyamurty et al., 1998). In Brazil, the cold fronts operate along the year and most significantly affect the South and Southeast Regions. They are responsible for rain, mainly in the south of the country. Oliveira (1986) built climatology of cold fronts and interaction with the convection on the Amazon, using satellite imagery. Lemos and Calbete (1996) continued the work of Oliveira, preparing the climatology of the systems front from 1987 to 1995. Recent studies establish a weather front of the systems in South America using data from the NCEP reanalysis/NCAR as Cavalcanti and Kousky (2003). All previous mentioned works showed that the frequency of cold fronts decreases at lower latitudes.

Rodrigues et al. (2004) estimated climatology of cold fronts at the Brazilian coast between 25°57' S and 29°23' S, based on 10-year period (1990-1999) of NCEP-NCAR reanalysis data. The cold front passages were objectively identified taking into account the wind shifts to a southerly direction. The results show that, on the average, 3 to 4 cold fronts reach the Brazilian coast at these latitudes, monthly, with an interval of 8 days. The composite data analysis, using the date of days of cold front passages as reference, shows clearly a climatological pattern of evolution, with cold front moving typically from southwest to northeast.

The changes in weather conditions observed in regions south and southeastern Brazil are generally associated with the transition or intensification of cold fronts, weather systems typical of middle latitudes in the Brazilian coast at all seasons of the year (Satyamurty et al., 1998). In the south-southeast coast of Brazil, these atmospheric disturbances can cause

elevations in the sea level. Significant changes in the currents and tides, in turn, can affect marine activities, fishing and navigation, hampering operations in ships, ports and platforms. Extreme elevations in the sea level may result in problems of coastal erosion, destruction of edge and saline intrusion. Truccolo and Franco (2000) identified a sea level response to the frontal passages, in the south region of the Brazilian coast. The cold fronts in the South American coast, in general, reach latitudes around 20°S, where begins its process of dissipation.

In southern Brazil, the studies of Oliveira (1986) and Lemos and Calbete (1996) identified a relatively greater frequency front from May to December, decreasing between January and April. In the southeastern coast of Brazil, these same authors found a number of frontal systems relatively higher in the winter months, when compared to the period of summer. The greater permanence of the systems, however, was observed during the summer, in association with the activity of the South Atlantic Convergence Zone (SACZ) (Satyamurty et al., 1998). Lemos and Calbete (1996) identified a monthly average of 3 to 4.5 systems reaching the south of Brazil between 1987 and 1995. Oliveira (1986), on the other hand, found a higher frequency of cold fronts, ranging from 6 to 7 between May and December, and 5 to 6 between January and April. He selected cases of cold fronts in four bands of latitude (between 45°S and 20°S) along the coast; through analysis of images from a geostationary satellite GOES-EAST, between the years 1975 and 1984.

2.2. The mean circulation

The South Atlantic plays a unique role in transporting energy towards the equator (Gordon, 1986), forming an important link in the thermohaline circulation. Nevertheless the actual knowledge about the variability of the South Atlantic circulation (and its interaction with the atmosphere) is poorly known if compared to the more studied North Atlantic Ocean. A major portion of variability in the tropical Atlantic currents seems to be driven by

large-scale seasonality in the trade wind regime and the latitude of the Intertropical Convergence Zone (ITCZ) (Stramma and Schott, 1999; Lumpkin and Garzoli, 2005). In similar manner, the dynamics that control the variability in the western boundary regime of the tropical South Atlantic could be a result of the seasonal changes of the surface wind speed. The ITCZ migrates meridionally, on seasonal time scale, leading to changes in the upper ocean parameter distribution and also in the ocean circulation (Stramma et al., 2005). This ITCZ seasonal cycle is the largest atmosphere-ocean signal in the tropical Atlantic. The surface currents reflect the response to the seasonally varying wind field and the migration of the ITCZ. As the ITCZ moves northward, the zonal currents (i.e., North Equatorial Current (NEC), North Equatorial Countercurrent (NECC) and South Equatorial Current (SEC)) are also carried northward.

Under this context, the sSEC is broad and slow flow (Stramma et al., 2003; Lumpkin and Garzoli, 2005) transporting subtropical water northwestward into the western Atlantic boundary until it encounters the South American continent. At the easternmost tip of South America, the sSEC bifurcates feeding two important western boundary currents. The southward limb of the sSEC as the Brazil Current (BC) carries about 4Sv (Stramma et al., 1999).

The northward limb of the sSEC merges with the North Brazil Undercurrent (NBUC). This strong western boundary current has a near shore core position at 50 km from the Brazilian coast; reaching down to about the 900 m level and its mean maximum of about 65 cm s^{-1} is at 180 to 250 m depth. The mean flow structure of the NBUC is already well developed at 11°S , indicating that the bifurcation of the sSEC is located well south of this section with a main maximum northward NBUC flow in July and minimum in October-November (Schott et al., 2005). The mean northward transport of the NBUC is about 25.4 Sv along the northern coastline of Brazil and a seasonal cycle of 2.5 Sv amplitude with its northward maximum in July. The interannual transport of the NBUC has small variations of the order of 1.2 Sv, with no detectable trend (Schott et al., 2005). The NBUC

supplies the eastward flow of the South Equatorial Countercurrent (SECC), which partially recirculates into the cSEC.

After passing Cape São Roque at 5°S, the central branch of SEC (cSEC) joins the NBUC, causing its vertical structure to change from an undercurrent to a surface-intensified current, namely the North Brazil Current (NBC). The NBC crosses the equator northwestward and retroflects into the zonal equatorial current system (Silveira et al., 1994; Stramma et al., 1990, 1995, 2005; Schott et al., 1998) feeding the NECC.

Recently, the sSEC dynamics has received more attention. In particular, the sSEC bifurcation region brings together multiple oceanic-weather interactions of great importance. Among these interactions they can be enumerated: (i) transfers of heat and mass between different layers of the tropical Atlantic subsurface; (ii) exchanges of heat and fresh water between the ocean and the atmosphere on the tropical Atlantic surface; (iii) links between climatic variability of the SST and the heat content of the upper layers of the tropical Atlantic and related atmospheric systems, which controls precipitation on the Brazilian Northeast.

The bifurcation also affects downstream mesoscale processes in the ocean. For example, in the region south of Cabo Frio (22°S), the BC presents a very energetic pattern, with frequent formation of strong cyclonic and anticyclonic meanders, which sometimes detach from the main flow in well developed rings. The frequency and intensity of these meso-scale processes are related to the behavior of the circulation at the sSEC bifurcation. However, the latitude where sSEC bifurcation occurs off Brazil is still poorly known.

The variability of the bifurcation of the sSEC also affects the Southwestern tropical Atlantic. The western boundary regime of the tropical South Atlantic in its several scales of variability has been the subject of numerous investigations (Molinari, 1983; Stramma, 1991; Stramma et al., 1995; Stramma and Schott, 1999; Stramma et al., 2005; Schott and Böning, 1991; Schott et al., 1993; Stramma et al., 1995; Rhein et al., 1995; Schott et al., 2005). The Deep Western Boundary Current (DWBC) transports cold

North Atlantic Deep Water toward the southern hemisphere, while the NBUC flows as an inter-hemispheric belt of warm surface waters northward to close the thermohaline overturning cell (Gordon, 1986; Schmitz, 1995). The SACW, between 100 and 500 m depth, is transported within the sSEC toward the Brazilian shelf, where it is carried toward the equator via NBUC and NBC (Stramma and Schott, 1999; Stramma et al., 2005).

Furthermore, the flow in the NBUC is of interest for a number of reasons. As already pointed out, the upper-layer western boundary flow carried by the NBUC is a crucial link within the Atlantic Subtropical Cell (STC) connecting the subduction regions of the subtropical South Atlantic and the eastward equatorial and off-equatorial undercurrents that supply the equatorial and eastern boundary upwelling regimes. Besides, in the 50–300m depth range, the NBUC could be an important role in the Atlantic STC.

The STC connects all processes of the subtropical to tropical ocean determining then, the water mass structure of the tropical ocean. Also, subduction processes, within the STC, bring surface waters below the mixed layer, where they will be advected towards the equator. Schott et al. (2005) showed the connection of the western boundary regime to the large scale tropical circulation. They suggest that, the NBUC seasonal variability is connected with the seasonal migration of the latitude of the sSEC inflow into the western boundary regime. Schott et al. (2005) also suggest that another source of seasonal boundary transport variability is the interior Sverdrup transport. Based on the NCEP reanalysis stresses, the Sverdrup transport has a southward maximum in July and a broad minimum during November–May with an annual range of 12 Sv. Discrepancies on seasonal curves of NBUC and Sverdrup transport, led them recommend a detailed investigation of the Rossby wave response in different parts of the basin to wind stress curl forcing at 10°–12°S.

Although the existence and importance of the bifurcation is well known, the observational and theoretical studies are not conclusive. Stramma et al. (2003) links the variability of the NBUC at 5°S to equatorial processes. On the other hand, Schott et al. (2005) links the seasonal cycle of

the NBUC at 11°S to seasonal migration of the sSEC bifurcation. Geostrophic flow fields have shown that the sSEC moves southward at increasing depth. Until recently, it was believed that the sSEC has a northernmost bifurcation in austral winter and a southernmost bifurcation in austral summer. Rodrigues et al. (2007) brought a new perspective to the seasonal variability of sSEC. They investigated the bifurcation using a reduced-gravity, primitive equation ocean circulation model. They found that the annual mean of the sSEC bifurcation starts at about 10°–14°S near the surface, and then it shifts poleward, while increasing depth, and reaches about 27°S at 1000 m. The bifurcation latitude has different variations for different depth ranges. For the first 100 m depth the bifurcation latitude varies 7°, 3° for 100 m to 400 m range depth, 1° for 400 m to 600 m and 2° below 600 m depth. The results of the model they use indicate that the seasonal variability of the bifurcation latitude in the upper thermocline is associated with changes in the local wind stress curl due to the annual north-south excursion of the ITCZ. Positive (negative) wind stress curl produces an anomalous anticyclonic (cyclonic) circulation, whose southward (northward) component near the western boundary causes the sSEC bifurcation to occur at lower (higher) latitude during the austral spring/summer (winter) months. Variability in the amplitude of local wind stress curl is due to the annual north–south excursion of the marine ITCZ complex. The local component of the forcing, responsible for most of the variability in the sSEC bifurcation, explains the decrease in the transport of both the sSEC and BC in June and July and the subsequent increase from September to November. When the sSEC bifurcation moves southward (northward), the NBUC transport increases (decreases) and the BC transport decreases (increases). It was obvious from their work that a detailed climatology should be constructed.

2.3. The water masses

The western boundary regime of the tropical South Atlantic Ocean is a belt of

exchange of warm and cold water masses as part of the MOC. Approximately 17-20 Sv ($1 \text{ Sv} \equiv 10^6 \text{ m}^3 \cdot \text{s}^{-1}$) of NADW pass southward through the equatorial zone, compensated by a net northward transport of warm and intermediate waters of Antarctic Bottom Water (Schott et al., 2005). Furthermore, the upper-layer western boundary flow, carried by the NBUC, is a crucial link within the STC connecting the subduction regions of the subtropical South Atlantic. The STC affects the tropical SST including all processes that connect the subtropical ocean to the tropics and thereby determine the water mass structure of the tropical ocean.

The Tropical Surface Water (TSW) is formed due to the intense radiation and the excessive evaporation in relation to rainfall, characteristic of the equatorial South Atlantic. The TSW with temperatures of about 27°C forms the mixed layer of the tropical Atlantic. In the sharp thermocline underneath, temperatures drop from 25 to 15°C over about 50 m in the vertical and the 20°C isotherm is often taken as a lower boundary of the TSW. This isotherm is often related to the isopycnal $\sigma_\theta = 25.8 \text{ kg} \cdot \text{m}^{-3}$ (Stramma et al., 2005). Imbedded in the TSW is the Salinity Maximum Water (SMW), also called Subtropical Underwater, characterized by a salinity maximum at densities slightly below $\sigma_\theta = 25.0 \text{ kg} \cdot \text{m}^{-3}$. The SMW is formed in the tropics/subtropics transition region by subduction and progresses equatorward as a subsurface salinity maximum.

The SACW is characterized by temperatures higher than 6°C and less than 20°C and salinity between 34.6 and 36 ups (Miranda, 1985; Silveira et al., 2000). Its formation is in the area of the confluence of the BC with the Falkland Current, which is responsible for its high salinity (Stramma & England, 1999). The SACW is located between the thermocline and the isopycnal $\sigma_\theta = 27.1 \text{ kg} \cdot \text{m}^{-3}$ at about 500 m depth and is characterized by a nearly linear T-S (temperature-salinity) relationship (Stramma et al., 2005). Two types of SACW are found, a lighter type of SACW, originating from the southwestern subtropical gyre and a denser type originated from the South Atlantic as well as from the South Indian Ocean. The latter is brought from the South Indian Ocean by the Agulhas Current. Then, the denser SACW is

carried into the equatorial region by the Benguela Current and then by the sSEC.

Silveira et al. (2000) describe the SACW as a body of water belonging to the Subtropical Gyre, which circulates with the South Atlantic and Benguela Currents, and reaches the coast of South America transported by the sSEC. The SACW bifurcates in two parts, as in the surface currents, one flowing towards the equator, and another southward. The exact location of the bifurcation of the SACW is uncertain, however there is consensus in the literature that at the south of Cabo de São Tome (22°S), the SACW flows to the south off the Brazilian coast. Estimates of the bifurcation of SACW were made by Wüst (1935) determining values extremes of temperature or salinity in the region of formation of this water mass. Defant (1941) confirmed the estimates of Wüst applying the geostrophic calculation. Other authors are also examining the zone of separation flow of SACW, as well as in Stramma and England (1999), which confirm the position of this zone in latitudes below 20°S.

Wüst (1935) defined the BC being formed by TSW and SACW, with a thickness of 400 - 700 m along the South-Southeast Brazilian. The lower limits of the southward-flowing BC water lies the oxygen minimum layer near the Brazilian coast, just above the Atlantic Antarctic Intermediate Water (AAIW).

The AAIW has thermohaline limits between 3° and 6°C and 34.3 and 34.6 psu. The AAIW and the upper Circumpolar Deep Water (uCDW) are located between the isopycnals $\sigma_\theta = 27.1 \text{ kg.m}^{-3}$ and $\sigma_\theta = 32.15 \text{ kg.m}^{-3}$. The AAIW originates from a surface region of the circumpolar layer, especially the surface waters in the northern Drake Passage and the Falkland Current loop and a southern boundary that is essentially the Subantarctic Front. The spreading of the AAIW from the South to the North Atlantic at the western boundary can be traced by following the salinity minimum. Stramma and England (1999) focused the axis of the bifurcation south of AAIW to 25°S, but with the axis of divergence occurring almost parallel to the slope.

The NADW, located just below the AAIW and part of the thermohaline

circulation, is characterized by values of temperature between 3° and 4°C and salinity between 34.6 and 35.0 psu, with levels between 1500-3000 m off the coast of southeast Brazil (Silveira et al., 2000). The NADW presents itself as an organized flow, flowing to the south along the contour west to around 32°S, transported with the Deep Western Boundary Current from the northern to the southern hemisphere, where at least part of the current returns toward the equator.

The Upper Circumpolar Deep Water (uCDW) located below AAIW has a source region different from the overlying AAIW, but both water masses flow from the South Atlantic toward the North Atlantic. The CDW is a large body of fresh, oxygen-poor, and nutrient-rich water compared with the North Atlantic Deep Water (NADW). The uCDW flows generally eastward in the Antarctic Circumpolar Current (ACC) and is found over a large density range. In the tropics the isopycnal $\sigma_{\theta} = 32.15 \text{ kg.m}^{-3}$ separates the uCDW from the southward NADW, however, in the subtropics the vertical extent of the uCDW increases and the isopycnal $\sigma_{\theta} = 36.9 \text{ kg.m}^{-3}$ better represents the lower boundary of this water mass (Stramma and Peterson, 1999).

Chapter 3

3. The study area and data

This thesis concentrates on the South Atlantic Ocean with focus more precisely at the upper layer of the western boundary of the tropical South Atlantic along the Brazilian shelf. The purpose is to introduce the area of study altogether with the data of relevant phenomena that influence it.

The data used in this work describe the mechanisms of the coupling ocean-atmosphere variability. Thus, it is analyzed ocean direct current measurements in a mooring array deployed by German CLIVAR (Climate Variability and Predictability Program) (Schott et al., 2005), satellite wind stress data (Zhang et al., 2006) and results from the Regional Ocean Model ROMS simulation (Silva et al., 2007).

3.1. The study area

The study area of the wind stress data is limited by the latitudes 40°S to 10°N, and longitudes 20°W to 60°W (Figure 3.1). Cross-shore and alongshore components of currents from an array of five current-meter moorings along

225 km across the North Brazil Undercurrent (NBUC) at 11°S are used to describe the mean structure of the currents and compare with model results as well as wind stress data.

Chart of area of interest with a schematic representation of mean currents involved in this study is showed in the large panel of the Figure 3.1. A mean latitudinal position of the sSEC is showed for three different water masses based on previous works. This figure also shows in the right side the moorings position at 11°S as well as the mooring array with the different depths of the measurements.

3.2. Moored array observations at 11°S

The current field data set used here was obtained during the period between March 2000 and August 2004 at the Brazilian shelf break, as part of the German CLIVAR tropical Atlantic Project. The aim was to investigate the deep western boundary current regime in this region as part of the global circulation and to analyze the equatorward return flow of the MOC in the upper layer. The data were collected in an array of five current-meter moorings (K1–K5) along 225 km across the NBUC (10°S–11°30'S), first deployed in March 2000 by Meteor cruise M47/1. The near-surface flow, at stations K1–K3, was covered by upward-looking ADCPs, while K4 carried an acoustic current meter at about 100 m depth. Mooring K5 was installed from March 2000 to February 2002 to observe the offshore deep flow. At the deepest levels, currents were recorded by acoustic current meters (ACMs).

The mooring array was deployed in the western boundary currents crossing the North Brazil Undercurrent, which transport the southern waters from South to North Atlantic as a limb of Meridional Overturning Cell (MOC) as a part of the Sub-tropical Cell. This last one connects the subduction regions of the subtropical South Atlantic with the eastward equatorial and off-equatorial undercurrents that supply the equatorial and eastern boundary upwelling regimes (Schott et al., 2005).

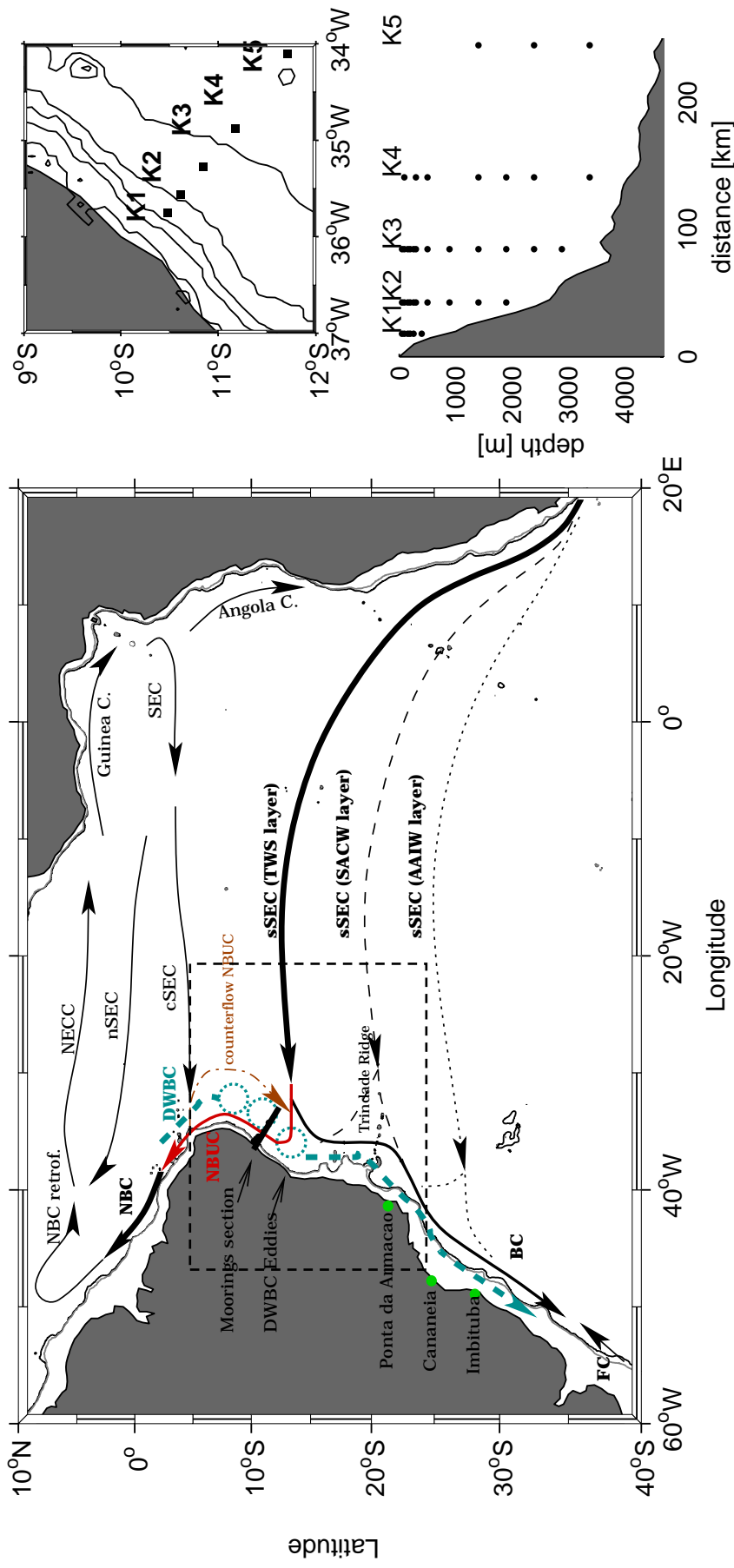


Figure 3.1. (left) Chart of study area with domain limited by 10°N-40°S and 20°E-60°W and location of the K1-K5 moorings along the offshore normal transect about 11°S. Schematic representation of mean zonal and meridional currents are indicated: The upper ocean northward NBUC flow (red solid line), and the deepest southward transport by the DWBC (blue dashed line). The sSEC bifurcation at 100m depth (solid line); between 200m and 500m depth (dashed line); between 500m and 1200m depth (pointed line), according with Stramma and England (1999). The three sea level Stations are indicated (green points). Dashed dark rectangle is the modeled area. (Right) On top the crossshore mooring array position. Bottom the depth measurements at the mooring array.

The K1 to K5 mooring lines were used in this work to estimate the monthly-averaged transports at 11°S. These data were also investigated through Principal Component Analysis (PCA) applied for a single field, meridional current only, while K3 and K4 data, for which simultaneous measurements of speed of currents and temperature are available to the same time interval, were also investigated through PCA for coupled fields (Table 3.1).

Table 3.1. Mooring time records, positions, instruments and current-meter depth. For K3 and K4 stations there are temperature measurements for the same time interval and depths.

<i>Station and time period of records</i>	<i>Lat/Lon</i>	<i>Instrument</i>	<i>Depth</i>
<i>K1 - 02/02/2002 to 17/01/2003 and 01/06/2003 to 18/08/2004</i>	<i>10° 16.0' S 35° 51.7' W</i>	<i>ADCP</i>	<i>32 to 400 m</i>
		<i>FSI-ACM</i>	<i>443 m</i>
		<i>ARGONAUT</i>	<i>622 m</i>
<i>K2 - 06/02/2002 to 04/05/2004</i>	<i>10° 22.8' S 35° 40.8' W</i>	<i>ADCP</i>	<i>39 to 400 m</i>
		<i>RCM</i>	<i>900 m</i>
		<i>FSI-ACM</i>	<i>1400 m</i>
		<i>ARGONAUT</i>	<i>1900 m</i>
<i>K3 - 21/03/2000 to 31/01/2002 and 12/05/2003 to 19/08/2004</i>	<i>10° 36.7' S 35° 23.4' W</i>	<i>ADCP</i>	<i>29 to 264 m</i>
		<i>RCM</i>	<i>491 to 2883 m</i>
		<i>ARGONAUT</i>	<i>888 m</i>
		<i>FSI-ACM</i>	<i>1386 m</i>
<i>K4 - 20/03/2000 to 18/08/2004</i>	<i>10° 56.5' S 34° 59.5' W</i>	<i>ARGONAUT</i>	<i>112 to 2402m</i>
		<i>RCM</i>	
		<i>FSI-ACM</i>	
<i>K5 - 21/03/2000 to 04/02/2002</i>	<i>11° 28.2' S 34° 12.9' W</i>	<i>ARGONAUT</i>	<i>1404 to 3404 m</i>
		<i>FSI-ACM</i>	

The K1 to K5 moorings line were used in this work to estimate the seasonal and intra-seasonal variability at 11°S. These data were also investigated through Spectral Analysis and Cross-correlation between alongshore currents and meridional wind stress. Tidal frequencies are removed from the observed currents by taking a 40-hour filter and sub-sampled every 12 hours. For the intraseasonal variability analysis one 10-30-days band pass filter was applied to calculate the cross-correlation with wind stress data.

3.3. Wind stress data

The wind stress data were obtained from the NOAA/NCDC (National Oceanic and Atmospheric Administration/National Climatic Data Center) available online at <http://www.ncdc.noaa.gov/oa/satellite.html>. In this data base surface wind stresses ($N.m^{-2}$) are estimated from blended sea surface wind speeds at 10 m above sea level have been generated from six satellites, on a global $1/4^\circ$ regular grid and for several time resolutions (Zhang et al., 2006). The surface wind fields are retrieved from various satellite instruments, e.g., the Special Sensor Microwave/Imager (SSM/I), the Tropical Rainfall Measuring Mission (TRMM) Microwave Imager (TMI), the Quick Scatterometer (QuikSCAT), and the Advanced Microwave Scanning Radiometer - EOS (AMSR-E), from ERS-1/2 and from the altimeter satellites TOPEX/POSEIDON and Jason. The ascending and descending satellite data with a $1/4^\circ$ resolution are used as input to blended products. The most recent versions of the Remote Sensing System (RSS) retrievals were used: Version 5 for SSMI ocean products, Version 3a for TMI ocean products, Version 3 for QuikSCAT winds, and Version 4 for AMSR-E ocean products. An objective analysis method, namely a spatial-temporally weighted interpolation, is used to generate 12-hourly blended product from multiple satellites. The averaging weights are determined by the normalized distances in both space and time from the data points to the grid interpolation points. The weight function has Gaussian characteristics with near zero lags and decreases more rapidly farther away, ensuring less smoothing from remote data points to the gridded values at grids with nearby observations. The gridded wind stress fields are produced for regular $1/4^\circ$ spatial grids from 0° to $359.75^\circ E$ in longitude and from $89.75^\circ S$ to $89.75^\circ N$ in latitude.

The blended speeds are then decomposed into (u, v) components using the NCEP Re-analysis 2 (NRA-2) wind directions interpolated onto the blended speed grid. The 6-hourly satellite-scaled global $1/4^\circ$ grid wind stress components are computed as:

$$\tau^x = -(V_s/V_m)^2 \tau_m^x \text{ and } \tau^y = -(V_s/V_m)^2 \tau_m^y \quad (3.1)$$

where V is the velocity estimated from its u and v components, the V_s indicates satellite-scaled values and V_m indicates NRA-2 model values interpolated to the satellite grid. The initial reanalysis produced using the NCEP model in cooperation with the National Center for Atmospheric Research (NCAR), usually referred to as NCEP-NCAR reanalysis, and is termed NRA. The wind stress data used in this study has 12 hourly temporal resolutions. The covered area was between 40°S to 10°N and 60°W to 20°E. A two days filter was used to derive the seasonal mean, standard deviation of data and spectral analysis. A low pass filter was applied in the spectral analysis where maximum correlation was found and a 10-30-days band pass filter was applied to calculate the cross-correlation with current data.

3.4. Sea level gauge

For the present work, three local stations along the Brazilian coast have data-available for the same period of the mooring measurements. The Ponta da Armação Station (22°53'S and 43°08'W) which is maintained by the Brazilian Navy Hydrographic Center (CHM) itself, and the Cananéia Station (25°01'S and 47°55.5'W), controlled by the Oceanographic Institute of the São Paulo University - IO/USP. The third source of daily sea level data was provided by the Brazilian Institute of Geography and Statistics (IBGE). The Imbituba Station (28°08'S and 48°24'W) is an IBGE's Geodetic Permanent Tide Gauge Network (RM PG), with daily sea level records in the period 2002-2004. The RM PG stations are part Global Sea Level Observing System of the Intergovernmental Oceanographic Commission of UNESCO (GLOSS/IOC), and have been used as a reference for studies related to climatic changes.

3.5. Chlorophyll data

MODIS-A is one of the five sensors on-board TERRA/AQUA satellite with 36 electromagnetic spectral bands from visible to thermal Infra-red (IR). MODIS Ocean data consist of 36 Ocean Color and 4 sea surface temperature (SST) parameters. There are an additional 38 parameters, such as wind speed, surface pressure, brightness temperatures, etc., that are used for quality control. The ocean parameters are grouped into 3 Ocean Color data types and one SST data type. Each data type is distributed as a separate HDF-EOS file. The ocean parameters are available in daily, 8-day, monthly and yearly average, and at 4.63 km, 36 km and 1° spatial resolution (Savtchenko et al., 2004). For this work, daily mapped 4 km images MODIS Aqua has been acquired into the same period of execution from moorings data, but the MODIS-A is available since July 2002. For this first year there are many gaps for the area of interest, thus the data are analyzed for 2003 and 2004. The area selected to analyze the chlorophyll concentration (mg m^{-3}), is from 22°S to 26°S and 43°W to 48°W.

3.6. The Regional Ocean Modeling System - ROMS

The data obtained from numerical simulations has been extremely important for the knowledge of the numerous aspects of the oceanic circulation. The success of the numerical modeling is related to low operational cost and the possibility of study large geographic areas. Based on this premises, this work focus the investigation in a temporal monthly scale, of the velocity and temperature data from the Regional Ocean Modeling System (ROMS).

ROMS has been used to model the circulation in different regions of the world oceans (i.e. Haidvogel et al., 2000; Malanotte-Rizzoli et al., 2000; Penven et al., 2000, 2001a,b; MacCready and Geyer, 2001; Lutjeharms et al., 2003). It solves the free surface with primitive equations in an Earth-centered rotating environment, based on the classical Boussinesq approximation and hydrostatic vertical momentum balance. The model considers coastline and terrain-following curvilinear coordinates, which

allows minimizing the number of dead points in computing the solution. The boundary conditions for the model are appropriate for an irregular solid bottom and coastline, free upper surfaces and open-ocean sides away from the coastline. These conditions include the forcing influences of surface wind stress, heat and water fluxes, coastal river inflows, bottom drag, and open-ocean outgoing wave radiation and nudging towards the specified basin-scale circulation. Upstream advection in ROMS is treated with a third-order scheme that enhances the solution through the generation of steep gradients as a function of a given grid size (Shchepetkin and McWilliams, 1998). Unresolved vertical subgrid-scale processes are parameterized by an adaptation of the non-local K-profile planetary boundary layer scheme (Large et al., 1994). A complete description of the model may be found in Haidvogel et al. (2000), and Shchepetkin and McWilliams (2003, 2005).

The study presented here deals with the ocean area near the Brazilian coast. Integration domains comprised within 5°S and 25°S, and 20°W and 47°W (Figure 3.1). An isotropic 1/12° horizontal grid was used for simulations, resulting in 323 x 249 horizontal mesh cells. Vertical discretization considers 40 levels. Bottom topography was derived from a 2' resolution database ETOPO2 (Smith and Sandwell, 1997), and a “slope parameter” $r = \nabla h/h < 0.20$ has been used to prevent errors in the computation of the pressure gradient (Haidvogel et al., 2000). At the three laterals open boundaries (North, East and South) an active, implicit, upstream biased, radiation condition connects the model solution to the ocean surroundings (Marchesiello et al., 2001). Horizontal Laplacian diffusivity inside the integration domain is zero, and a 16-points smooth increasing is imposed (up to $10^4 \text{ m}^2 \text{ s}^{-1}$) in sponge layers near open ocean boundaries. The model equations were subjects to non-slip boundary conditions at solid boundaries. A basin scale seasonal hydrology derived from WOA 2001 database (monthly climatology at 1° resolution) was used to infer thermodynamics (temperature and salinity) and geostrophy induced currents at the open boundaries. The circulation was forced at the surface by winds, heat fluxes and fresh water fluxes climatology derived from the COADS ocean monthly fluxes data at 0.5° resolution (Da Silva et al., 1994).

The model ran from a state of rest during 10 years. After a spin-up period of about five years, the model has achieved a statistically steady state. All the numerical results examined correspond to the last year of simulation (year 10).

3.7. Simple Ocean Data Assimilation – SODA reanalysis data

The Simple Ocean Data Assimilation (SODA) version 2.0.2 is a reanalysis of ocean climate. SODA uses the Geophysical Fluid Dynamics Laboratory-Modular Ocean Model (GFDL-MOM) version 2.2, which is a numerical representation of the ocean's hydrostatic primitive equations. The model is forced by observed surface wind stresses from the COADS data set (from 1958 to 1992) and from NCEP (after 1992). The wind stresses were detrended before use due to inconsistencies with observed sea level pressure trends. The model is also constrained by a sequential data assimilation approach of observed temperatures, salinities, and altimetry using an optimal data assimilation technique, in which a numerical model provides a first guess of the ocean state at the update time. The correction of the first guess is based on estimates of the errors contained in the model forecast (the difference between the forecast value and true value of a variable such as temperature at a particular location and time) and in the observations. SODA uses advanced error statistics that are flow dependent, anisotropic, and latitude-depth dependent. The observed data comes from: (1) The World Ocean Atlas 1994 which contains ocean temperatures and salinities from mechanical bathythermographs, expendable bathythermographs and conductivity-temperature-depth probes; (2) The expendable bathythermograph archive; (3) The TOGA-TAO thermistor array; (4) The Soviet Sections tropical program; and (5) Satellite altimetry from Geosat, ERS/1 and TOPEX/Poseidon.

Chapter 4

4. The western boundary variability of the South Atlantic at 11°S

In the western tropical Atlantic strong western boundary currents contribute to the inter-hemispheric transport of water mass properties. The current system is characterized by the interaction of the wind driven meridional current system, the MOC and the STCs. The NBUC supplies the upper layer warm waters along the coast that impact a multitude of importance climate phenomena, while the NADW mass from the north is transported via DWBC at lower depths into the South Atlantic. In this chapter the pathways and variability features of this complex flow pattern will be summarized.

4.1. The mean boundary current structure at 11°S cross section

In order to describe the mean current regime at 11°S, an average section is calculated from the current measurements. The current vectors are rotated

clockwise by an angle of 36° parallel to the coast. The arithmetic mean (2000-2004) of crossshore and alongshore velocity is derived at every instrument depth and interpolated onto a regular 5 km by 20 m grid using Gaussian weights (Figure 4.1). Both the crossshore and alongshore mean present maximum velocities centered at about 250 m depth at K2 and K1 (Figures 4.1a, c). At a distance of approximately 20 km from coast, the crossshore component is towards the continent (Figure 4.1a), where the shelf breaks, and positive from here until 100 km reaching to about 1000 m depth. Further down, between K3 and K4, a mean westward crossshore component (Figure 4.1a), towards the continental slope, that associated to the southward alongshore component (Figure 4.1c) confirms the mean southwestward flow, representing the DWBC at 1500-3500 m. The standard deviation shows more crossshore variability from 100 m eastwards K5 (Figure 4.1b). Higher variability is centered at the K4 position at 2000 m depth. In this position, the eddy model used by Dengler et al. (2004) produced more vigorous eddy activity from April to September.

In the alongshore component a maximum northeastward core is centered at 250 m depth and situated about 50 km from the coast (Figure 4.1c), where the transport is stronger (Schott et al., 2002; Stramma et al., 2003; Schott et al., 2005). The measurements at K3 in the upper 500 m are located at the eastern flank of the NBUC. K4 is positioned outside the equatorward boundary current. Farther offshore there is a weak mean southward flow (Figure 4.1c) at about 500-1500 m depth which is only covered by mooring K4. The return flow of the MOC, also referred to as the upper limb, is compensated with the southward flow of cold water masses in the DWBC. The average current core of the DWBC is centered at mooring K3. The mooring K5 offshore has only provided a two-year-long measurement and the observations are confined to deeper layers below 1500 m with modest flow. There is stronger variability at the core centered in the NBUC and DWBC, with less but not unnoticed variability is the southward flow at 500-1500 m in K4 position.

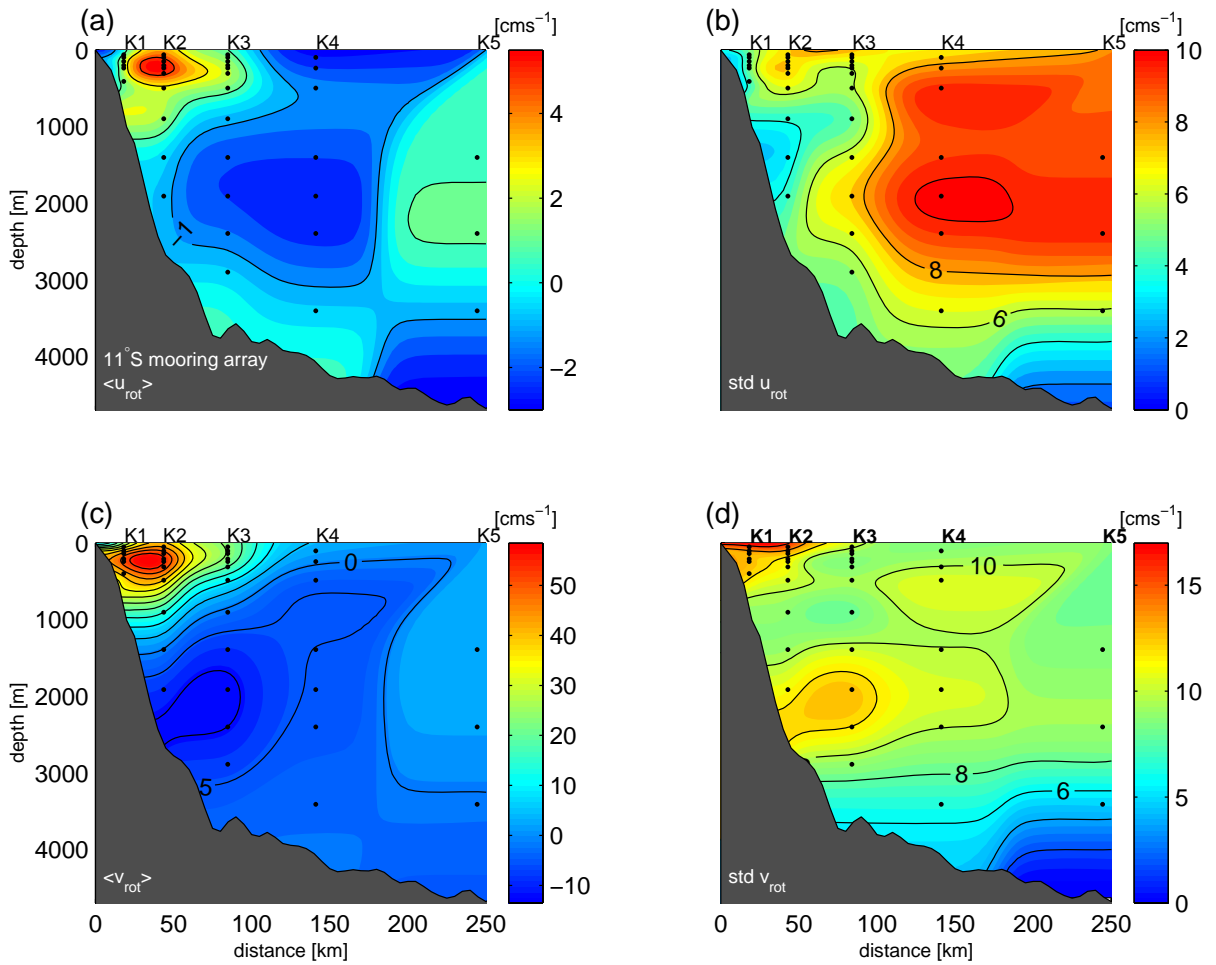


Figure 4.1. Mean currents: (a) crossshore component, (b) standard deviation of crossshore, (c) alongshore component (Adapted from Schott et al., 2005), (d) standard deviation of alongshore. Instrument depths are marked with a black dot.

4.2. Seasonal and intraseasonal variability

The intraseasonal variability (hereafter ISV) in the near surface layer measurements at 100 m depth will be discussed based on current anomalies shown in Figures 4.2 a-e, at mooring positions K1 to K5 for the years 2000 to 2004. The time series are 40-hour low-pass filtered to eliminate tidal effects and the current vectors are rotated clockwise by an angle of 36° parallel to the coast. The mean velocities as shown in Figure 4.1 are subtracted, respectively. However, the anomalies at the near shore position K1 (Figure 4.2a) show mainly high-frequency variability. Velocity changes sign two to three times a month and the fluctuations exceed 50 cm.s^{-1} amplitude. Besides these dominant high-frequency fluctuations, variability

exists with periods of 2-3 months (e.g. austral fall to winter 2002). The dominant signal at K2 is characterized by fluctuations with periods of about 2-3 months similar to K1. The amplitudes of the high-frequency (< 1 month) signal decreases at K2 (Figure 4.2b) which consequently means that these fluctuations are confined to the near boundary region. Further offshore two to three monthly fluctuations are again the dominant signal but those amplitudes scale down with increasing distance from the NBUC current core.

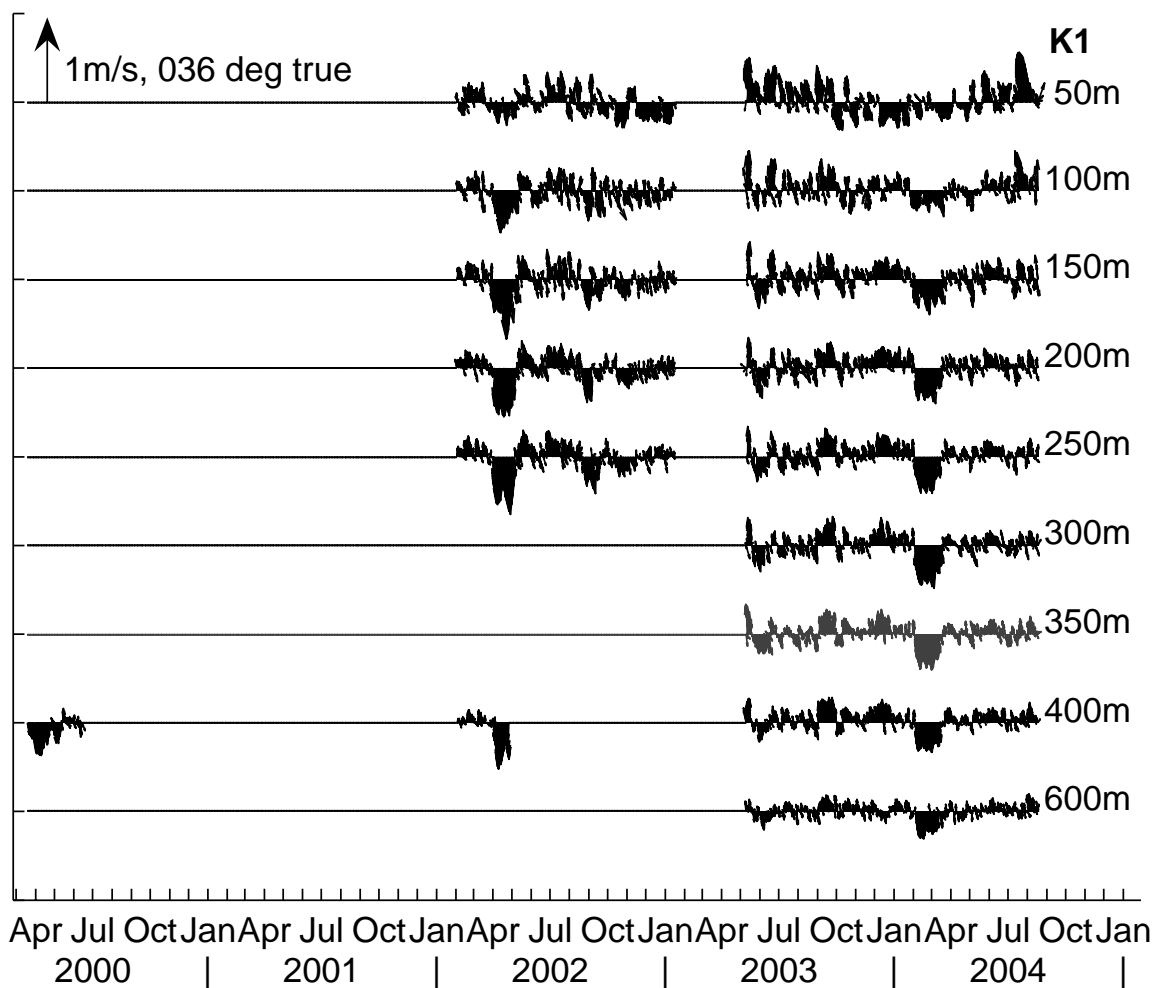


Figure 4.2 a. Combined vector time series of 40-hour low-passed current anomalies from March 2000 to August 2004 of the mooring K1. The time series are rotated 36° parallel to the coast (adapted from von Schuckmann, 2006).

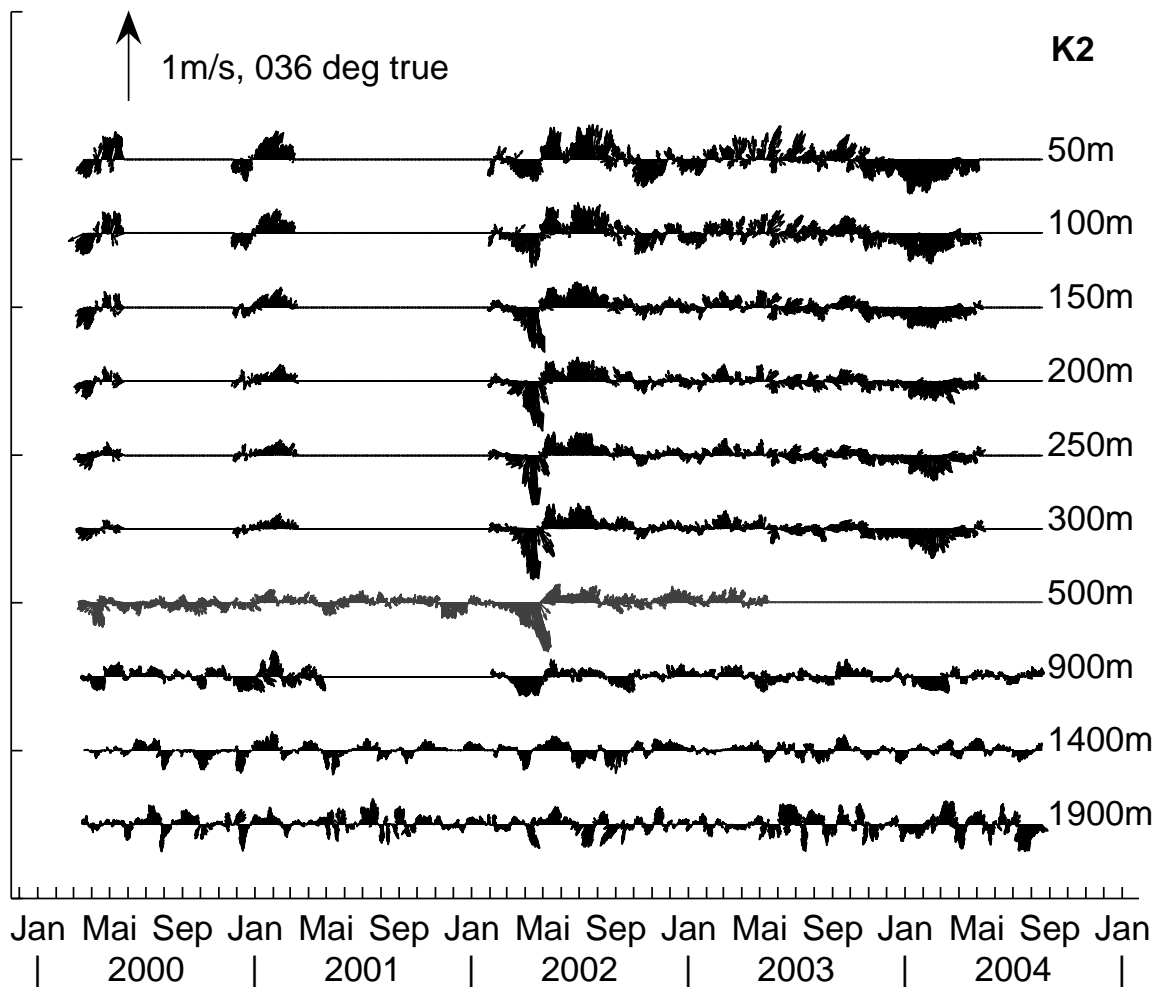


Figure 4.2 b. Combined vector time series of 40-hour low-passed current anomalies from March 2000 to August 2004 of the mooring K2. The time series are rotated 36° parallel to the coast (adapted from von Schuckmann, 2006).

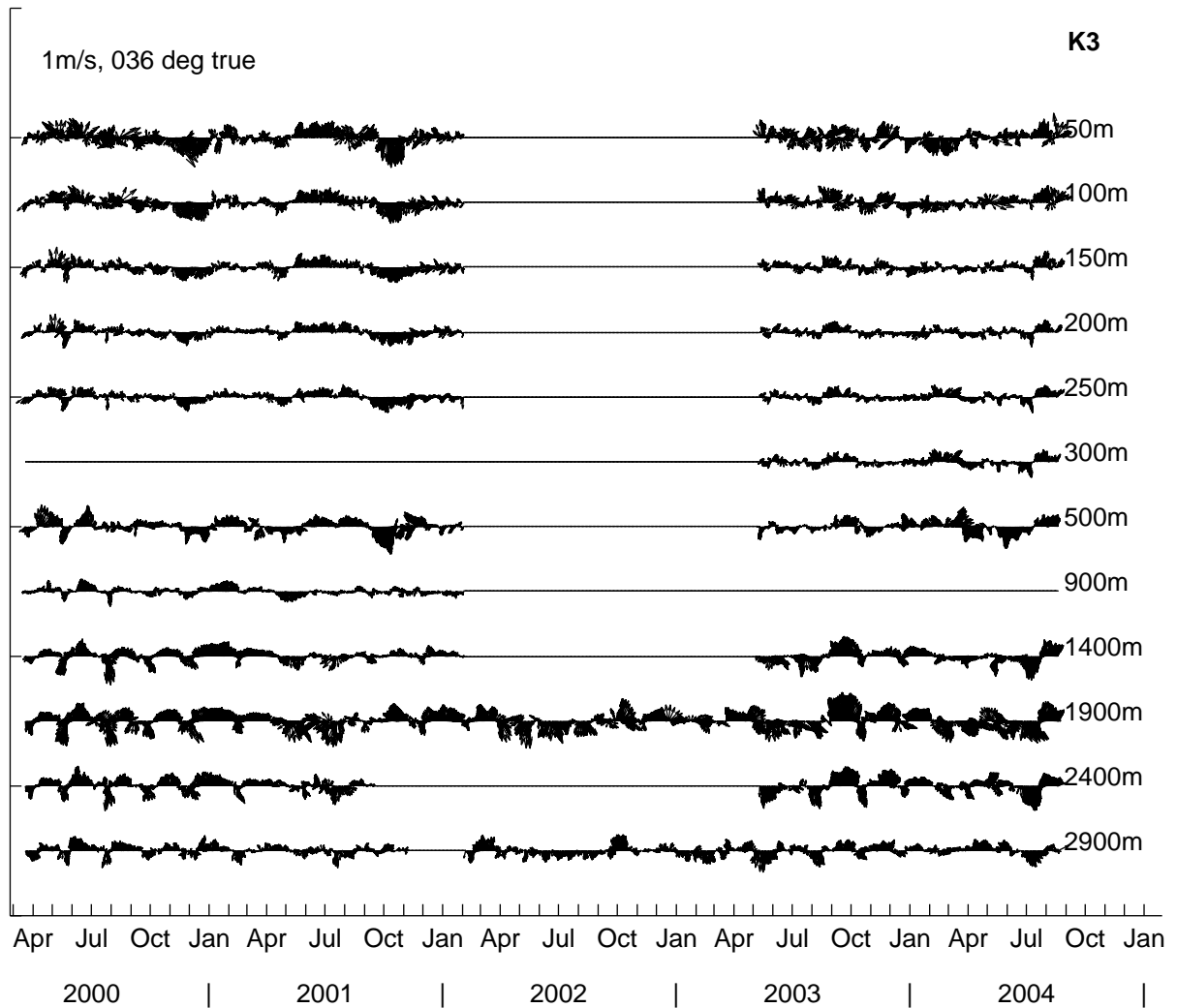


Figure 4.2 c. Combined vector time series of 40-hour low-passed current anomalies from March 2000 to August 2004 of the mooring K3. The time series are rotated 36° parallel to the coast (adapted from von Schuckmann, 2006).

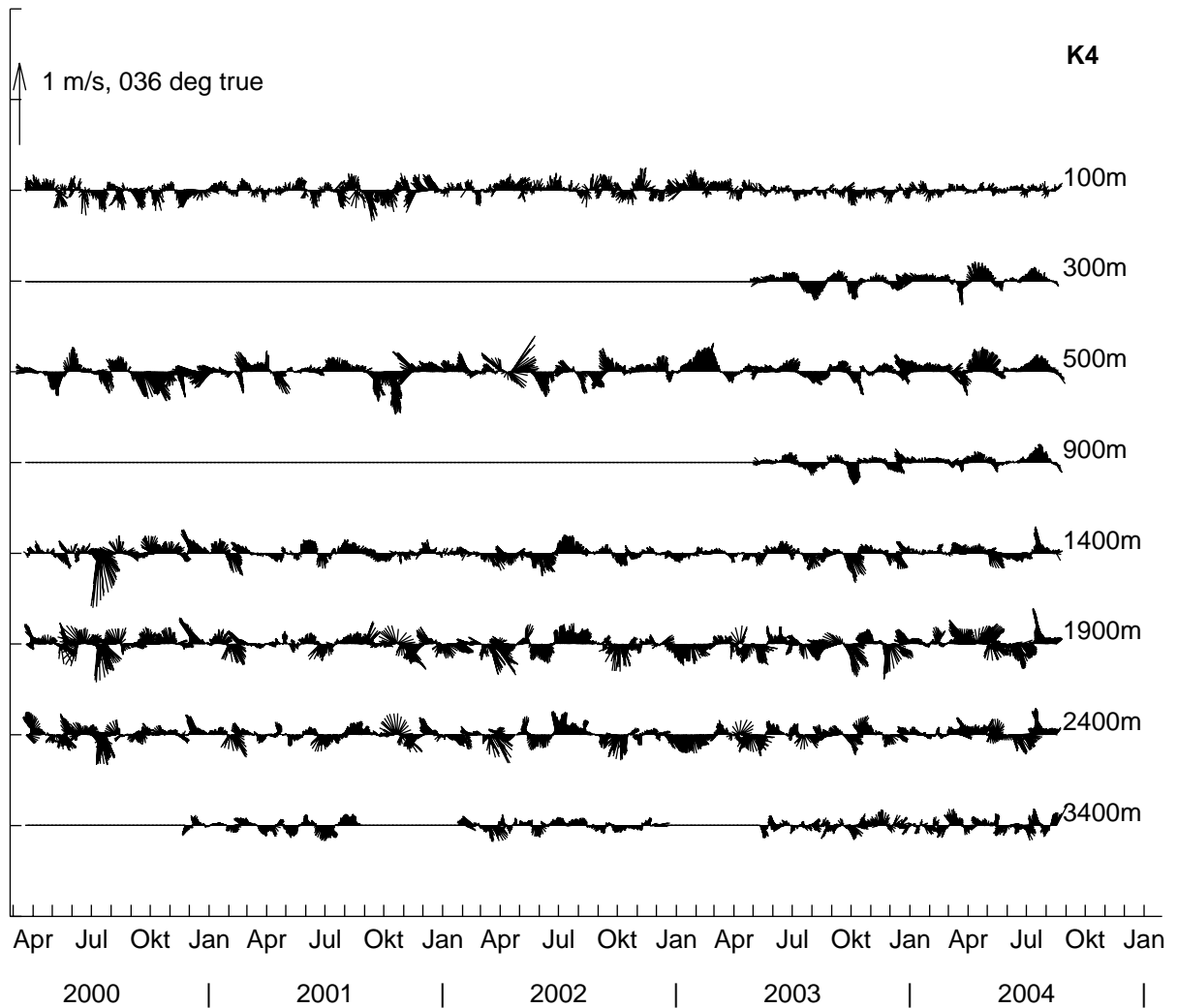


Figure 4.2 d. Combined vector time series of 40-hour low-passed current anomalies from March 2000 to August 2004 of the mooring K4. The time series are rotated 36° parallel to the coast (adapted from von Schuckmann, 2006).

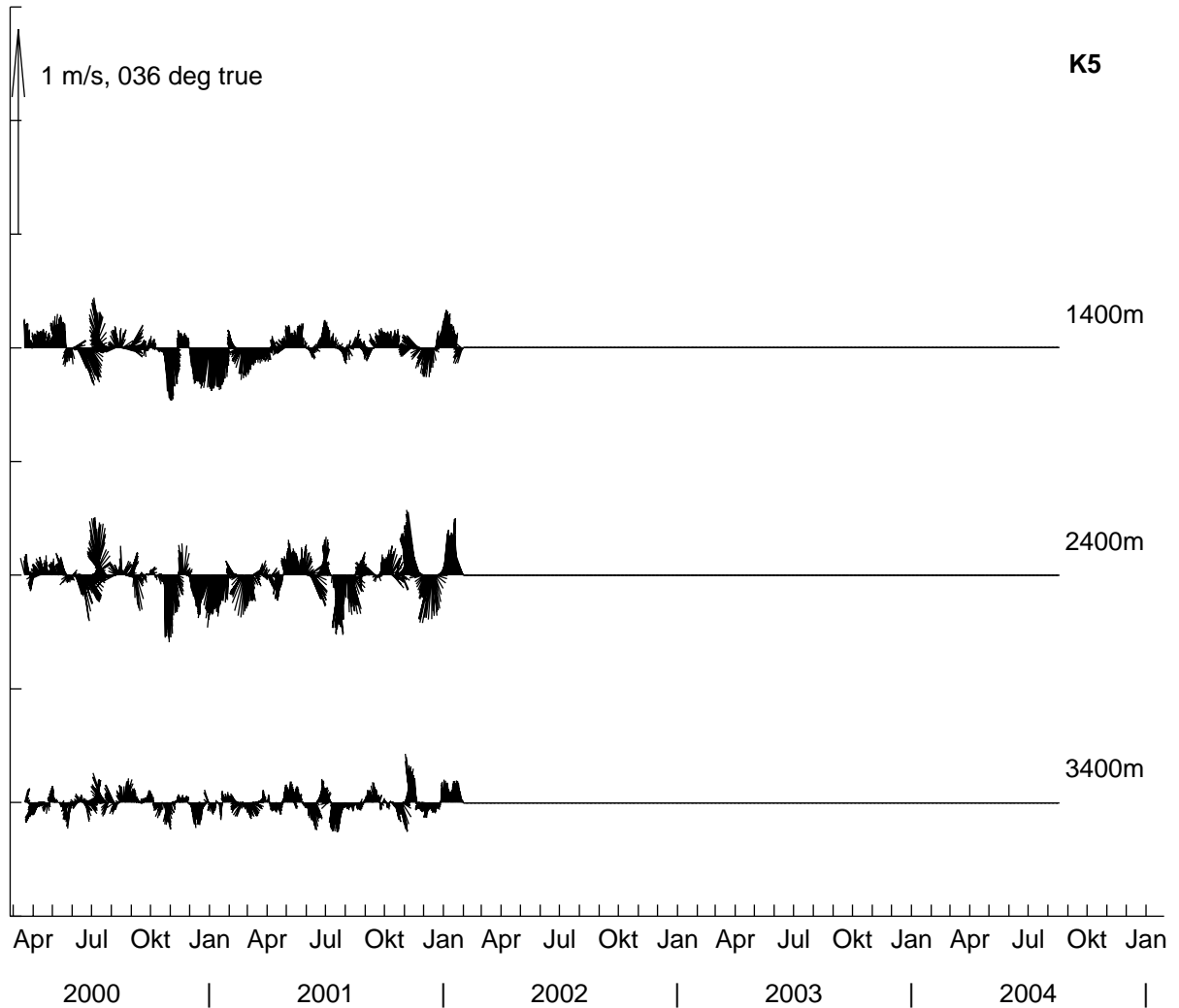


Figure 4.2 e. Combined vector time series of 40-hour low-passed current anomalies from March 2000 to August 2004 of the mooring K5. The time series are rotated 36° parallel to the coast (adapted from von Schuckmann, 2006).

For the seasonal mean alongshore component (Figure 4.3), the strongest values are present in June, July and August, at center of the NBUC. The presence of a mean southward flow at 300-900 m offshore to the NBUC (about 150 km from the coast) can be observed still in the upper layers (Figures 4.3e and g).

At lower depths, in the DWBC, the southward center flow is more attached to coast in June, July and August, and broader and weaker in September, October and November. More variability is present for March, April and May, mainly in the NBUC position and DWBC. At K3 position the

variability is pronounced about 2000 m depth in December, January and February. The mean NADW current is strongest near 2000 m at station K3, and mean offshore northward recirculation at 1400 and 2400 m at station K5 can be observed.

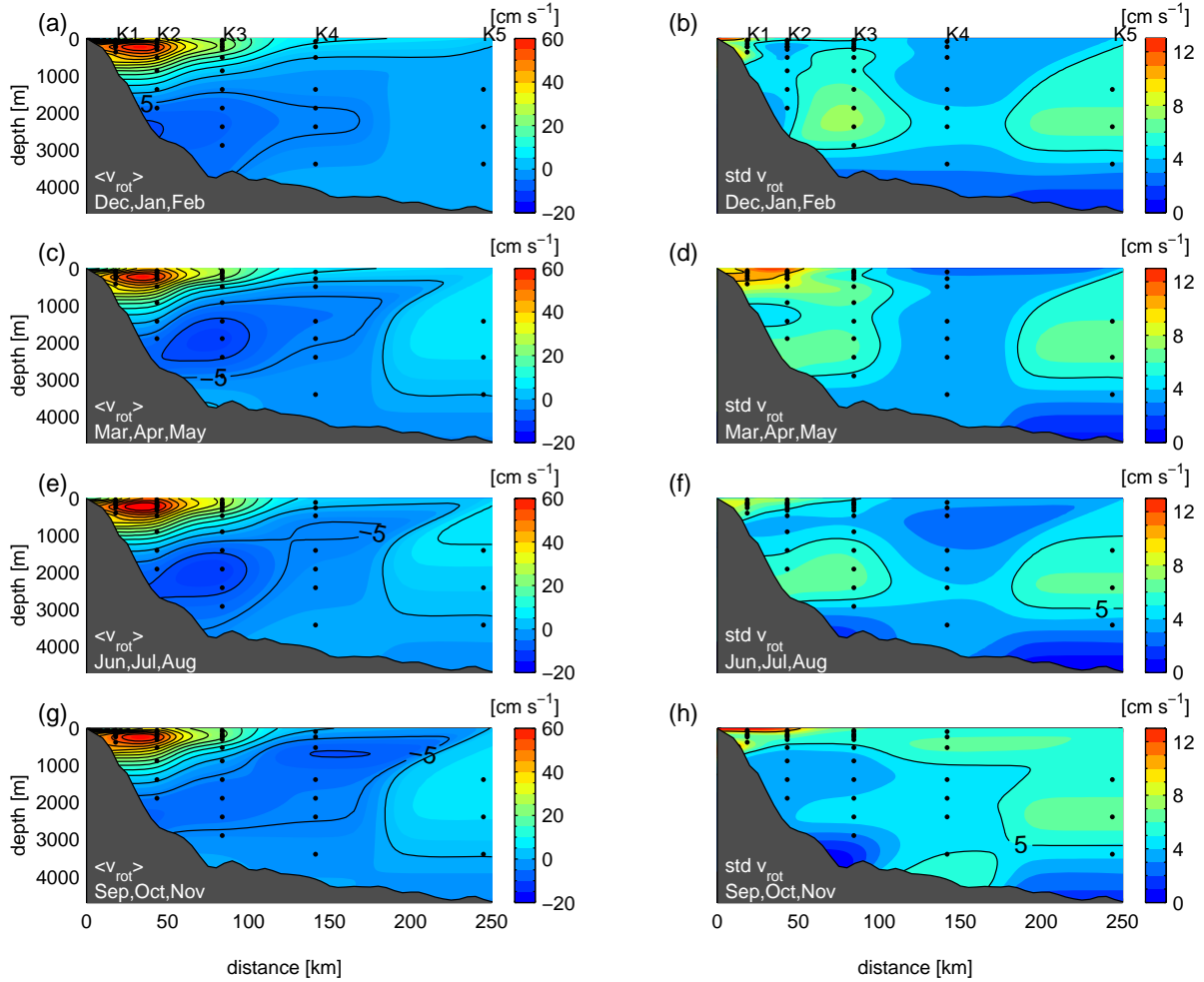


Figure 4.3. Seasonal alongshore current: (a, c, e, g) mean component, (b, d, f, h) standard deviation.

In the mooring K1 is found mainly high-frequency variability, with velocity changes of 2-3 times a month, in the near surface layer for the years 2000 to 2004. Besides these dominant high-frequency fluctuations, there is variability with periods of 2-3 months. The dominant signal at K2 was characterized by fluctuations with periods of about 2-3 months similar to K1. The amplitudes of the high-frequency signal diminish at K2, which means that these fluctuations are confined to the near boundary region.

Offshore, the 2-3 months fluctuations are again dominant, but those amplitudes scale down with increasing distance from the NBUC core.

The spectral distributions of the current records between 50 and 300 m depth at mooring position K1 to K4 are shown in Figure 4.4. Sections of the time series without interruption are used for spectral analysis. The power spectral density is calculated for each complete part of the combined current meter records with comparable window length and then the average power spectral density is composed in order to determine reliable spectral distributions at each mooring position. For the spectral average the short measurement periods in the years 2000 and 2001 at K2 are neglected for the power spectral density estimates. To preserve the signal variance, under the spectral curve, the power spectral density versus the frequency gives the true signal variance within the band of each frequency interval. Finally, the power spectral density of the cross-shore and alongshore component are summed. In addition, the 95% significance level is dashed for the single spectra at position K1-K4.

Significant signals at periods between 10-14 and 14-30 days have been detected in the spectral analysis of current meters at surface as well as at deeper measurements, mainly close to the coast. More variance is dominant at high-frequency in mooring K1, not only at the surface, but also at deeper depth, mostly for 10-30 days period. For mooring K2 this high-frequency signal is present at 50 m and 100 m depth, decreasing gradually, with less energy at high-frequencies for deeper depths, where the low-frequency signal is dominant. The high-frequency signal in K2 is about 50% of the variance at lower frequencies. At the mooring K3 these high-frequency signals is present at the surface and gradually decrease with depth. Except for one significant peak of energy, that reaches down to 250 m depth in the high frequencies. The variance in K3, for 14-30 days period is dominant at 100-250 m depth. In the mooring K4 the signal at lower frequencies is dominant but at 300 m depth one peak of energy, with 14-30 days period is also present. The high-frequency signals are evident mostly close to coast, at mooring K1. Further offshore this signal is more apparent at upper depths and these amplitudes

scale down with increasing distance from the NBUC current core.

The spectra at K3 and K4 have smaller energy amplitudes, which decrease with depth. The highest variances are present at periods of 40-60 days.

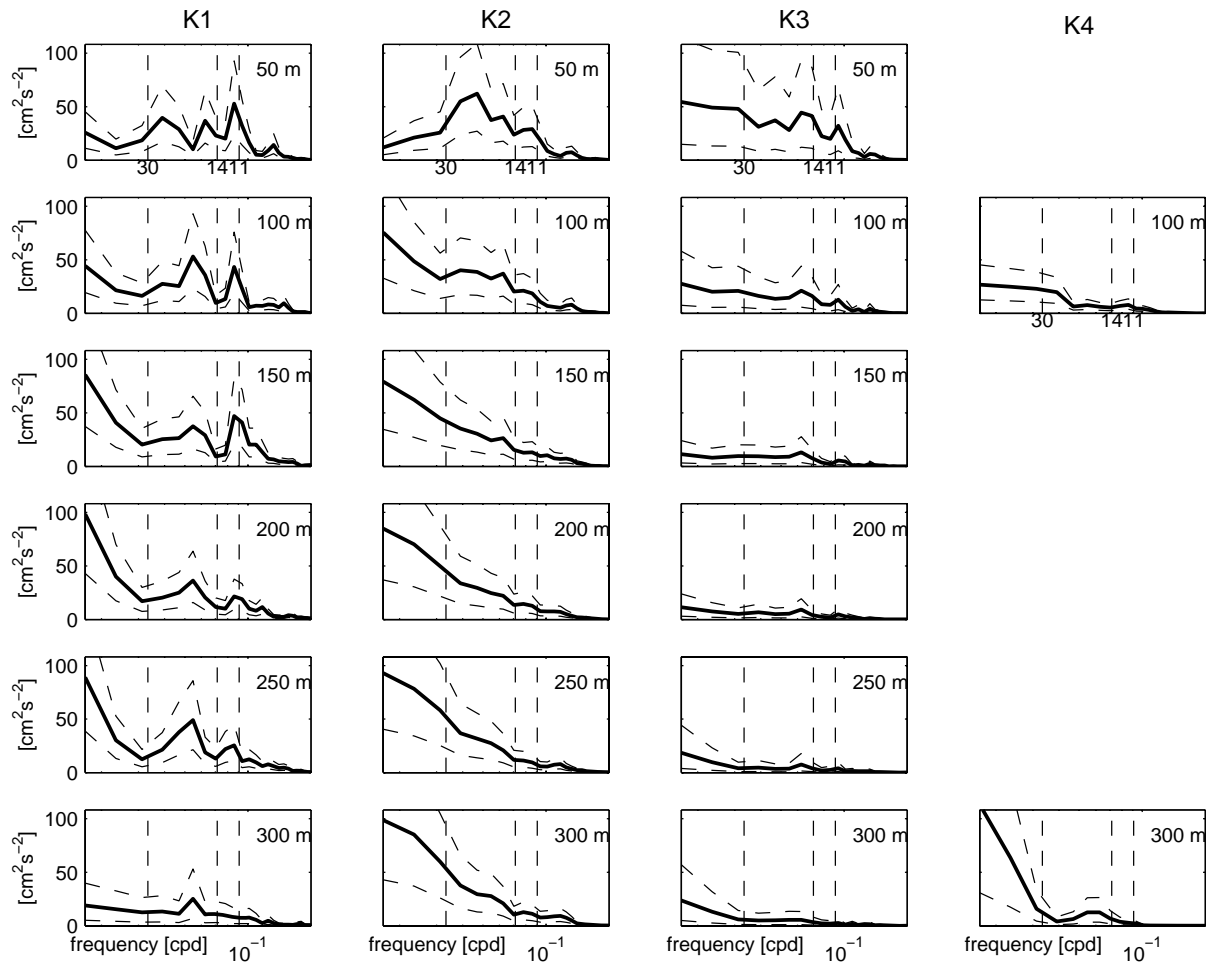


Figure 4.4. Variance preserving spectrum of kinetic energy [$\text{cm}^2 \text{s}^{-2}$] (solid line), for moorings K1-K4, at 50 to 300 m depth, from March 2000 to August 2004, with the respective 95% confidence interval (dashed line).

4.3. Principal Component Analysis – PCA

Principal Components Analysis (PCA) (Preisendorfer, 1988; Jolliffe, 2002) is a method for analysis based in a decomposition of a signal or data set in terms of orthogonal basis components (Proper Orthogonal Decomposition- POD)

which are determined from the data. It is the same as performing an Empirical Orthogonal Functions (EOF) analysis on the data, except that in the EOF the components of the basis are continuous instead of discrete as in POD. The PCA is a way of identifying patterns in data, and to analyze its variability.

Technically speaking, PCA is a linear transformation of the data to a new coordinate system such that the greatest variance by any projection of the data comes to lie on the first coordinate (called the first principal component), the second greatest variance on the second coordinate, and so on.

Principal Components of velocity data along the 11°S transect and velocity and temperature along the same transect were obtained to provide a compact description of the variability. In this work the Principal Component (PC) for the single field of velocity of the currents and also the PC for the coupled fields of velocity current and temperature is computed.

The PCA applied to the velocity field decomposes the data in an orthogonal basis, with the first mode (the greatest variance mode) corresponding to the first eigenvector of such decomposition and the corresponding eigenvalue giving the variance of this mode. In general, each the k -th mode e_k accounts for a variance, $\sigma_k = \frac{\lambda_k}{\sum \lambda_i} \times 100$, where λ_k is the eigenvalue of the k^{th} eigenvector e_k . In this work, the Singular Value Decomposition algorithm was applied to the sample data to obtain eigenvalues, eigenvectors and time varying amplitudes (PC). The projecting coefficients obtained by the expansion of the sample data onto the eigenvectors, that is the time varying amplitudes, are the principal components, also called expansion coefficients (Vautard et al., 1992).

The PCA of the coupled fields of the velocity and the temperature allows the identification of pairs of coupled spatial patterns and their temporal variation, with each pair explaining a fraction of the covariance between the two fields. The methodology is similar to the one described above, the only difference is that, now, the first mode correspond to the greatest variance

mode of both fields. In other words, the first mode of the coupled fields corresponds to the mode of the greatest correlation between the two fields. Each pair of data of the two fields corresponds to the same time interval.

The data of the velocity is projected onto the basis generated from the two fields. The same applies for the temperature field. The projecting coefficients obtained by the expansion of the sample data onto the eigenvectors, the principal components (PC), correspond now, to the temporal evolution of the coupling strength between the two fields. The significance of this coupling is characterized by the squared covariance fraction (SCF) explained by each mode. If $\gamma_k = \Gamma(k, k)$ is the i^{th} singular value, the fraction of squared covariance (SCF) is given by $SCF_k = \gamma_k^2 / \sum \gamma_k^2$. The coefficient of correlation (CC) of the PC is also calculated to quantify the degree of correlation of the compound of the two fields.

The empirical Orthogonal Functions analysis of the meridional component of current fields were computed in K1, K2, K3 and K4 moorings to provide a simpler description of their variability. Usually, most of the variance of the spatially distributed time series is retained in the first few EOFs functions. In this study, a singular value decomposition of the data matrix was used to obtain eigenvalues, eigenvectors and time varying amplitudes, or principal components, of the sample covariance matrix. Table 4.1 summarizes the results of EOF analysis for the meridional component of current fields from the moorings. A single field analysis was done for those stations.

The K1 mooring is located approximately 10 km from the coast, which goes northward in the western boundary regime. The first EOF mode is located at approximately 300 m depth and account for 90% of the total variance. The spectrum clearly shows dominant mode of variability at 14-30 days. The second mode for K1, with only 10% of the total variance, shows also a peak at nearly 60 days. The first mode of variability for K2 corresponds to 99% of total variance. The dominant mode of variability for K2, located in the NBUC core, approximately 50 km from the coast, has the most variance at 14 days and also between 30 and 60 days.

Table 4.1. EOF analysis applied to the alongshore component of the current at 11°S. The SFC is Squared Fraction Covariance for each mode in alongshore velocity of current from mooring data. The column “Period (days)” shows the periodicity of the maximum variance for each mode in single field analysis.

<i>Mooring</i>	<i>EOF Mode</i>	<i>SCF (%)</i>	<i>Period (days)</i>	<i>Depth (m)</i>
<i>K1</i>	<i>1°</i>	<i>90</i>	<i>14-25-60</i>	<i>300</i>
	<i>2°</i>	<i>10</i>	<i>60</i>	<i>100</i>
<i>K2</i>	<i>1°</i>	<i>99</i>	<i>14-25-60</i>	<i>50-200</i>
<i>K3</i>	<i>1°</i>	<i>63</i>	<i>14-25</i>	<i>100</i>
	<i>2°</i>	<i>34</i>	<i>14</i>	<i>300-500</i>
<i>K4</i>	<i>1°</i>	<i>81</i>	<i>14-30-60</i>	<i>1900</i>
	<i>2°</i>	<i>15</i>	<i>60</i>	<i>500</i>
<i>K5</i>	<i>1°</i>	<i>97</i>	<i>25-60</i>	<i>2400</i>

Despite of the large variability observed in the NBUC at 5°S (Schott et al., 1998) be related to equatorial processes, and not to the sSEC (Stramma et al., 2003), the large variability computed at 11°S is mostly influenced by the migration of the sSEC (Schott et al., 2005).

According to Schott et al. (2005) the NBUC and DWBC transports are not correlated. These authors claim that a possible reason for intraseasonal variance in the NADW domain has been identified as upstream instability from eddies passing into the DWBC.

The variance preserving spectrum of the PCAs for the moorings K1 to K5 show the main period band of most variance. K3 and K4 are located in the NADW. The first EOF mode in the K3 mooring is responsible for 63% of the variability and it is located at 100 m depth. A second mode corresponds to 34% of the total variability and it is centered between 300 and 500 m depth.

The variance for K4 has a pronounced maximum located at 1900 m depth, approximately at the NADW core. The amplitude of this mode has a periodicity of 14-30 and 30-60 days (Figure 4.5d). The first maximum is about 30 days and the second maximum peak is 60 days, in agreement with Schott et al. (2005).

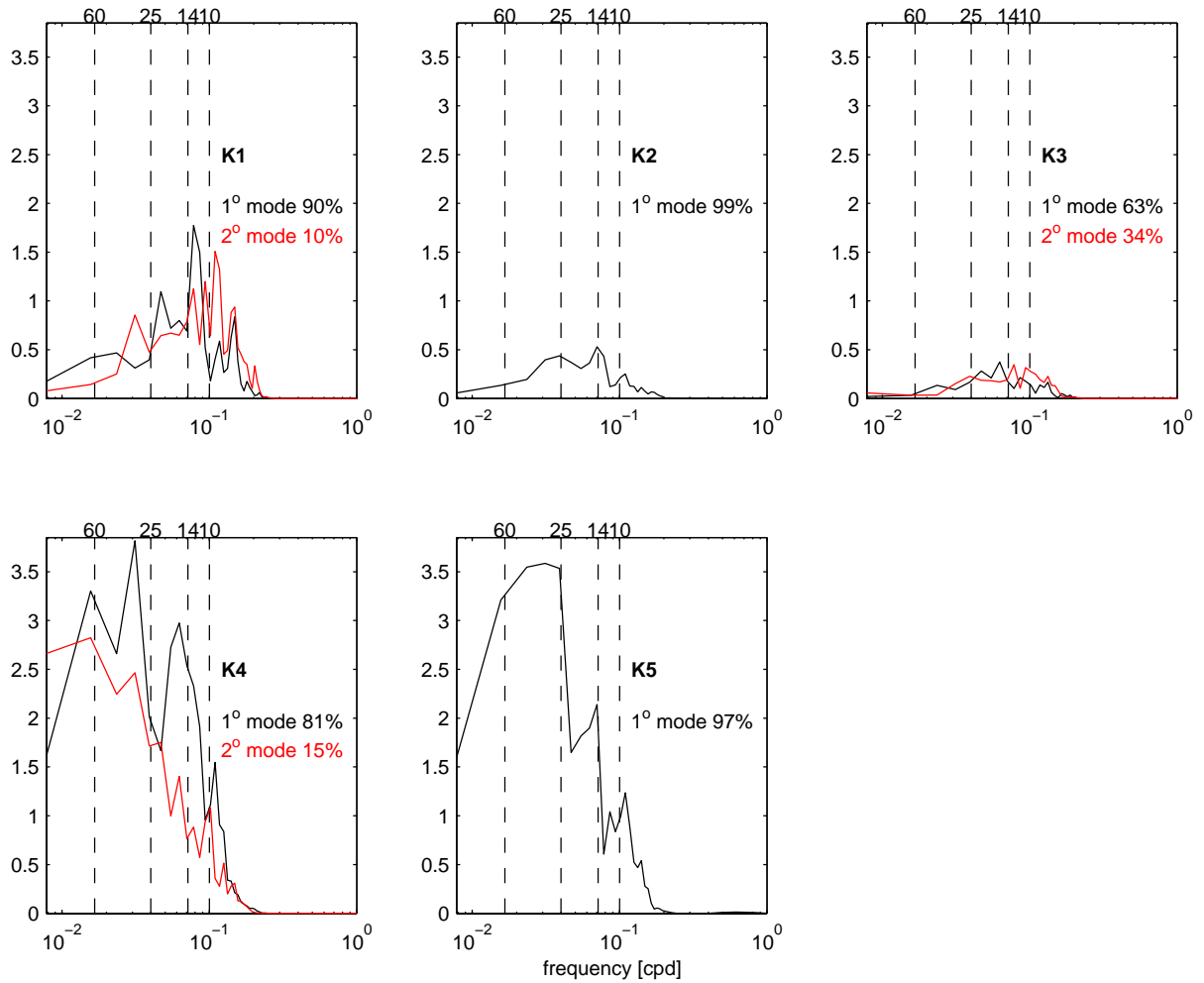


Figure 4.5. Variance preserving spectrum of the first Principal Component for current in the: a) K1, b) K2, c) K3, d) K4 and e) K5 stations.

On the other hand, the second EOF mode, in K4 station, is responsible for 15% of the variance (Table 4.1) at 500 m depth. The first maximum of this EOF corresponds to a periodicity of 30 and 60 days. In this position, below the STC level, Schott et al. (2005) found a substantial and persistent recirculation offshore from the NBUC along 5°-11°S. Particularly at 500 m depth, at 11°S, they found a statistically significantly southward current with approximately 6.8 cm.s^{-1} . This counterflow suggests an offshore band of intermediate water recirculation in this latitude range, up to 5 Sv and reaching down to NADW densities.

There are several possible explanations for the origin of this flow. One

would be the deflection of zonal currents. Northwest of the 5°S section, there is a westward flow across the 35°W section (Schott et al., 2005). In the opposite direction there is an eastward flow by the South Equatorial Undercurrent (SEUC) at 150-400 m depth, between 2.5°–4°S, and the Southern Intermediate Countercurrent (SICC) at 1.5°–3.5°S, reaching 500-1200 m depth. However, no evidence of a southward deflection has been reported for these currents, because the SICC and SEUC transport stays nearly constant until 28°W section. The other possible explanation would be an inflow from the east as part of the deep SEC, which gets deflected southward before reaching the Brazil coast and thus, forms an offshore counterflow to the deep NBUC. It could be also explained by a retroflexion of the deep NBUC just a little bit north of the northeastern tip of Brazil, to supply the southward offshore flow across 5°S.

However, we found two options in the analysis of numerical results obtained from SODA reanalysis and the numerical results from ROMS model (1/12°). Those results and discussion are planed in the section 6, where the ROMS and SODA results are explained.

In the calculation of the EOF analysis for two coupled fields, temperature and current measurements for the same time interval were used for each K3 and K4 stations and the results are summarized in the Table 4.2.

Table 4.2. EOF analyses applied to the (coupled field) alongshore current-temperature along transect 11°S. CC is the correlation coefficient, which quantifies the strength of the coupling.

<i>Mooring</i>	<i>EOF Mode</i>	<i>SCF (%)</i>	<i>Period (days)</i>		<i>Depth (m)</i>
			<i>Velocity</i>	<i>Temperature</i>	
<i>K3</i>	<i>1°</i>	<i>99</i>	<i>61</i>	<i>61</i>	<i>1885</i>
<i>K4</i>	<i>1°</i>	<i>98</i>	<i>67</i>	<i>67</i>	<i>1906</i>

The Correlation Coefficient (CC), the strength of the coupling, was computed giving a value of 0.60 (CC varies from 0 to 1). The coupled fields' analysis shows, through Principal Component Analysis, a stronger coupling for the temperature and the velocity of K3 at about 2000 m depth. The temperature is strongly coupled to the current of the mass of water at this depth. On the other hand, in K4, the coupling between the temperature and the current fields is not as strong as in K3, with a CC value of 0.34. The periodicity of the projection of the coupled fields onto the current and the temperature values agree with the single field analysis.

In the Principal Component Analysis of the EOF1 for the temperature and current for K3, from March 2000 to September 2001, there is a distinctive trend for a stronger coupling, mainly in the first 12 months of data, from March 2000 to February 2001. The PCA for temperature and current are synchronized each quasi-two month, where there is a trend for more variance at the same time for the two fields. This EOF1, which represents the core of the NADW as part of the MOC of the Atlantic, is an area of quasi-permanent coupling of temperature and current. This knowledge allows estimations of how much the current field contributes for the interhemispheric heat transport along this level. This depth is at the axis of the DWBC, which carry the NADW southward accomplished by migrating anticyclonic eddies.

The results found here show eddies of 60-70 days variability in agreement with predictions of Dengler et al. (2004). The DWBC break up into

a series of anticyclonic eddies, denoted by their positive bowl-shaped temperature anomaly. This bowl-shaped temperature shows that more high temperatures are concentrated into eddies at the DWBC level. It shows a strong coupling between high velocities from eddies and temperature anomalies inside them. In this thesis the first EOF in K3 responds for 60% of the variability at 2000 m depth. Consequently, eddies transporting positive temperature anomalies in DWBC are responsible for 60% of the heat transport at this depth.

Chapter 5

5. Wind stress variability in the South Atlantic

The horizontal force of the wind on the sea surface can be understood as the vertical transfer of horizontal momentum. Thus, momentum is transferred from the atmosphere to the ocean by wind stress. It is also the most important forcing for upper ocean circulation; all large scale basin ocean circulation theories and models begin with at least a specification of the surface stress or curl of the stress (Harrison, 1989; Trenberth et al., 1990; Münchow, 2000; Meacham, 2000; Fennel and Lass, 2007). Besides, the ocean dynamics, poleward of about 5° latitude, is largely governed by the wind stress curl through the Sverdrup relation. The aim of this chapter is to describe the variability of 3 years of wind stress which will be proved to be the main ingredient in the explanation of the seasonal variability of the sSEC bifurcation as well as correlation with sub-seasonal scale phenomena, studied in Chapters 6 and 7, respectively.

5.1. Wind-forced motions

Before turning to the results I will describe here the spatial and temporal characteristics of the wind stress datasets. It is important to establish the winds as being representative of the atmospheric seasonal oscillation, prior to demonstrating its connection to the current signals. The wind stress curl was estimated using the wind stress (τ) components from the following equation:

$$\nabla \times \tau = \frac{\partial \tau^y}{\partial x} - \frac{\partial \tau^x}{\partial y} \quad (5.1)$$

where:

$$\partial \tau^y \cong \Delta \tau^{[40^\circ \text{S} \rightarrow 10^\circ \text{N}]}$$

$$\partial \tau^x \cong \Delta \tau^{[60^\circ \text{W} \rightarrow 20^\circ \text{E}]}$$

$\hat{c}x$ = west-east (longitudinal) distance between each τ^y

$\hat{c}y$ = south-north (latitudinal) distance between each τ^x

For this work, the zonal and meridional mean wind stress, between December 2001 and February 2005, are compatible with literature (Trenberth et al., 1990; Harrison, 1989; Castelão and Barth, 2006). A negative field for zonal wind stress exists approximately for the entire domain (Figure 5.1a). A positive field of meridional wind stress is restricting to equatorial latitudes in the western part of the South Atlantic Ocean and cover entire eastern South Atlantic. (Figure 5.1c). Higher variability is found at South (Figures 5b,c), which is mostly under the influence of synoptic and mesoscale meteorological systems, inducing significant disturbances in the ocean. The next Figures show that the high variability of the wind stress components is most concentrated south 20°S. The curl presents a negative

field approximately between 10°S and 10°N (Chelton et al., 1990) with more variability southward. A negative stress curl exists close to Brazilian shore at 22°-26°S (Castelão and Barth, 2006), where an abrupt change of direction of the coast line exists. Rodrigues and Lorenzetti (2001) showed that coastline irregularities and bottom topography effects affect the spatial pattern of upwelling in this region.

The equatorward boundary of the subtropical gyre is associated to the zero wind curl line. At this line, the meridional Sverdrup transport is zero by definition. In the northern limit of the subtropical gyre the sSEC flows westward, and the zero curl line can be associated to the seasonal migration of the sSEC. According with the Sverdrup theory the latitude of the bifurcation of the sSEC can be obtained from the position of the zero line of zonally integrated wind stress curl. The following analysis contributes to the understanding of the seasonal migration of the sSEC discussed in the next chapter.

Figures 5.2 to 5.5 show the seasonal variability for zonal and meridional wind stress and curl. The wind stress components and curl are presented with their respective standard deviation.

The negative component of zonal wind stress covers most of the South Atlantic. While the meridional component is positive for the entire eastern part of South Atlantic and it is bounded to the north of 5°S and equator in the east part, for December, January and February (Figure 5.2). To the south of 5°S, at the western part, the meridional component of wind stress is negative, which combined with negative zonal component forms a predominantly wind from the northeast in the austral summer. Cyclonic meanders are strongly generated mainly by wind from northeast in Austral Summer in the region at 22°-26°S close to Brazilian coast (Castelão et al., 2004; Campos et al., 2000; Castro and Miranda, 1998).

The zero line of wind stress curl in Austral Summer is about 10°S close to Brazilian coast and at higher latitudes at east part of the South Atlantic basin. Smaller variability for zonal and meridional wind stress and curl is found for this period.

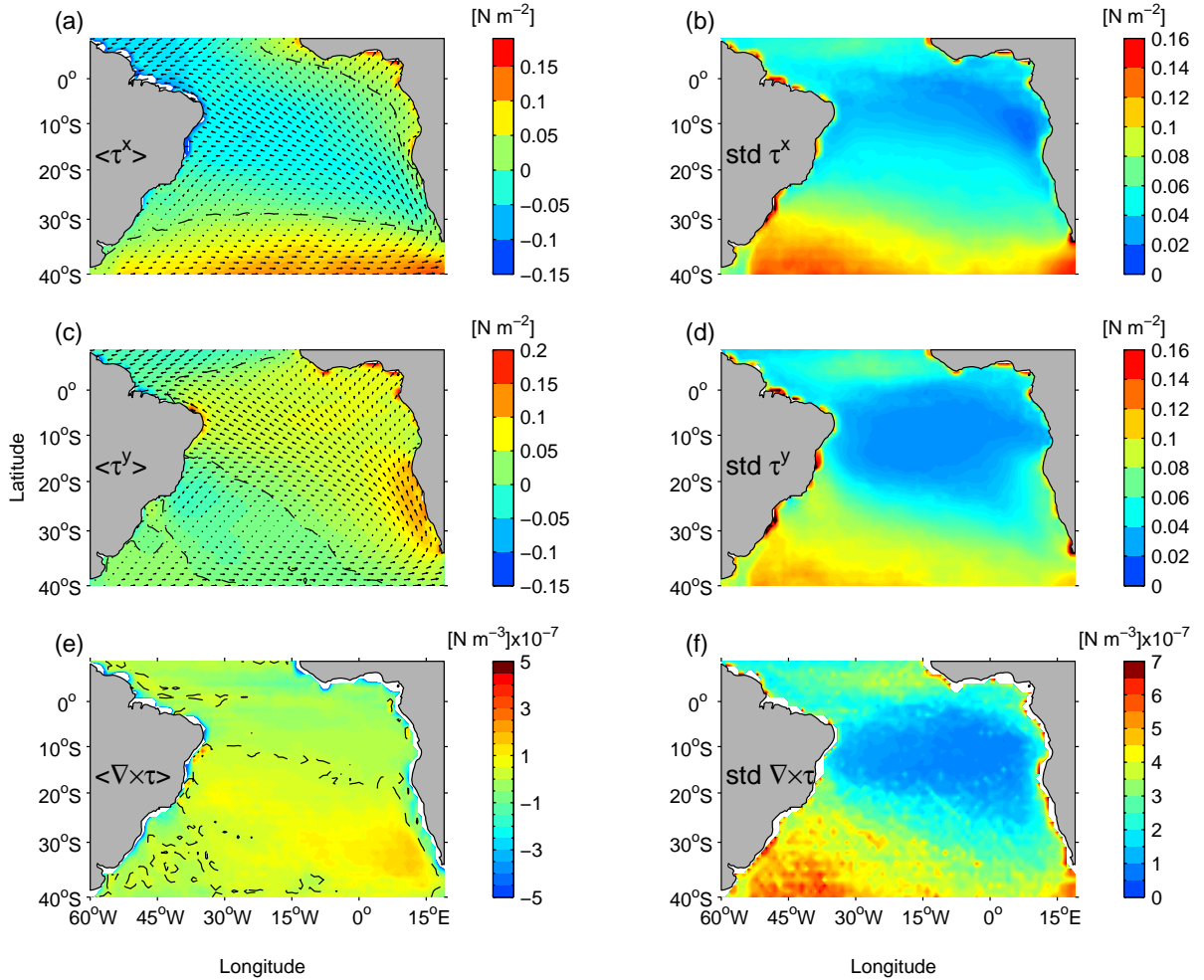


Figure 5.1. Mean (Dec/2001-Feb/2005): (a) zonal component, (c) meridional component and (e) curl of wind stress; (b), (d) and (f) respective standard deviations.

In March, April and May (Figure 5.3) the meridional component is stronger than December, January and February (Figure 5.2) and its zero stress curl line is about 18°S. A center of negative stress curl is found close to the American continent, between 22° and 26°S, this centre is already found in literature (Castelão and Barth, 2006). A second less significant center of negative stress curl is identified attached to the coast, between 11°S and 14°S at 38°W. The zero line of wind stress curl remains about 10°S. There is more variability in wind stress curl in this period than in December, January and February, mainly in the equatorial band.

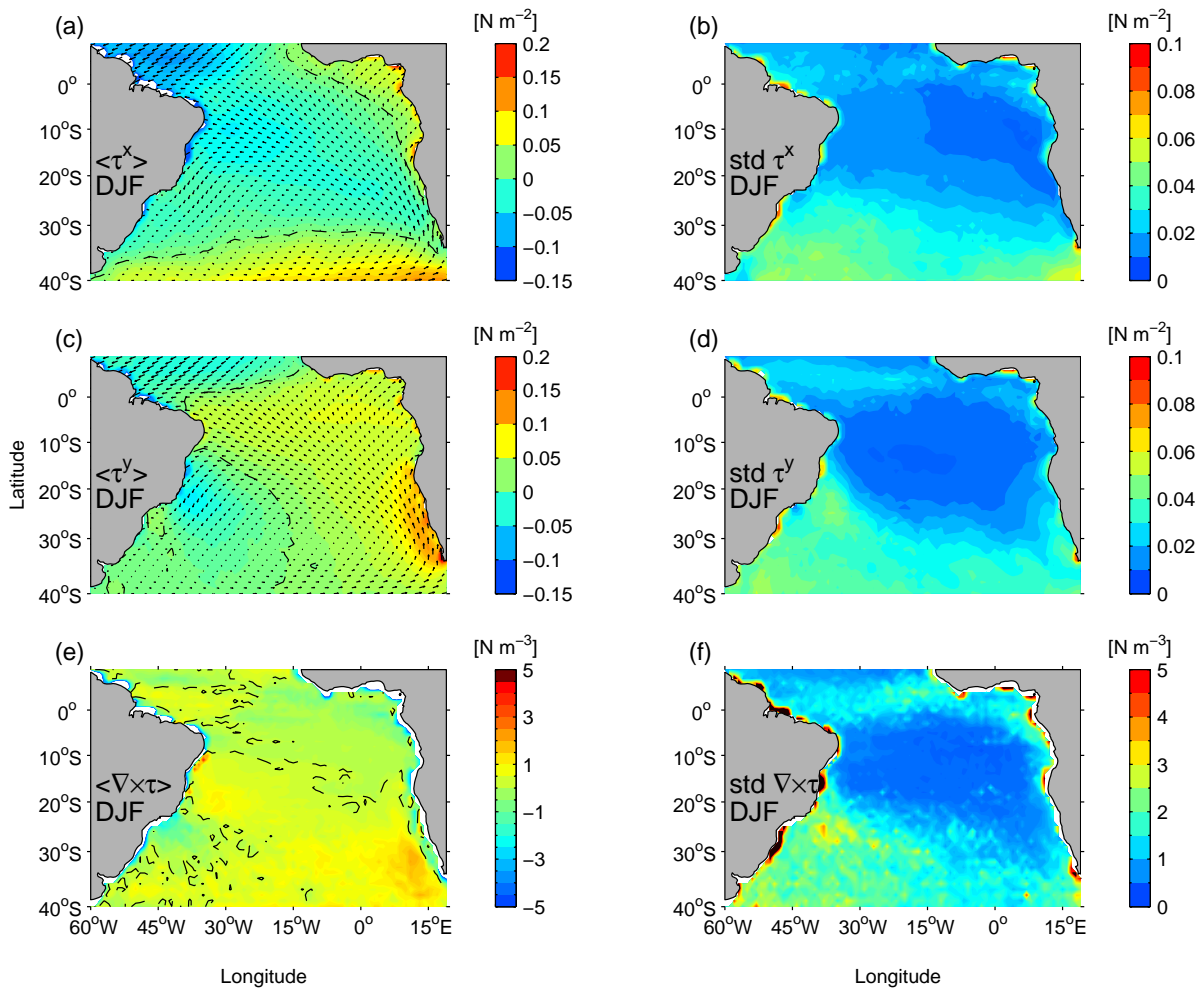


Figure 5.2. Seasonal mean for December, January and February: (a) zonal component, (c) meridional component and (e) curl of wind stress. (b), (d) and (f) respective standard deviation.

In June, July and August the strongest values are found in the meridional component of wind stress (Figure 5.4). For this period there are extreme alongshore currents in the NBUC, which coincides with the maximum northward transport of the NBUC in July (Schott et al., 2005).

The predominantly wind is from Southwest at south of 25°S. The wind stress curl is negative mainly between 10°S and 10°N. The negative centers of wind stress curl at 11°-14°S and 22°-26°S remain. This period presents the strongest variability in the wind stress curl field, south of 20°S and in the equatorial band, concentrated at about 5°N. The zero line of wind stress curl shifts southward about 15°S.

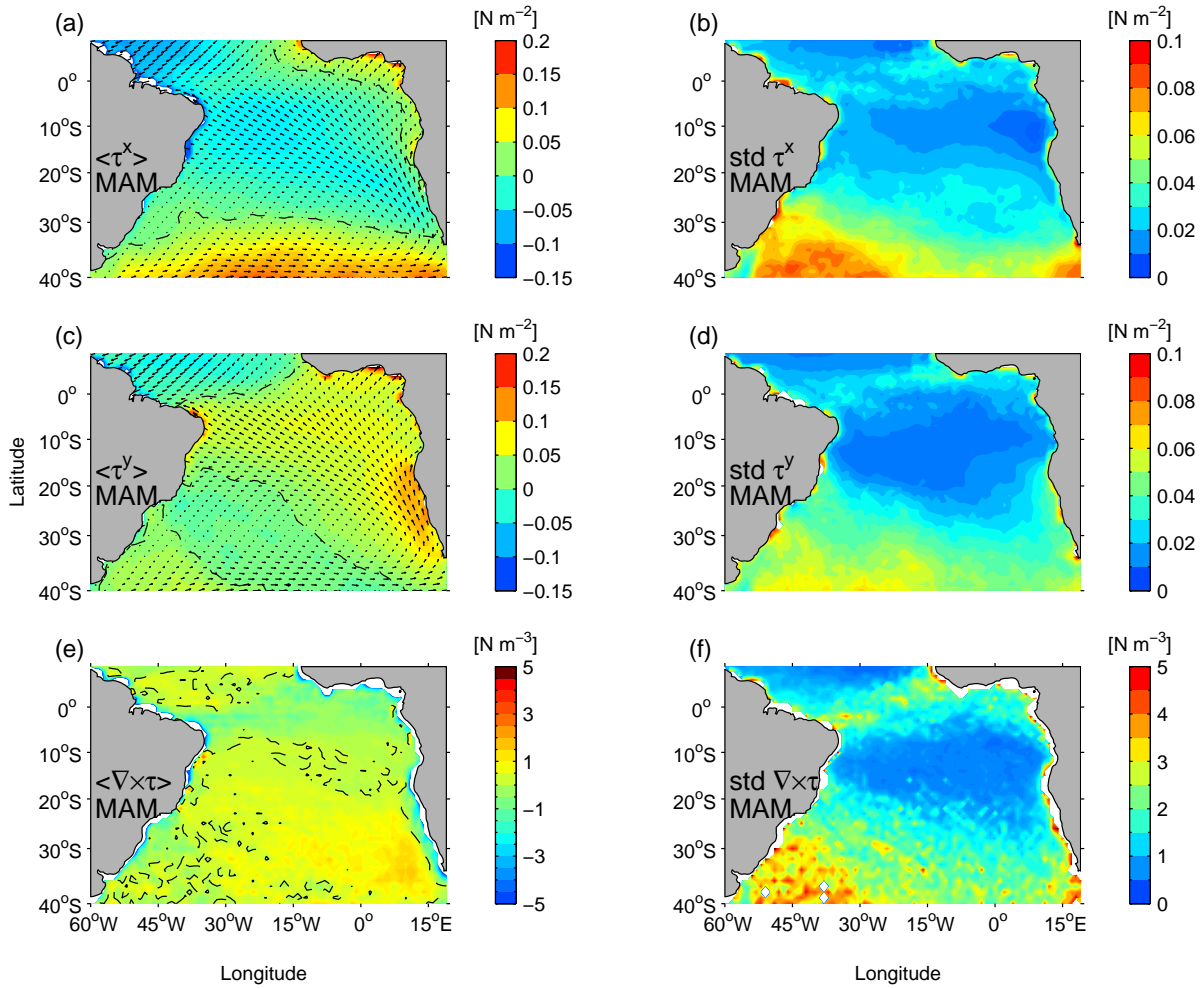


Figure 5.3. Seasonal mean for March, April and May: (a) zonal component, (c) meridional component and (e) curl of wind stress. (b), (d) and (f) respective standard deviation.

For September, October and November, the zero line of meridional wind stress moves more north, about 12°S and the second center of negative stress curl at 11°-14°S disappears but the center at 22°-26°S remains (Figure 5.5).

The zonal component of wind stress is approximately constant for all periods, with strongest negative values in June, July and August but stronger variability is found for March, April and May. The zero line of wind stress curl shifts again northward about 10°S.

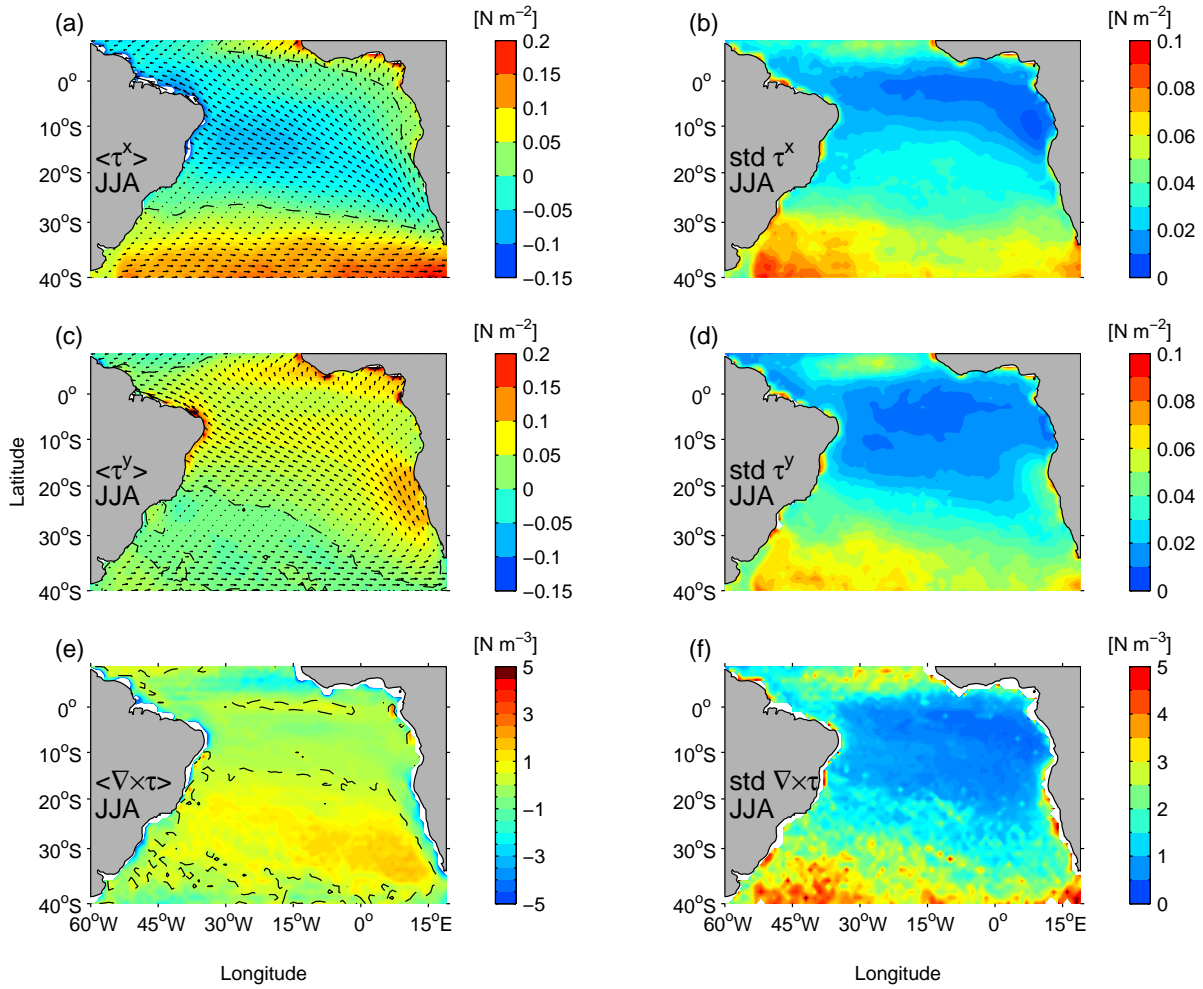


Figure 5.4. Seasonal mean for June, July and August: (a) zonal component, (c) meridional component and (e) curl of wind stress. (b), (d) and (f) respective standard deviation.

The seasonal means of wind stress curl shows a southernmost zero line for the months of June, July and August, which means that the northern limit of the subtropical gyre at these months has its southernmost position. Furthermore, as the sSEC is a north limb of the subtropical gyre, it is expected that southernmost bifurcation of the sSEC to be at these months.

The meridional excursion of the zero line of wind stress curl (shown in Figures 5.2 to 5.5) indicates a northernmost position about 10°S and the southernmost position is about 15°S; which is consistent with COADS monthly mean climatology (Rodrigues et al., 2007). According with the Sverdrup theory of the oceanic circulation, the northward mass transport of wind driven currents is equal to the curl of the wind stress. Thus, the line of

zero curl gives an estimative of the bifurcation latitude for a steady-state barotropic ocean, based on Sverdrup model.

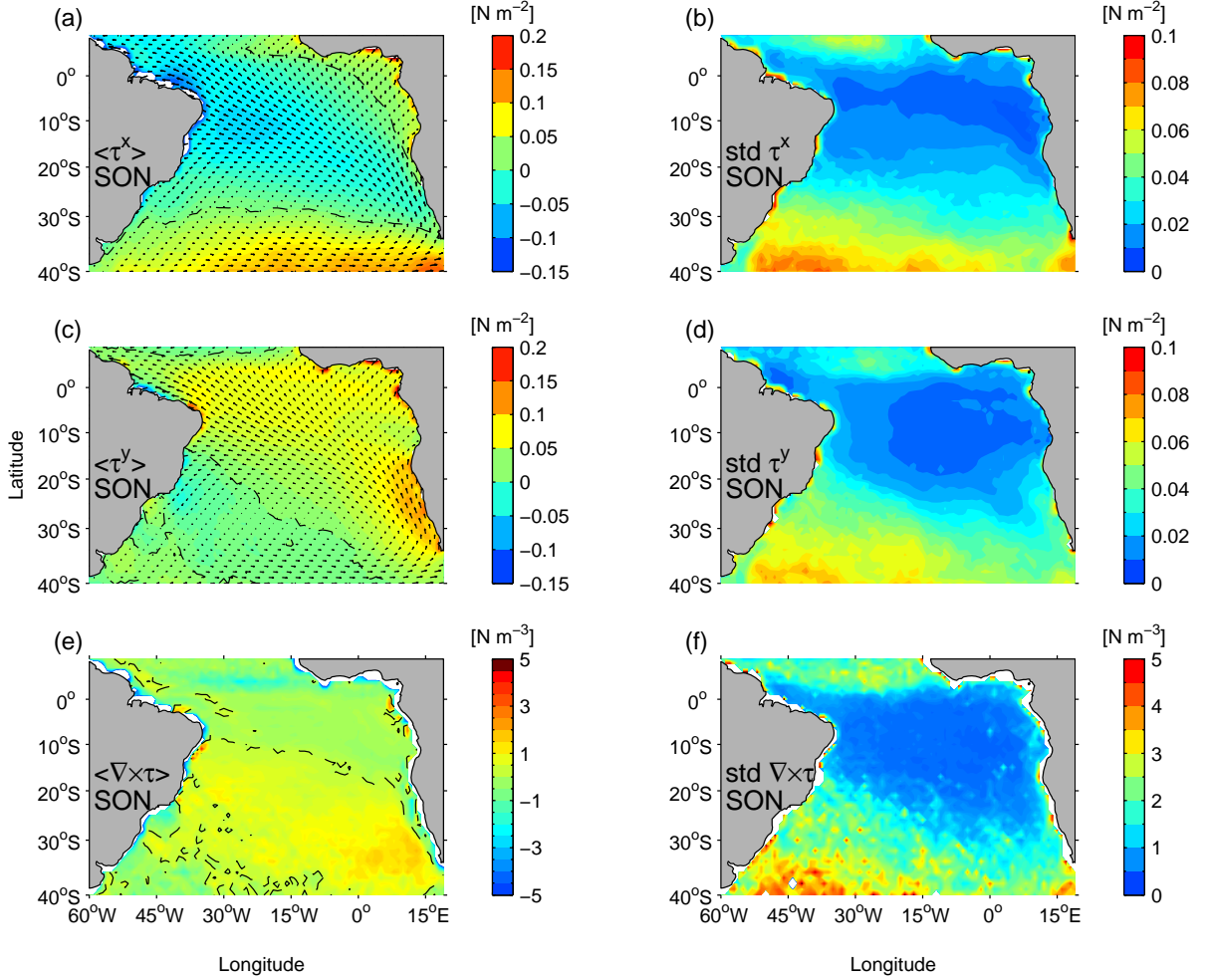


Figure 5.5. Seasonal mean for September, October and November: (a) zonal component, (c) meridional component and (e) curl of wind stress; (b), (d) and (f) respective standard deviation.

A map of the average variance preserving spectrum of kinetic energy of wind stress for the band of frequency corresponding to 10-30 days period is shown in Figure 5.6.

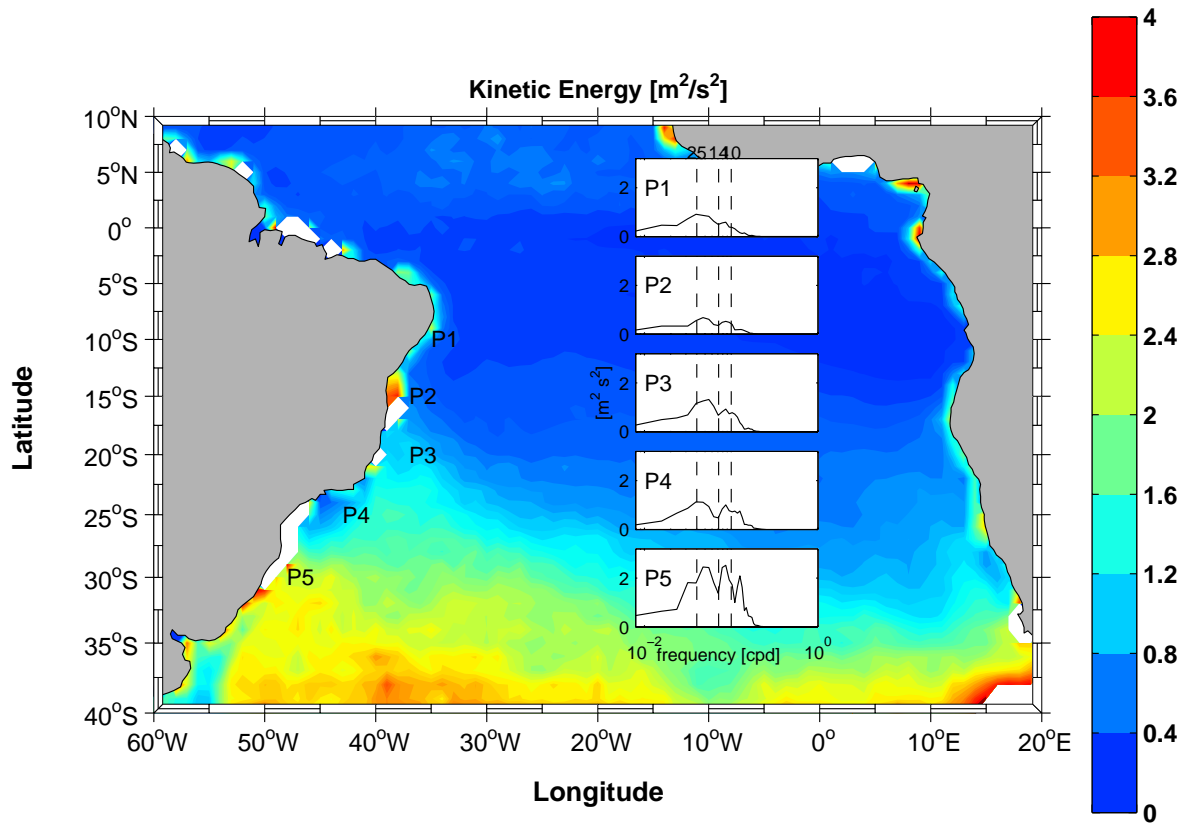


Figure 5.6. Variance preserving spectrum of kinetic energy on 10-30 days band, calculated using 3 year records of wind stress [$\text{m}^2.\text{s}^{-2}$] along the western boundary of the South Atlantic.

Close to Brazilian coast the variability increase southward. The map of averaged variance shows strong variability located close to coast at about 30°S . Additionally, the local variance preserving spectrum of kinetic energy of wind stress for some local points close to the coast are over plotted showing stronger signals mainly at periods between 10 and 30 days. In the south this signal is more evident and more energetic. The spectral signals are similar to the signals found in the current measurements at 11°S (Figure 4.4), confirming so, a connection between the currents measurements and the wind stress variability along the Brazilian coast.

The seasonal variability of 3 years of wind stress was described here. The data were used to estimate the curl of wind stress. The field data of the components of wind stress such as the curl of wind stress were consistent

with previous works and proved to be an important tool in the explanation of the seasonal variability of the sSEC bifurcation. The analysis here showed will help to confirm the seasonal variability of the sSEC in the next chapter. This is important because the wind stress curl is the main component to analyze the meridional transport along the northern limb of the subtropical gyre. This premise is based on Sverdrup theory of oceanic circulation.

The variance preserving spectrum of kinetic energy on 10-30 days band identified the main region of higher variability of winds. This region corresponds with variability at higher frequencies of the current measurements, which will be studied in the Chapter 7.

Chapter 6

6. ROMS results and SODA reanalysis

In this chapter the simulation of the ROMS and SODA reanalysis dataset are used to analyze the seasonal variability of the sSEC. The model results help us to analyze the oceanic mechanisms on different space and time scales, whereas observations are often limited. In the first instance it is important to see whether the numerical and reanalysis results yield seasonal variability similar to that observed in the southern tropical Atlantic.

6.1. Meridional variability and depth dependence

As already pointed out, the seasonal variations of the winds are associated with the north-south excursion of the atmospheric Intertropical Convergence Zone (ITCZ). The southeast trade winds are most intense and penetrate into the north hemisphere during the northern summer when the ITCZ is between 10° and 15°N. During those months the surface currents are particularly strong.

The ITCZ reaches its southernmost latitude in March and April,

bringing a rainy season to northeastern Brazil. In some years the rains fail, corresponding to years of drought. The droughts characteristically occur when the South Atlantic Subtropical High (SASH) expands equatorward and the ITCZ moves farther north. During those periods, the South Atlantic trade winds become stronger than normal and anomalously cold surface water appears in much of the equatorial Atlantic.

Annual changes in SST of the tropical Atlantic are of 6° - 8°C , substantially greater than the interannual (Peterson and Stramma, 1991). The SST variations in the tropical Atlantic play an important role modulating the climate variability, in particular over the adjacent continental regions (Kayano et al., 2005). This thermal gradient also acts through the buoyancy forcing over the space-time variability of the high to low pressure areas in the atmosphere.

The dynamics that controls the migration of the sSEC bifurcation in the western boundary South Atlantic can be a result of the seasonal changes of the surface winds speed, which is in great part driven by SST seasonality. A seasonal meridional change in the SST along the South Atlantic western boundary can be observed (Figure 6.1).

The western hemisphere warm pool alternates with the northern South America as the seasonal heating source for the Walker and Hadley circulations (Wang and Enfield, 2003). The monthly averaged fields of temperature of the ROMS confirm the existence of a South Atlantic warm pool, marked by high values of SST ($\sim 28^{\circ}\text{C}$), that occurs during November from the equator to about 14°S . These high temperatures remain until April, when these high SST values shifted northward, and warmer waters are only observed at the ocean area closer to the equator and limited to 8°S . This seasonal difference in SST fields creates a seasonal meridional temperature gradient along the South Atlantic, which drives the atmospheric general circulation that, in turn, feedbacks the upper ocean layer circulation through wind stress.

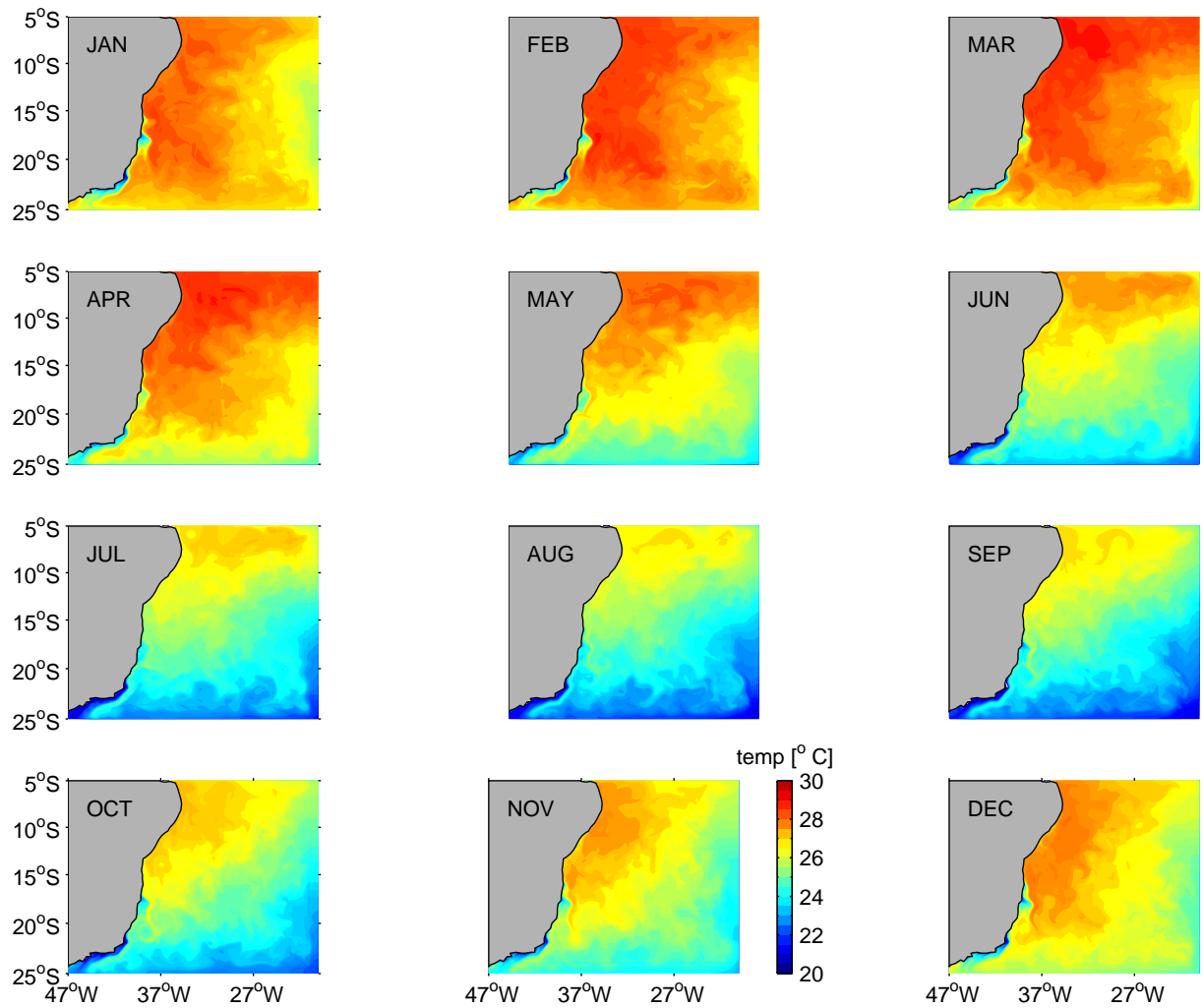


Figure 6.1. Monthly mean distribution of SST obtained from the last year of the climatological ROMS simulation.

Based on previous results cited in the literature, it is known that the sSEC at 10°–20°S feeds the NBUC, mainly in the SACW layer at 100–500 m depth (Stramma and England, 1999; Schott et al., 2005). The northward extension of the subtropical gyre reduces with increasing depth and reflects a poleward shift with depth. As we will see, the present chapter does not only support a seasonal variability on the position of the sSEC divergence, but also indicates its depth dependence. According to the model results, the sSEC bifurcation shifts southward as ocean depth increases.

The mean monthly horizontal velocity fields during the last year of a climatic run of the ROMS model are shown in Figure 6.2 at 200 m depth.

The red points in Figure 6.2 indicate the position of the sSEC bifurcation. The 200 m depth is approximately the level of the NBUC core (Schott et al., 2005). In January the sSEC bifurcates about 10°S at 200 m depth, but a great part of its southward left branch retroflects into NBUC at 12°S (Figure 6.2). At this latitude the meridional velocity component is reversed. The sSEC is stronger in the austral summer (DJF). An anticyclonic eddy exists in those months close to Brazilian coast between 12°-15°S. This mesoscale structure represents the Ilhéus Eddy, which has been already identified from sea measurements during austral summer (Silveira et al., 2006; Soutelino, 2008). It is suggested here that this eddy contributes to reduce the northward transport of the NBUC in austral summer. In austral winter the sSEC is weaker and the anticyclonic eddy is not present between 12°-15°S.

Toward to the south, the BC flow also presents eddy structures at about 15°-20°S, caused by the interaction between alongshore currents and complex topography of the Brazilian coast. The position of the BC changes considerably with time. Sometimes the greater part of the BC turns eastward, north of this complex bathymetry and then turns back to the west close to coast (Campos et al., 1995). It is important remember that at this latitude exists the Vitoria-Trindade Ridge and Abrolhos Bank. The eddy characteristic is typical of this area. More to the south, between 20°S and 31°S, the continuous Brazil Current is still associated with eddies and meanders (Schmid et al., 1995).

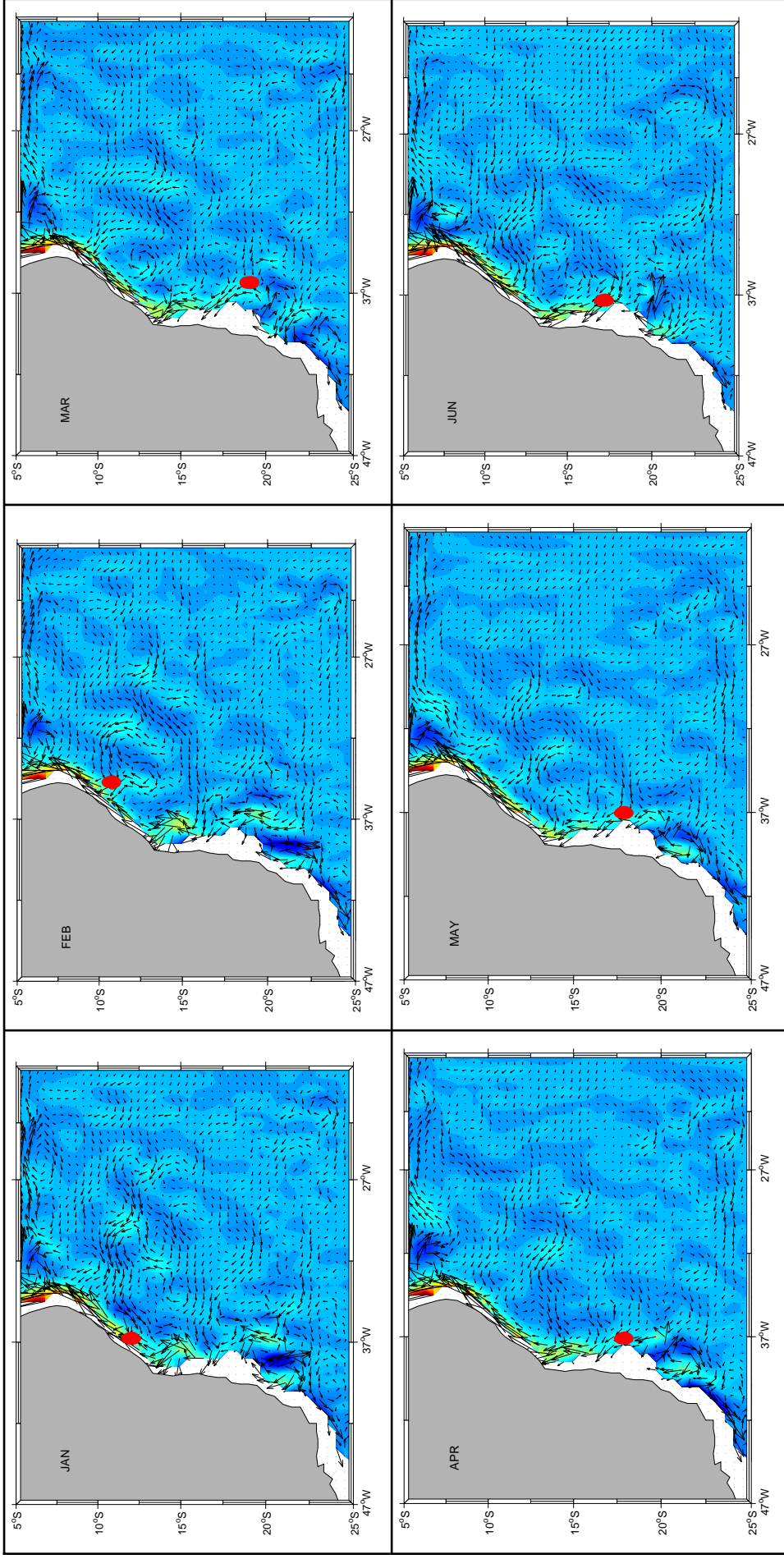


Figure 6.2. Monthly mean horizontal current (m.s^{-1}) fields at 200 m depth obtained from last year of the climatological ROMS simulation. Red points represent the location of the sSEC bifurcation.

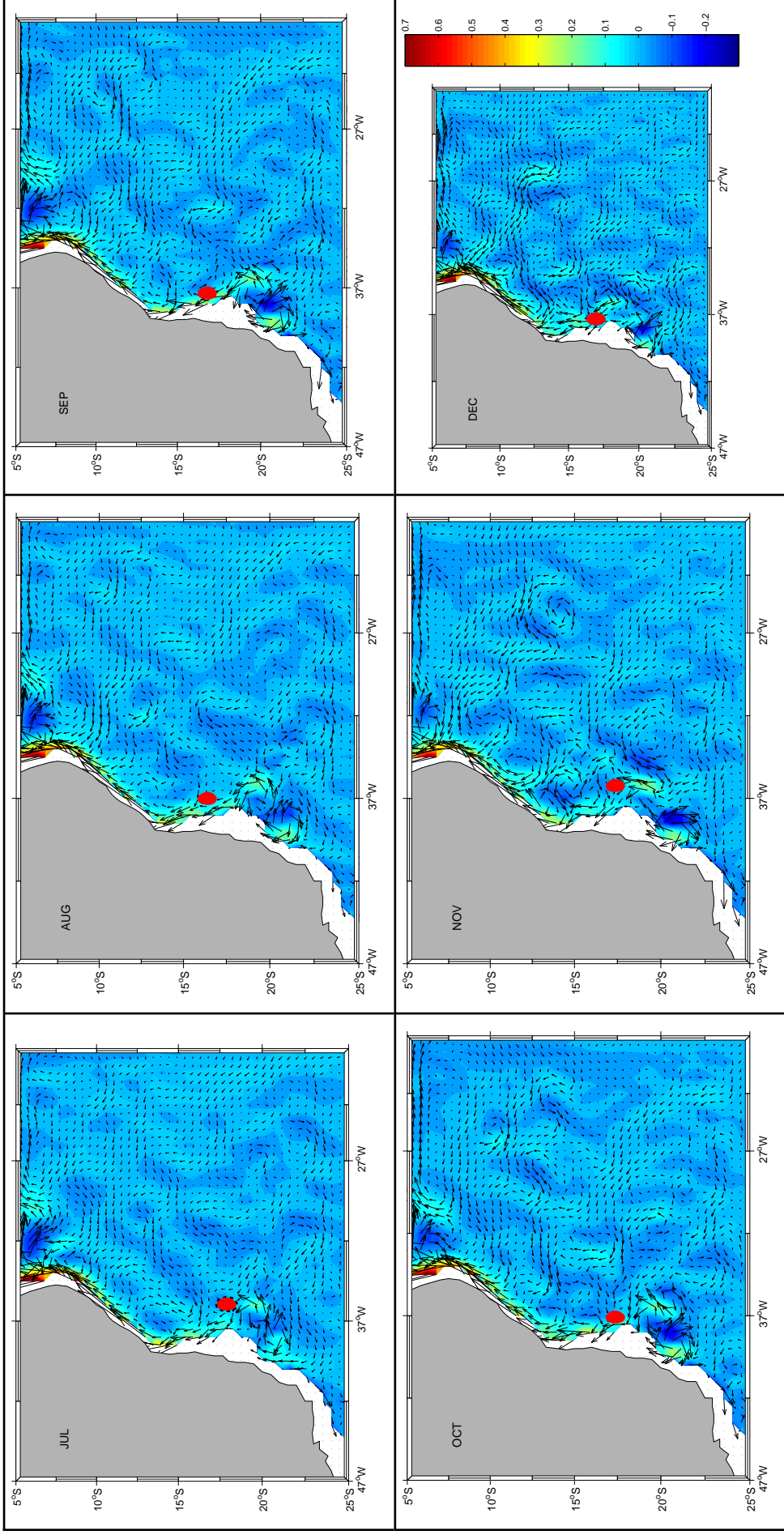


Figure 6.2. (Continuation) Monthly mean horizontal current ($m.s^{-1}$) fields at 200 m depth obtained from last year of the climatological ROMS simulation. Red points represent the location of the sSEC bifurcation.

Figures 6.3 and 6.4 abridge the depth dependence of the sSEC bifurcation latitude. In these figures the sSEC bifurcation is represented by black line, where the modeled meridional velocity (averaged within a 1° longitude band off the Brazilian coast) is zero. The white areas in Figures 6.3 and 6.4 represent Vitoria-Trindade Ridge and Abrolhos Bank.

At 200 m depth, the southernmost position of the sSEC bifurcation is in the March, April, May mean and the northernmost position is at September, October and November. The seasonal profiles confirm that the sSEC bifurcation shifts southward at lower depths.

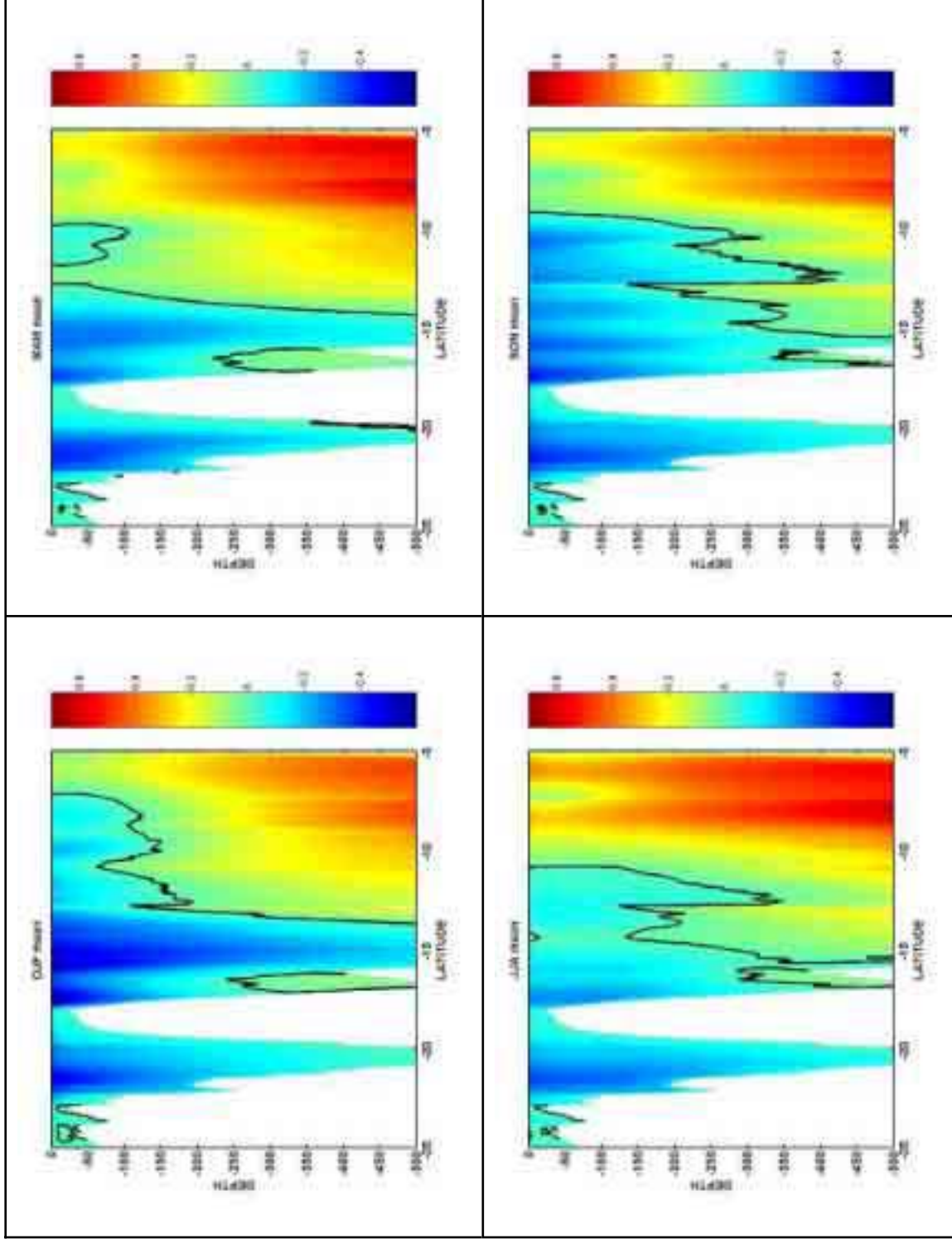


Figure 6.3. Seasonal averaged (three months) meridional velocity ($m.s^{-1}$) obtained from last year of the climatological ROMS simulation. The velocities are averaged within a 1° longitude band off the Brazilian coast. The dark line is the contour of zero velocity that represents the bifurcation of the SSEC. The white areas represent Vitoria-Trindade Ridge and Abrolhos Bank.

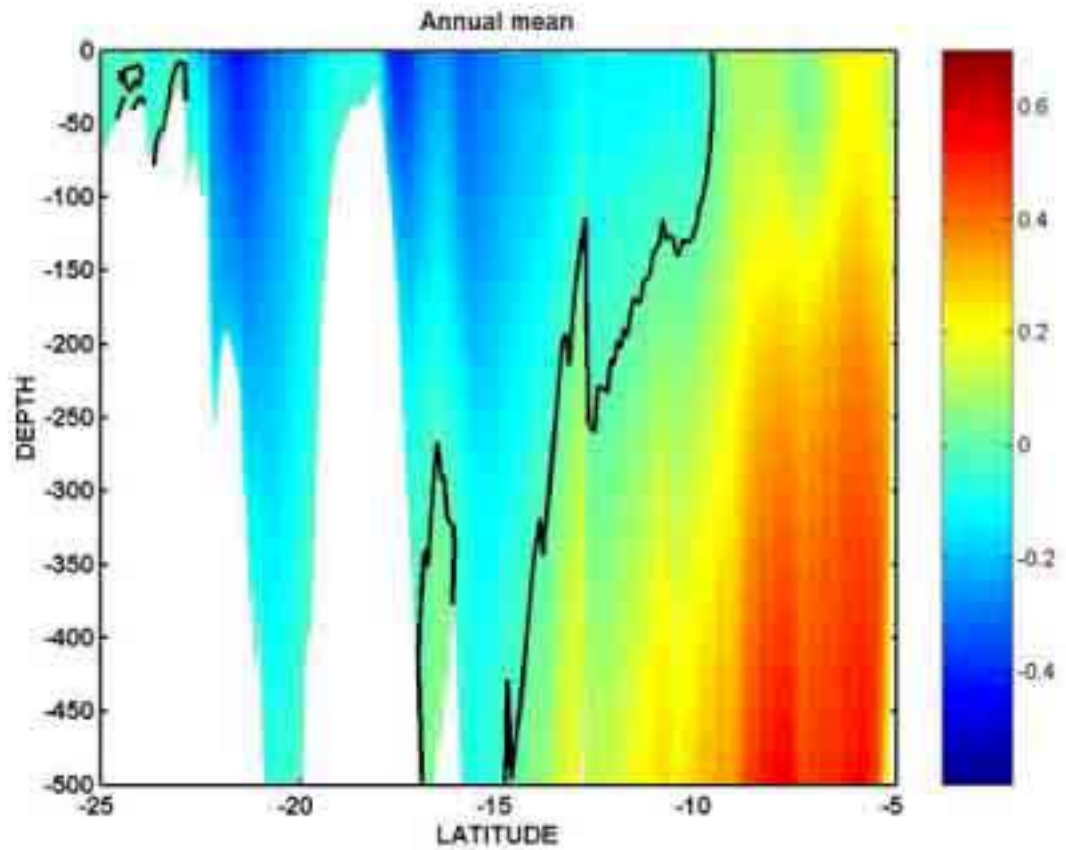


Figure 6.4. Annual averaged meridional velocity (m.s^{-1}) obtained from last year of the climatological ROMS simulation. The velocities are averaged within a 1° longitude band off the Brazilian coast. The dark line is the contour of zero velocity that represents the bifurcation of the sSEC. The white areas represent Vitoria-Trindade Ridge and Abrolhos Bank.

Complementary, the Figure 6.5 shows the seasonal bifurcation of the sSEC obtained from the last five years of the ROMS simulation. The results are extracted from 200 m depth layer. The bifurcation of the sSEC is represented here by the white line where mean alongshore velocity (also averaged within a 1° longitude band off the South American coast) is zero. According to Figure 6.5, the sSEC bifurcation occurs at 19°S in May-June and close to 13°S from September to January.

In austral winter, the model reproduces the intensification of the NBUC and the southernmost position of the sSEC bifurcation. On the other hand, in austral summer, the NBUC is weaker while the sSEC has its northernmost position. It is important remember that, in austral summer an

anticyclonic eddy attached to Brazilian coast exists, between 12°-15°S at 200 m depth (Figure 6.2). Our theory is that this eddy reduces the northward transport of the NBUC in austral summer.

The seasonality of this bifurcation agrees with recent results of Rodrigues et al. (2007) about the seasonality of the sSEC. The model results are also consistent with field measurements in which the strongest value of the NBUC are found in austral winter and weaker in austral summer.

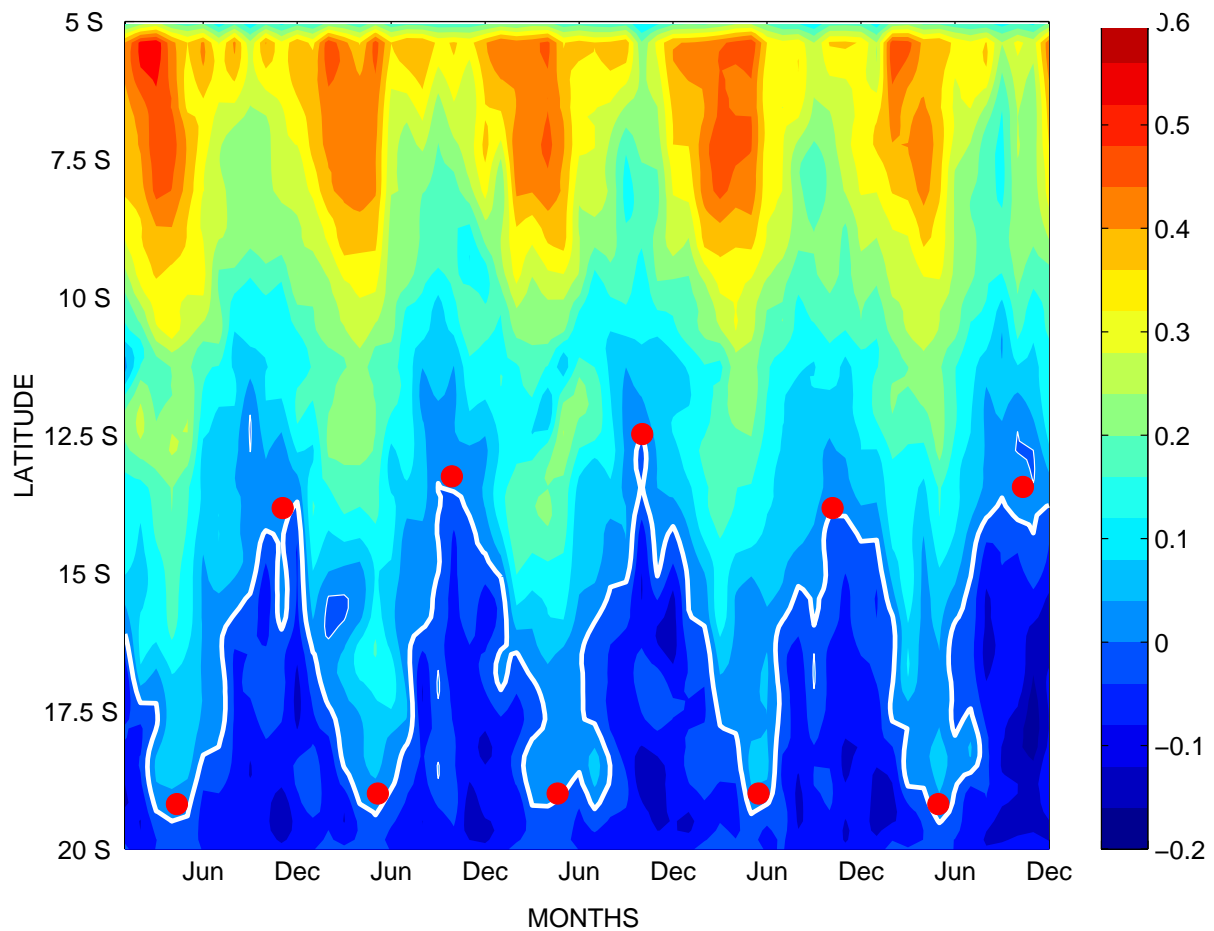


Figure 6.5. Hovmoeller of the meridional component of velocity ($m.s^{-1}$) at 200 m depth. Results from the last 5 year of simulation of ROMS model. The alongshore component is a mean of 1° longitude from the coast. The white line represents the locations where the western boundary currents are reversed. Extreme positions are indicated by red points.

6.2. Current structure and transport variability at 11°S

6.2.1. Northward NBUC transport

The time series of the NBUC transport anomaly calculated from 11°S moorings data is plotted in Figure 6.6. It shows strong fluctuations with amplitudes of about ± 15 Sv. Fluctuations with bimonthly periods are dominant within the NBUC. Mean NBUC transport at 11°S accounts for 25.7 Sv. The combined annual and semiannual harmonics cycle result in a maximal northward NBUC transport in austral winter (July) with minimum in October and November.

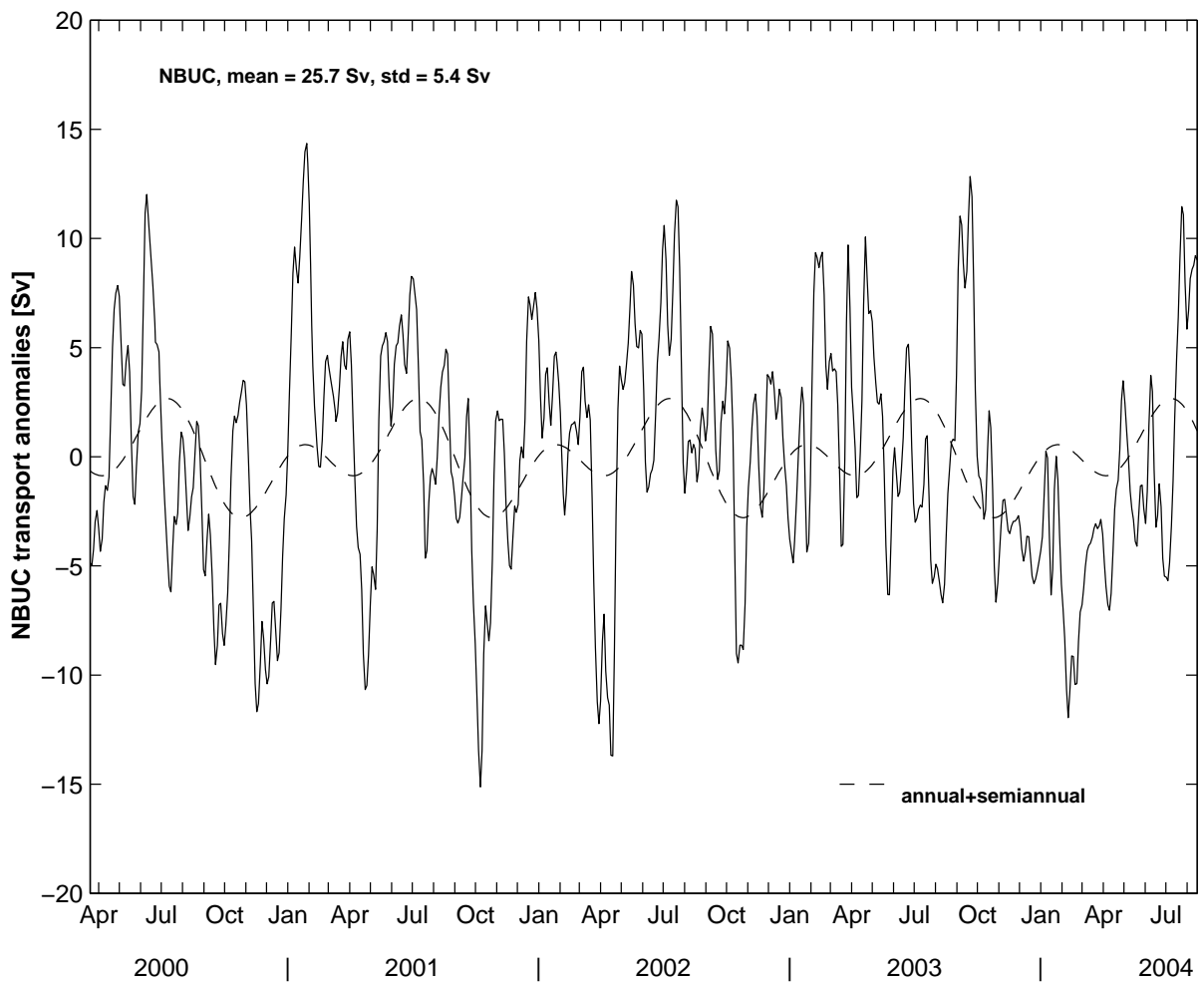


Figure 6.6. NBUC transport anomalies at 11°S (German CLIVAR data) and the superposition of annual and semiannual harmonics (dashed line). Adapted from von Schuckmann (2006).

Based on mooring data, mean alongshore transport values obtained from ROMS simulation at 11°S are presented in the next Figures 6.7 and 6.8, for November and July, respectively. The isopycnal $\sigma_\theta = 32.15 \text{ kg.m}^{-3}$, about 1100 m depth in Figures 6.7 and 6.8 indicates the lower boundary of the upper warmer waters, as well as the lower boundary of the AAIW. This is the layer where most of the northward NBUC transport occurs. Below 1200 m depth the NADW extends to about 4000 m depth ($\sigma_\theta = 45.9 \text{ kg.m}^{-3}$). This is the place where the DWBC acts transporting cold waters from the North hemisphere with a net transport southward. The isopycnal of $\sigma_\theta = 45.9 \text{ kg.m}^{-3}$ separates the lower NADW from the northward spreading Antarctic Bottom Water (AABW). The limits of the water masses found in these sections agree with previous works (Stramma and England, 1999; Stramma and Peterson, 1990).

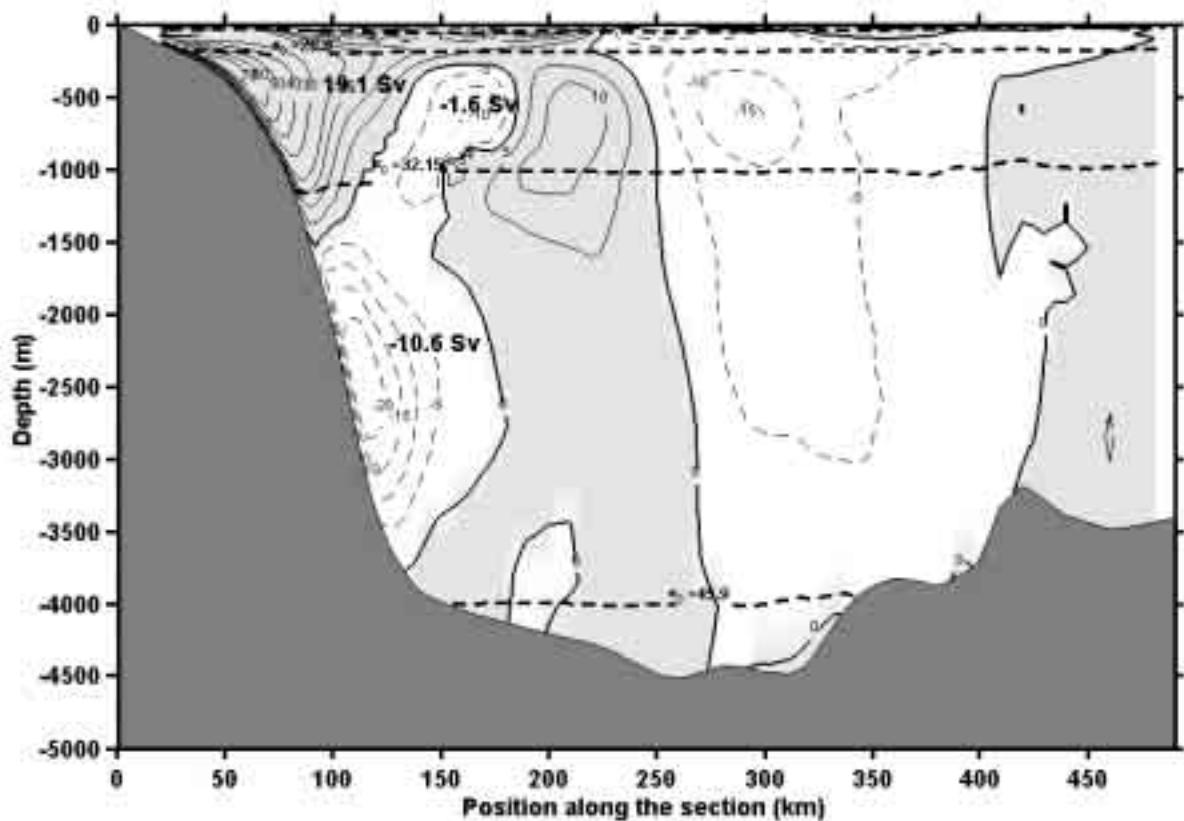


Figure 6.7. Meridional transport obtained from ROMS simulation at 11°S: November. Positive values are indicated by solid lines corresponding to northward currents, while negative southward transport is represented by dashed sections. Horizontal dashed lines indicate the boundaries between different water masses.

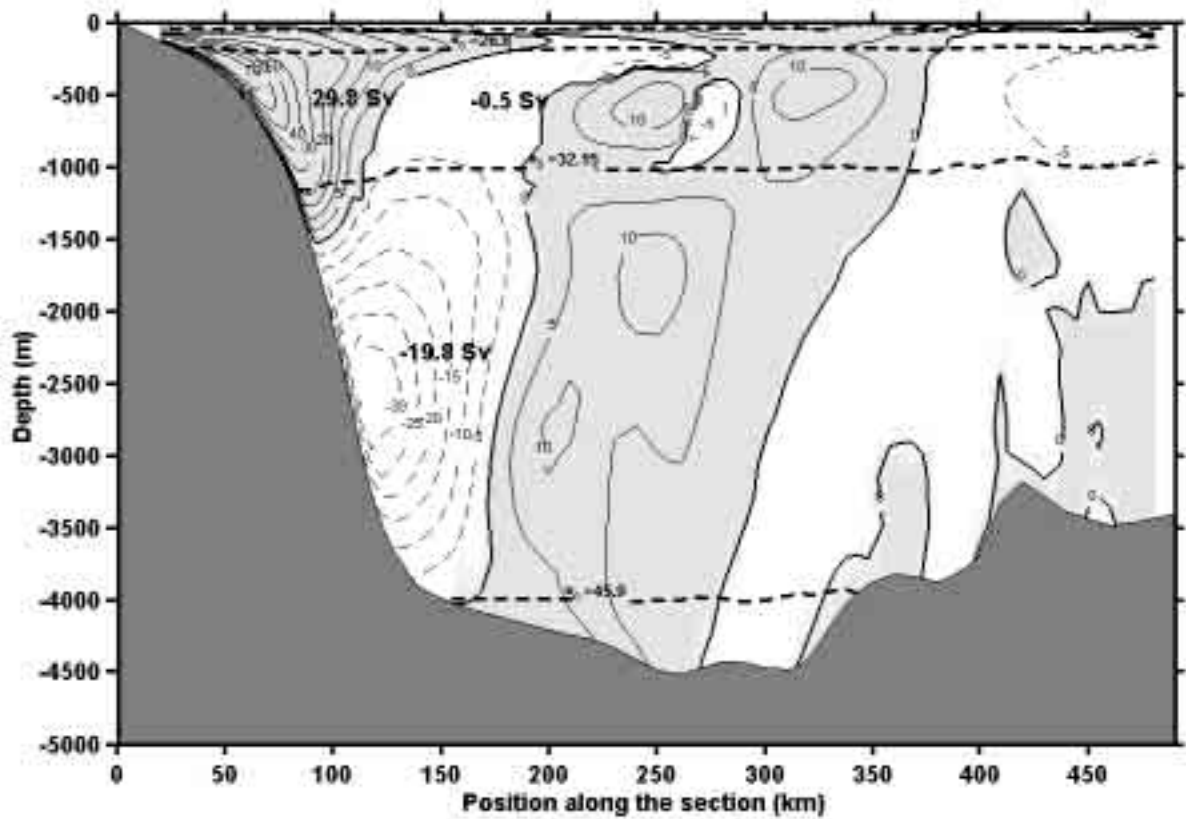


Figure 6.8. Meridional transport obtained from ROMS simulation at 11°S: July. Positive values are indicated by solid lines corresponding to northward currents, while negative southward transport is represented by dashed sections. Horizontal dashed lines indicate the boundaries between different water masses.

The transport sections presented here contribute to infer about the level of coupling between the seasonal cycle of the NBUC and the alongshore intrannual variability of the sSEC bifurcation. Rodrigues et al. (2007) showed that, when the sSEC bifurcation is located more southward, the NBUC transport is more intense. Whereas, as the sSEC bifurcation is displaced northward, the NBUC transport is weaker. This is based on the fact that the inflow of the sSEC into the western equatorial regime feeds the NBUC mainly in the depth range of the Central Water Layer (100–500 m). As a consequence the seasonal migration of the sSEC could be responsible for the NBUC transport seasonality (Schott et al., 2005).

The northward NBUC with its core is situated about 50 km from the coast, at 180–250 m depth, where the transport is stronger (Figure 6.7). This

has been also detected from field measurements (Figure 4.1c, Chapter 4). Toward the surface the velocities decrease considerably, confirming the undercurrent characteristic of the NBUC. Still in the upper layers, model transects indicate the presence of a mean southward counterflow at 300-900 m offshore the NBUC (about 150 km from the coast). This southward flow was evidenced from ADCP measurements (Figure 4.1c, Chapter 4), as well as in the Principal Component Analysis of the Chapter 4.

The climatological modeling results confirm a stronger northward transport of the NBUC during the austral winter of 29.2 Sv (arithmetic mean over 90-day time period) with approximately the same magnitude of the moorings data for the same period (27.7 Sv). During austral summer, less accentuated northward transport is verified from the model results (20.8 Sv, Figure 6.9) and field measurements (22.7 Sv).

The previous analyses suggest that there is a link between the strength of NBUC transport at 200 m depth and the latitude where the sSEC bifurcates near the Brazilian edge (Figure 6.5). When the sSEC bifurcation is southward, during austral winter, the NBUC transport is stronger. Model results indicate that the NBUC at 11°S presents an almost steady flow, reaching down to about 900 m depth, with a slower transport during austral summer (November) and a slightly higher northward transport in winter (July). These same features are observed at the experimental transects obtained from moorings data (Schott et al., 2005). Mean annual northward NBUC transport calculated from model is 23.4 Sv. This value is in good agreement with the 25.4 Sv estimated by Schott et al. (2005). The K1-K2 moorings data indicate the presence of the NBUC core in July at about 200 m depth (Figure 4.1c, Chapter 4) and higher velocities of about 70 cm.s⁻¹. The November measurements indicate a NBUC core at 200 m depth, with velocities reaching 35 cm.s⁻¹ at that latitude. Model results to November show a subsurface NBUC core situated at about 250 m depth, and velocities of up to 70 cm.s⁻¹. In July, the numerical NBUC core is situated close to 300 m depth, with maximum velocities of about 72 cm.s⁻¹, which is in good agreement with experimental values estimated from the direct

measurements of Schott et al. (2005).

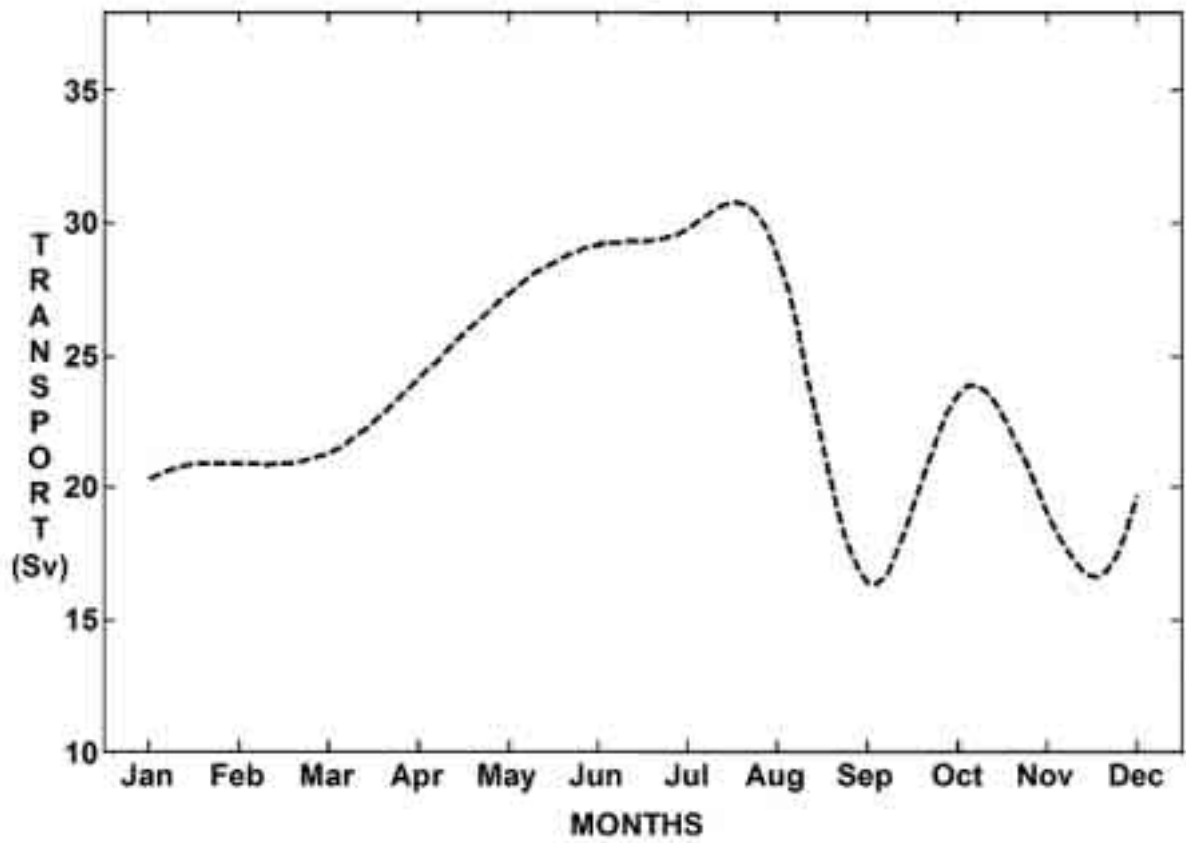


Figure 6.9. NBUC transport at 11°S for the last year of the climatological ROMS simulation.

The current structure obtained from ROMS in a section at 11° S (Figure 6.10) is representative of the alongshore current measurements from the moorings section (represented in Figure 4.1c). Monthly averaged sections for the last year of simulation of ROMS are represented in Figure 6.10. The core of the NBUC is well formed at this latitude, and the maximum alongshore currents reaches 70 cm.s^{-1} as in Schott et al. (2005).

The higher values of the DWBC from measurements (see Figure 4.3) are found in a mean section for June, July and August, where the DWBC is more defined and attached to coast. In the results from ROMS (Figure 6.10) the DWBC is more defined and stronger as other months in July and August. Both experimental (Figure 4.1c) and model information (Figure 6.10) suggest that the NBUC is originated further south than 11°S, and that it is

already well developed at this latitude.

6.2.2. Southward DWBC transport

Below the northward NBUC transport of warmer waters, the negative sections show the presence of the DWBC (Figures 6.7 and 6.8), transporting NADW between 1100 and 3500 m depth at 11°S. Much more instable than the NBUC, the deeper and colder DWBC flow presents more or less alternated periods with northward and predominantly southward transports along the continental slope. The dynamics in this latitude is very different from previous upstream measurements of the DWBC along the Brazilian shore. For example, Fischer and Schott (1997) observed, just north of the equator (44°W), a southward DWBC that is never reversed in direction. More to the south (at a crossshore 5°S Section), a mean southward DWBC transport of about 25.5 ± 8.3 Sv was estimated by Schott et al. (2005), with no significant signals of DWBC recirculation. Dengler et al. (2004), trying to explain the observed discrepancy in meridional DWBC transport along these latitudes, used the K1-K5 data to show that the southward transport of deep water across 11°S is accomplished by migrating anticyclonic eddies. The eddy model used by Dengler et al. (2004) produced more vigorous eddy activity from April to September, presenting an eddy activity caused by seasonal variations in strength of the upstream DWBC between 4°S and 8°S, which leads to enhanced eddy generation. These authors also speculate that the eddy variability can be associated to the long-term MOC variations.

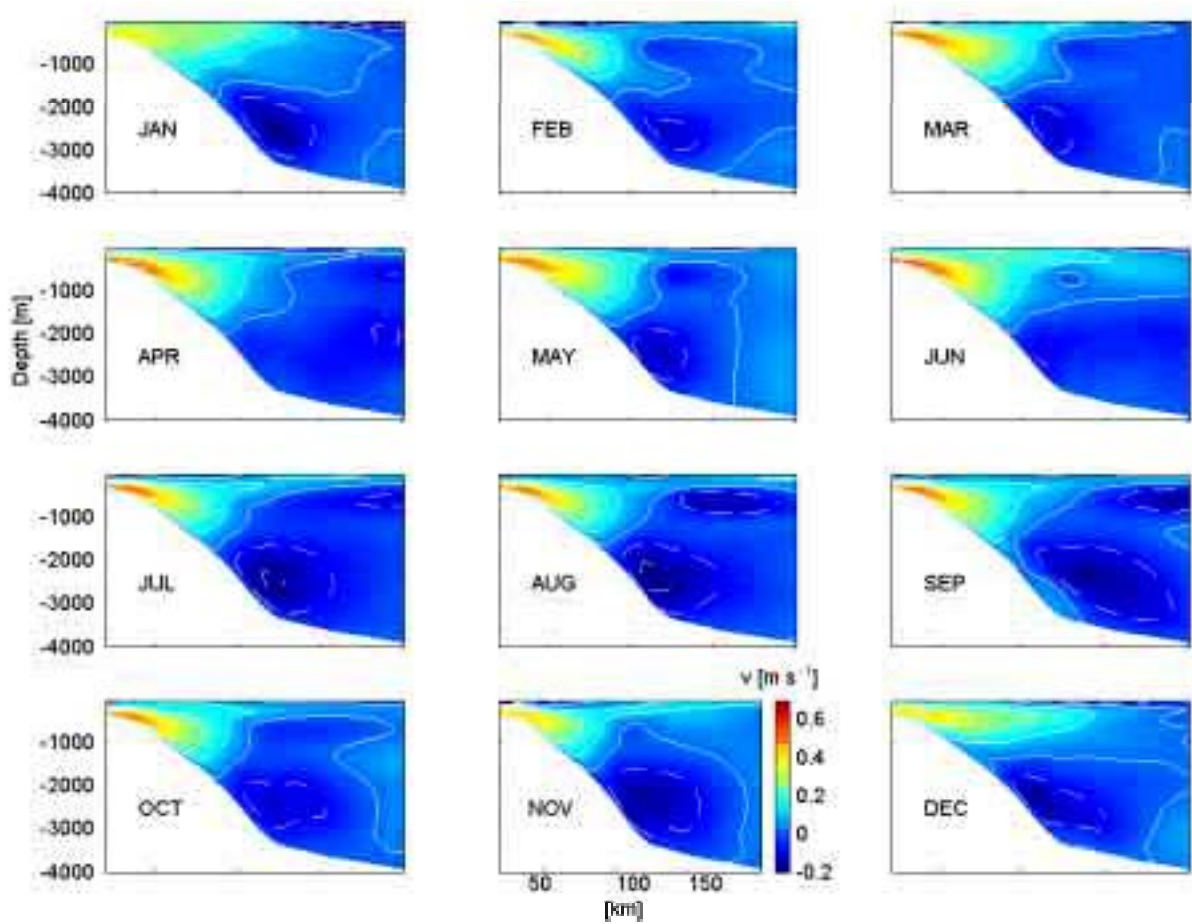


Figure 6.10. Alongshore monthly mean velocities obtained from last year of the ROMS simulation Section at 11°S. Positive values are indicated by solid lines corresponding to northward currents, while southward flow is indicated by dashed sections.

Model results also indicate eddy-forming activities along the year with different intensities, at the NADW layer between 10°S and 17°S. After examining all monthly-averaged model charts, in order to identify the most distinct periods concerning eddy development, August and February were chosen to represent the horizontal current field obtained from simulations at 1900 m. The numerical results from ROMS climatological modeling agree with mean experimental data and previous works (Dengler et al., 2004; Schott et al., 2005). According to simulations, the upstream DWBC between 7°S and 10°S is reinforced during austral winter (August), when more vigorous and well developed eddies begin to be formed at 10°S and are well developed at 12°S and 14°S-15°S (Figure 6.11). These anticyclonic structures

shown a mean radius of 72 km and horizontal velocity of about 42 cm.s^{-1} at 1900 m, in agreement with the average eddy scales found from the eddy model fitting of Dengler et al. (2004). During the austral summer (February), the upstream DWBC flow is clearly reduced, and less well defined eddies are present (Figure 6.12).

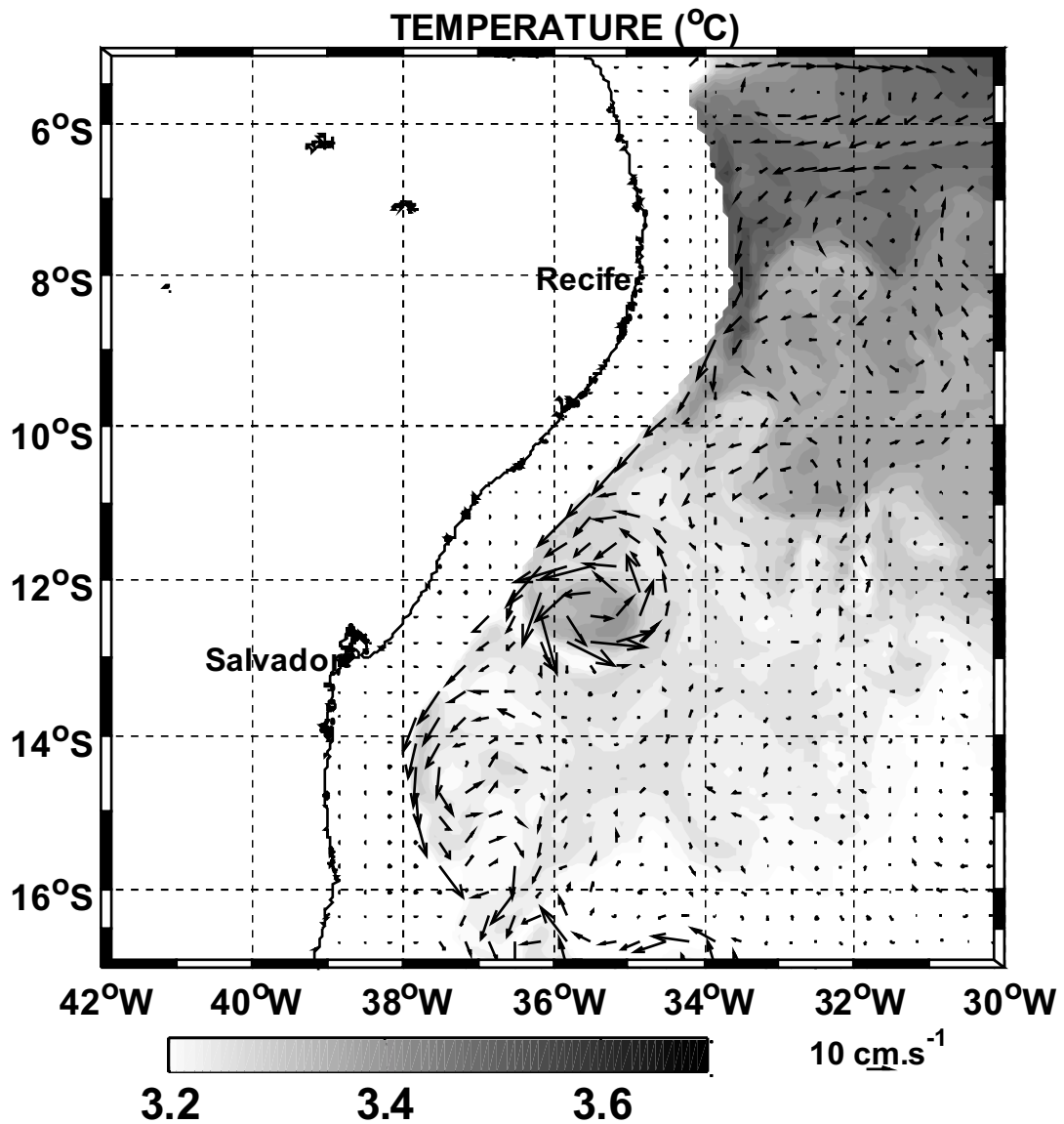


Figure 6.11. Horizontal current fields obtained in ROMS simulations at 1900 m depth: August.

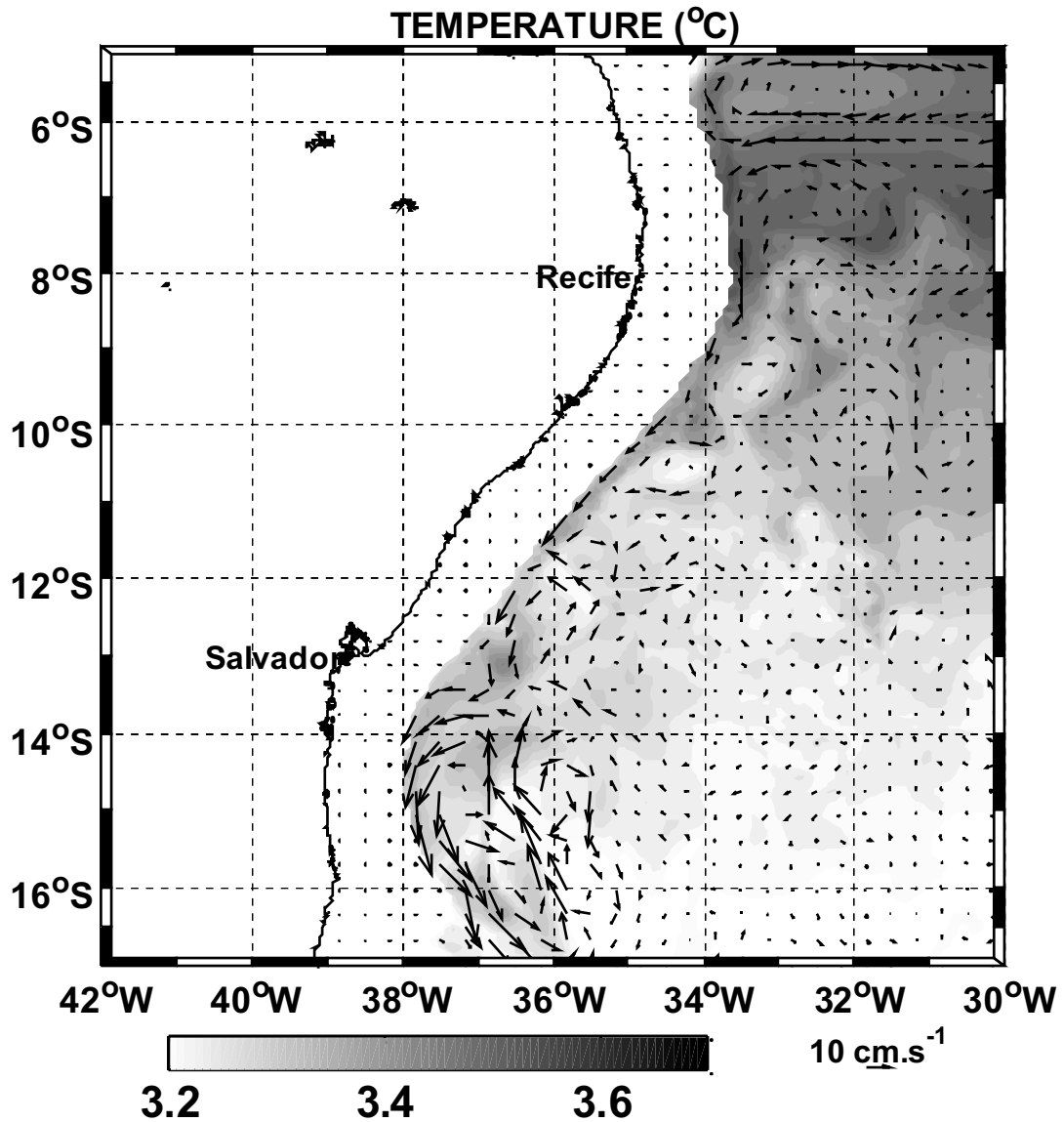


Figure 6.12. Horizontal current fields obtained in ROMS simulations at 1900 m depth: February.

6.3. Climatology of the SODA reanalysis

The analysis of the combined current records in the Chapter 4 has shown that 2-3 months variability exists in the NBUC domain. The intraseasonal variance shows maximal values when the mean northward NBUC velocity becomes maximal and the variance decreases with increasing distance from the undercurrent core (e.g. K2 mooring at 250 m depth, Figure 4.1c). This indicates that a mode of ISV exists with periods of 50-100 which is connected to the NBUC domain. The combined annual and semiannual cycle

result in maximal northward NBUC transport in austral winter and minimum in October to November (see also Schott et al., 2005, their Figure 12).

Monthly averaged alongshore current for 47 years of SODA reanalysis are examined to identify the bifurcation of the sSEC. The area covered here is from 20°S to 5°S and from 41°W to 30°W. Such as in ROMS results, the alongshore current fields of SODA reanalysis in Figures 6.13 and 6.14, the bifurcation latitude of the sSEC is defined as the place where the western boundary currents are reversed. Thus, the bifurcation is chosen where the alongshore component of the zero velocity (dashed line) reaches the coast. These sites are represented by black points in Figures 6.13 and 6.14.

In 200 m depth, the northernmost position where the alongshore currents are reversed occurs in December and January at about 15°S. The southernmost position occurs in from May to August at about 18°S (Figure 6.13). In 500 m depth, the alongshore current are reversed northernmost at about 17°S in October and November while the southernmost reversed currents is from March to July at about 19°S. These fields are an important confirmation the depth dependence of the bifurcation of the sSEC, as was described by Rodrigues et al. (2007) and Cirano et al. (2006), and also obtained in ROMS model results in this work.

The results from SODA reanalysis were also analyzed in horizontal charts at 500 m depth. This analysis shows a counterflow off the NBUC from January to March, which reaches 10°S such as identified in Schott et al. (2005). From May to September this counterflow reaches higher latitudes, which suggest another feeding contribution. We can speculate here that this contribution may come from the deep cSEC, which shifts southward and feeds the NBUC counterflow.

The temporal evolution of the offshore counterflow to the NBUC suggests that this flow persist during the whole year. This phenomenon is important because it reduces the net heat transport toward the Northern Hemisphere. However, this counterflow still remains an open question, which needs to be confirmed by sea measurements altogether with

numerical simulations involving the ocean area north of 5°S.

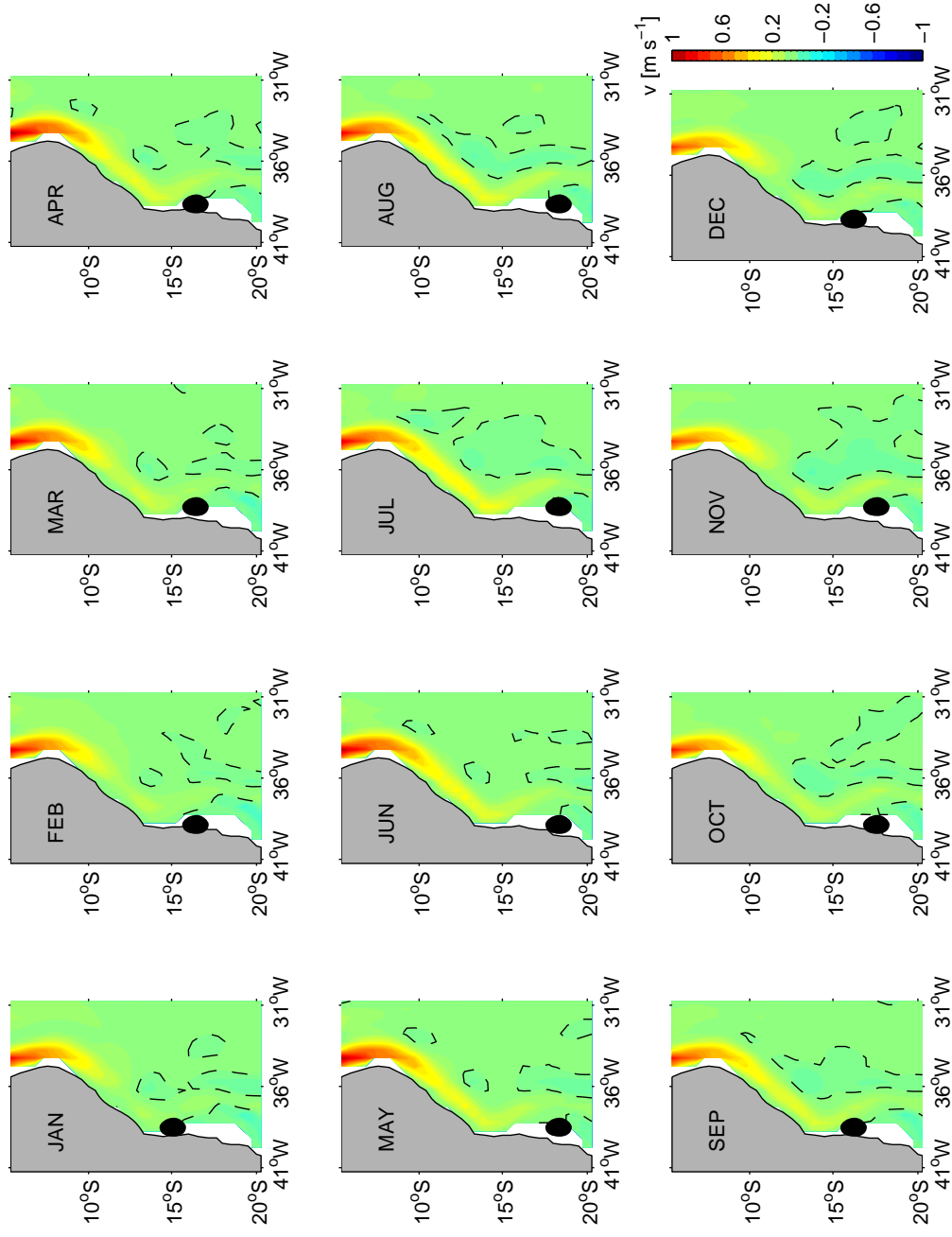


Figure 6.13. Monthly mean horizontal current fields at 200 m depth obtained from 47 years of the SODA reanalysis. Black points are the sites where the alongshore component of the zero velocity reaches the coast.

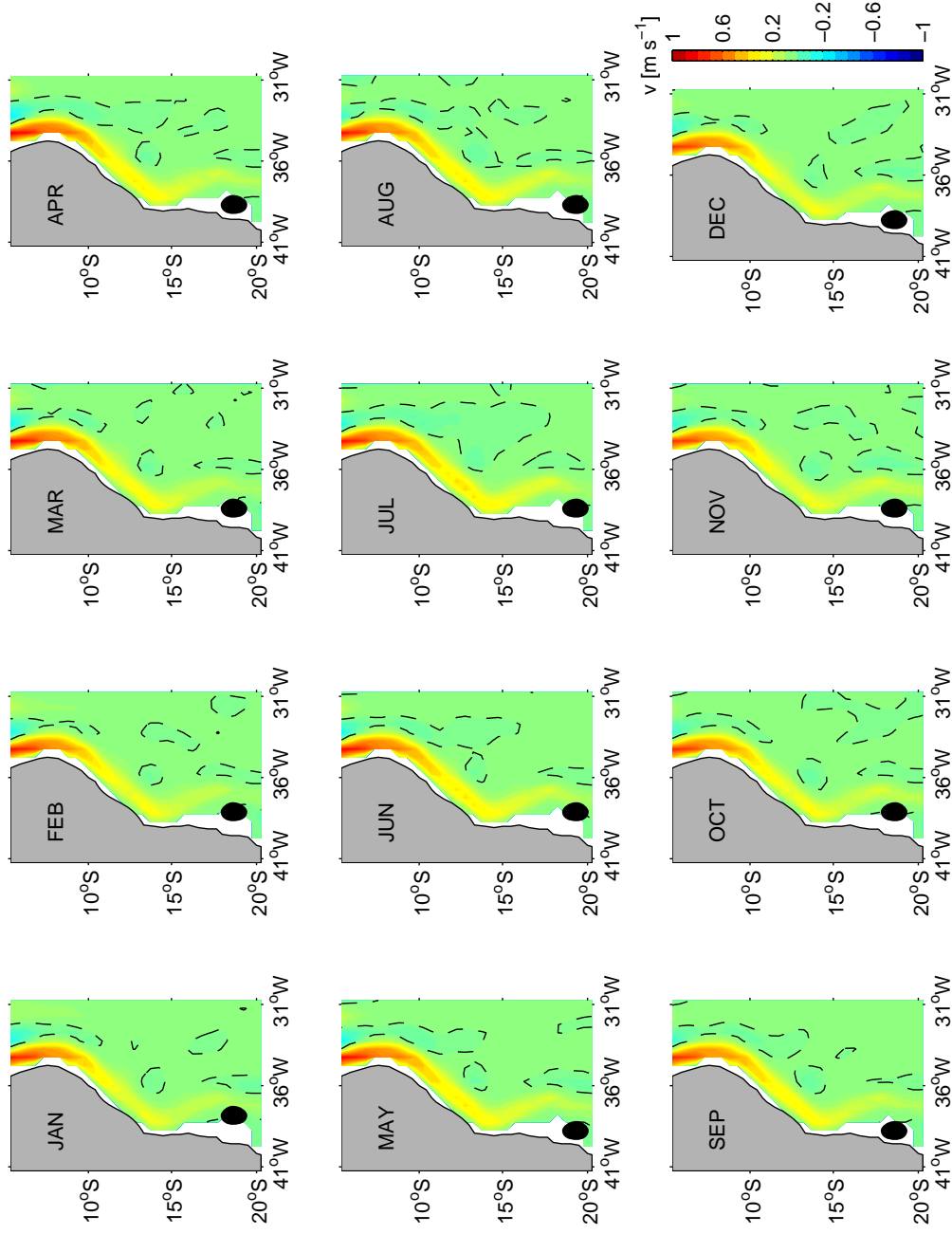


Figure 6.14. Monthly mean horizontal current fields at 500 m depth obtained from 47 years of the SODA reanalysis. Black points are the sites where the alongshore component of the zero velocity reaches the coast.

6.4. Summary

The main goal behind this chapter was to investigate the presence and the dynamic of the southern band of the South Equatorial Current (sSEC) as well as the vertical structures in the western Atlantic Ocean boundary comprised within 5°S-25°S and 20°W-47°W. These coordinates limits the area where the sSEC encounters the South American continent and bifurcates, with the water flowing north and south as two western boundary currents, the NBUC and the BC, respectively. This is a region of complex links between climatic variability of the SST and heat content of the upper layers of the tropical Atlantic, atmospheric convective systems and precipitation on the adjacent continent, especially on the Brazilian Northeast region. It is particularly interesting on evaluating the capacity of a specific numerical modeling technique on reproducing seasonal transport of heat and oceanic mass between different sectors of the subsurface tropical Atlantic and identifies the temporal scales of occurrence of these phenomena.

6.4.1. The bifurcation of the southern branch of the SEC

Numerical transports and currents results were compared to ocean measurements obtained from moorings data deployed at 11°S by the German part of CLIVAR program, from March 2000 to August 2004. These comparisons suggest that the climatological modeling approach employed here reproduces the main features of the circulation observed from field measurements. Numerical currents and transports distributions, from the climatological model, along water depth are similar to CLIVAR measurements. An important characteristic found in the simulated sSEC divergence is that it shifts southward as ocean depth increases: it varies from 8°S at 100 m depth to about 20°S at the 500 m depth.

Model results show a strong northward under surface speeds up to 70 cm.s⁻¹ near 5°S, corresponding to the NBUC field data such as in Stramma et al. (2003). Despite of the larger variability observed at this latitude, the NBUC at 5°S has to be related to equatorial processes and not to sSEC

variability (Schott et al., 1998; Stramma et al., 2003). Nevertheless the NBUC at 11°S can receive influences from seasonal migration of the sSEC (Schott et al., 2005). One of the main goals of this study was to quantify the variability of the flow in the NBUC level, and whether its dynamics is or not associated to the sSEC migration. The model simulations presented in this work stressed a seasonal migration of sSEC at 200 m depth, with a southernmost shift at about 18°S in May-June and northernmost at 12°S from September to January.

The seasonal wind stress curl, in Chapter 5, indicate a southernmost zero line for the months of June, July and August, which means that the northern limit of the subtropical gyre at these months is more southward. Furthermore, the sSEC is a north limb of the subtropical gyre. Thus, it is expected that southernmost bifurcation of the sSEC to be at these months. The maximum northward zero line of wind stress curl was about 10°S and the southward maximum was about 15°S. The southernmost position of wind stress curl (Chapter 5) was in austral winter. Furthermore, the southernmost position of the sSEC bifurcation was found also in austral winter, from ROMS results and from SODA reanalysis results (Figure 6.15).

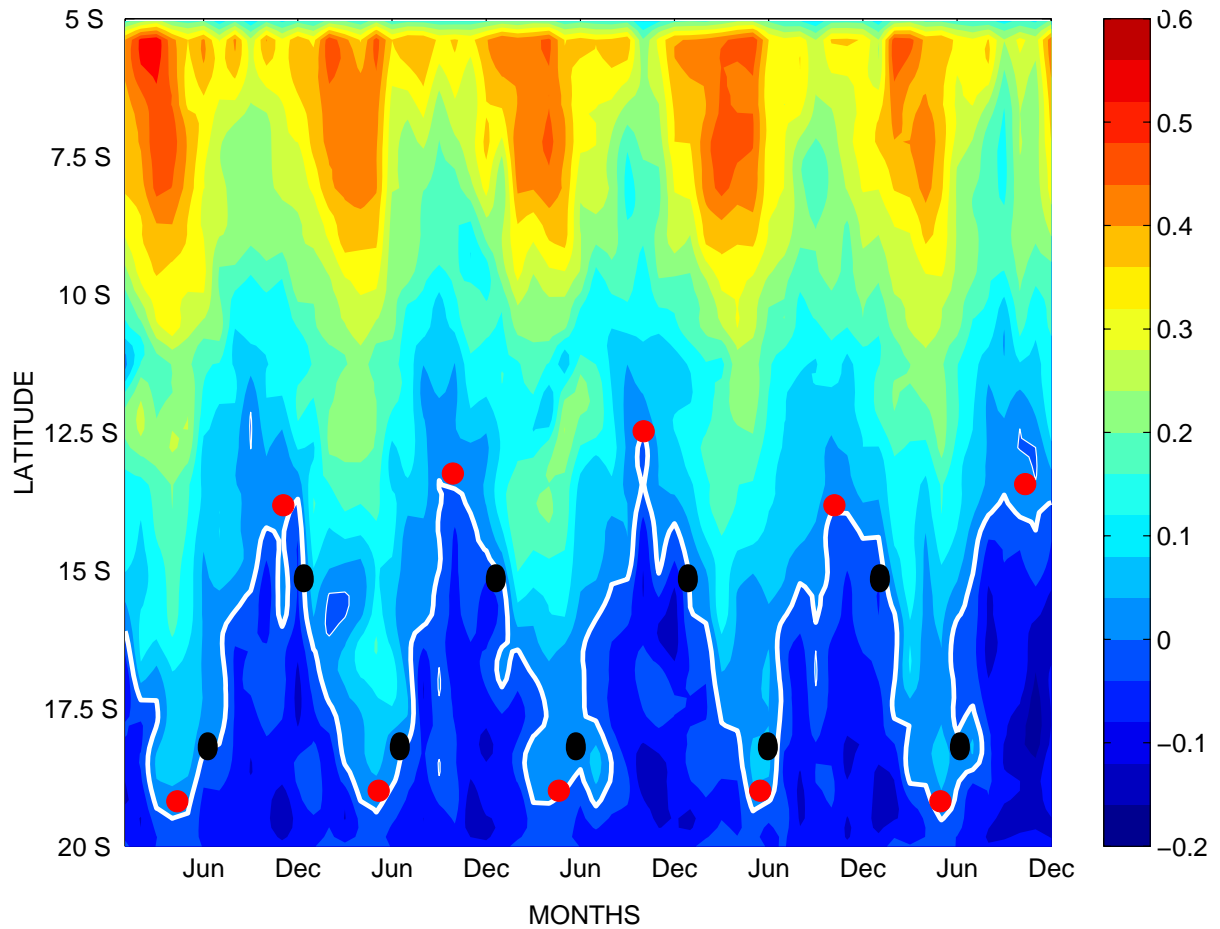


Figure 6.15. Hovmoeller of the meridional component of velocity (m.s^{-1}) at 200 m depth. Results from the last 5 year of simulation of ROMS model and climatological SODA reanalysis. The alongshore component is a mean of one degree of longitude from the coast. The white line represents the site where the western boundary currents are reversed in ROMS simulations. Red points represent the location of the sSEC bifurcation from ROMS model, and black points are the sites where the alongshore component of the zero velocity reaches the coast in SODA reanalysis.

6.4.2. The eddies at NADW core

The NADW variability observed from mooring K4 in deeper layers seems to be linked to upstream instability from eddies' passage in the DWBC. The PCA indicated a cycle of about 14-30-60 days (EOF1 = 81%) for the core of the DWBC at 1900 m depth.

According to simulations, the upstream DWBC between 7°S and 10°S is reinforced during austral winter (August), enhancing eddies generation. The ROMS simulation indicates that the DWBC breaks up into eddies reproducing anticyclonic structures with the same order of magnitude of the average eddy scales estimated from moorings data (Dengler et al., 2004). On the other hand, the simulated upstream DWBC flow is clearly reduced during the austral summer (February), and less well defined eddies are present. Eddy formation in the Southern Hemisphere is indicated as a counterpart to NBC rings. Furthermore, the DWBC eddies here represented are a major component of the cold water branch of the MOC.

6.4.3. The counterflow offshore the NBUC

The Principal Component Analysis (PCA) for currents give 60 days variability (EOF2 = 14%) in K4 mooring at 500 m depth (Table 4.1, Chapter 4), where Schott et al. (2005) found a substantial and persistent recirculation offshore from the NBUC along 5°-11°S. The counterflow suggests an offshore band of intermediate water recirculation in this latitude range, amounting to about 5 Sv and reaching down to NADW densities. This counterflow is important because it reduces the liquid content of heat transport toward the Northern Hemisphere.

In the ROMS simulations we found this well formed counterflow just offshore of the NBUC at 11°S, with more intense flow in November and less intense in July, when no retroflexion of the NBUC was verified.

The SODA reanalysis data analyzed in a horizontal section at 500 m depth indicated a retroflexion in the NBUC from January to March, which reaches at 10°S such as in Schott et al. (2005). In May to September there is

another contribution for the counterflow. It would be the westward flow from the deep cSEC shifting southward and feeding the counterflow.

The PCA for coupled fields does not show strong coupling in the first EOF at K4 station. However, the temperature is strongly coupled to the velocity current at the core of the DWBC for the first year of K3 mooring data, which reveals that these two fields have phase zero each two months. There is a tendency for more variance at the same time for the two fields.

A strong coupling was found between temperature and current measurements at mooring K4. This coupling can be linked to the bowl-shaped temperature anomaly found in eddies at the DWBC core. The results from ROMS model shows that higher temperatures are concentrate into the eddies at the DWBC level. It shows a strong coupling between high velocities from eddies and a high temperature into this eddies.

Table 6.1 resumes the main results found in this chapter.

Table 6.1. Comparison between this work and related works.

	<i>Other works</i>	<i>This work</i>
sSEC bifurcation 100m	<p>10°-14°S (annual mean) (Rodrigues et al., 2007)</p> <p>9°S - 15°S (annual mean at level of Tropical Water, between 0-116 m) (Cirano et al., 2006)</p> <p>14°-16°S between 0-100 m (Stramma and England, 1999)</p>	ROMS - 8°S
sSEC bifurcation 200m	<p>17°S in July and 13°S in November (Rodrigues et al., 2007)</p> <p>25°S (at level of the Central Water, between 116-657 m) (Cirano et al., 2006)</p>	<p>ROMS - 19°S in May-June and 13°S from September to January</p> <p>SODA - 18°S in May to August and 15°S in December and January</p>
sSEC bifurcation 500m	20°-24°S between 400 and 500 m (Stramma and England, 1999)	<p>ROMS - 20°S</p> <p>SODA – between 17°S and 19°S</p>
Eddies into DWBC	8°-16°S (Dengler et al., 2004)	between 7°S and 10°S
Counterflow offshore the NBUC	500 m (Schott et al., 2005)	mean southward counterflow at 300-900 m offshore the NBUC (about 150 km from the coast) (ROMS)

Chapter 7

7. Intraseasonal variability on the North Brazil Undercurrent forced by remote winds

The spectral analysis of both current meters measurements at 11° S and wind stress (Figures 4.4 and 5.6 of the Chapters 4 and 5, respectively), along the western boundary of South Atlantic, have revealed 10-14 and 14-30 days oscillations. This evidence altogether with the fact that non local forcing was found at those frequencies, clearly suggests that fluctuations in the current signals are due to wind stress forcing. Furthermore, the spectral analysis of the Principal Components for different depths in the moorings K1 to K4 shows a dominant mode of variability for 14 and 30 days. In this chapter the Coastal Trapped Waves theory is examined as a mechanism to explain these intraseasonal fluctuations.

7.1. Coastal trapped waves

While the dominant fluctuation in the NBUC core, at about 50 km from the coast, have a period of about two months (Schott et al., 2005), biweekly

signals are the dominant modes at western flank of the NBUC, about 10 km from the coast (von Schuckmann, 2006). As mentioned in the Chapter 1, it is unclear how these high-frequency fluctuations are generated. In this chapter we investigate which are the prime candidates as physical mechanisms for driving these signals on the western tropical South Atlantic.

It is well known that, intraseasonal fluctuations in the upper-ocean circulation can be excited through several dynamic processes such as local wind forcing, wind forcing in remote areas via waveguide dynamics, mean flow instability, and resonance due to coastline geometry (Brink, 1989; von Schuckmann, 2006). When these signals are located at coastal zone, the motion of the oceanic waters over the continental shelf and slope may be influenced by the earth's rotation, density stratification, offshore current regime, slopping bottom topography and the presence of a coastline (Allen, 1980).

Together with these coastal effects, Coastal Trapped Waves (hereafter CTW) appear important to be quite of attention. The existence of these waves depends entirely on the presence of a shallow shelf between the coast and the deep ocean. The CTW propagate along the continental slopes and shelves of the world's coastlines, leaving the coast on the right-side in the Northern Hemisphere, whereas on the left in the Southern Hemisphere. They have periods of days to 2-3 weeks and wavelengths of the order of 2000 km, determined by the atmospheric weather patterns. When stratification of the shelf waters is taken into account, their shape and associated currents are further modified, and they can have strongest currents at mid-depth. The effect of CTW on shelf currents and sea level variations can vary with the seasons due to fact that the stratification in shallow water is strongly affected by the seasons. For arbitrary topography and stratification, free-wave mode, similar to the barotropic Kelvin wave, plus an infinite set of higher mode, more slowly propagating waves (Brink, 1991), explain the variations in sea level and alongshore current over the continental shelf for typical periods ranging from the inertial period out to about 20 days. Wind and tides in coastal regions at sub-inertial frequency force those waves with

periods ranging from days to weeks. Since continental shelf is a transition zone between the coastline and the open ocean, the CTW transport materials (e.g., nutrients and pollutants) from regions near the coastline to and from the open ocean, and along the continental margins. Thus, the CTW modulate the upwelling system and primary productivity in the coastal regions.

Previous studies have confirmed the presence of the CTW with typical periods of 5-20 days. Brink et al. (1984) associated these waves with remote wind forcing. Battisti and Hickey (1984) determined that the pressure and alongshore velocity fields in the Northwest Pacific can be a response of the wind-forced CTW. The variance in sea surface pressure off Oregon and Washington was found to be generated by wind forcing between San Francisco and Cape Mendocino, California. The signal propagates 900 to 1300 km northward to Washington-Oregon arriving 3 to 4 days later. Camayo and Campos (2006) found 6-11 and 20-90 days oscillations off the western coast of South America, with strong correlation between sea level and alongshore wind stress (Spillane et al, 1987; Enfield, 1987). Strong upwelling and downwelling with biweekly period was also found throughout the year at the Indian Ocean equator, associated to continuous 10-20 days oscillations of meridional velocity in the upper ocean. The meridional oscillation was associated with an equatorially trapped wave forced by subseasonal variability of wind stress, with 4000 km wavelength, moving west about 350 km per day (Miyama et al, 2006).

Surface equatorial Kelvin waves travel very fast, at about 200 m.s^{-1} . However, in the thermocline they are much slower, typically between 0.5 and 3.0 m.s^{-1} (43.2 to $259.2 \text{ km.day}^{-1}$). They may be detectable at the surface, as sea-level is slightly raised above regions where the thermocline is depressed and slightly depressed above regions where the thermocline is raised. Smith (1978), for example, found a persistent poleward propagation of fluctuations in currents and sea level along the Peru coast between 10°S and 15°S with a wave speed of about 200 km.day^{-1} . Enfield and Allen (1980) also estimated the wave phase speed as the ratio of alongshore station separation to the corresponding lag. Brink (1982) pointed out the agreement between CTW

theory and observation. For the case of observations made off Peru in 1977, his results indicated free wave phase speeds of about 200 km.day^{-1} , as well as sea level and alongshore velocity fluctuations in the 5-10 day period band. Spillane et al. (1987) found oscillations with intraseasonal periods of 36-73 days over alongshore distances of several thousand kilometers, at the eastern Pacific, also close to the coast of Peru. They investigated these oscillations using spectral methods and EOF analysis, which revealed that the intraseasonal sea level variability has a peak in spectral density along the coasts of South America, Central America and Mexico, with poleward phase propagation of $150\text{-}200 \text{ km.day}^{-1}$. Enfield (1987) extends the work of Spillane et al. (1987) in order to see if the oceanic oscillation is related to its atmospheric counterpart. He found coincident phases of wind and sea level high, indicating that the intraseasonal sea level variations pointed out by Spillane et al. (1987) are forced in the western equatorial Pacific by the counterpart oscillation in the atmosphere. Their results are consistent with previous studies, which have found propagation at speeds of 216 to $259.2 \text{ km.day}^{-1}$.

More recently Camayo and Campos (2006) used wavelet analysis to study the intraseasonal current oscillations along the coast of Peru, with strong correlation between sea level and local wind. Their results suggested remotely forced internal Kelvin waves with periods between 6 and 11 days, southward propagating with phase velocities between $160\text{-}260 \text{ km.day}^{-1}$, barotropic shelf waves propagated southward with velocities between 110 and 150 km.day^{-1} , such as baroclinic Kelvin waves with period between 10 and 20 days, with velocities approximately of 200 km.day^{-1} .

The observed oceanic oscillations near the Brazilian shelf around 11°S , discussed in the Chapter 3, are related to its atmospheric counterpart. The German CLIVAR measurements obtained from four current-meter moorings array across the NBUC reveal a considerable 10-30 days current variability. The wind stress and sea level data also reveal variability within the same intraseasonal time-scales at the western boundary of the South Atlantic. These findings suggest that oscillations in the currents are forced by CTW

generated by remote winds. The hypothesis here is that these oscillations can be associated to remote winds and coastal wave forcing.

7.2. Cross-correlation method

The cross-correlation function is a quantitative operation in the time domain to describe the relationship between data measured at a point and data obtained at another observation point. The cross-correlation function is given by equation:

$$\psi_{xy}(t_l) = \lim_{T \rightarrow \infty} \frac{1}{T} \int_0^T F_x(t) \cdot F_y(t + t_l) dt \quad (7.1)$$

where $F_x(t)$ is the magnitude of the signal at point x, at time t, and $F_y(t + t_l)$ is the magnitude of the signal at a point y a time (t_l) later. By varying t_l , the relationship between the signals at x and y as a function of time is obtained.

For each cross-correlation between two signals, the lag is calculated. The data used are based on time series of wind stress for South Atlantic Ocean, on time series at 100m depth of current measurements from the mooring K1-K4 at 11°S, sea level and Chlorophyll concentration data. Only continuous series of these data were used, for gaps of one and maximum three days, linear interpolation was used.

The EOF analyses of the meridional component of current fields computed in K1, K2, K3 and K4 moorings was described in Chapter 4. Typically, most of the variance of the spatially distributed time series is retained in the first EOF modes.

As already discussed the K1 mooring is located approximately 10 km from the coast. The first EOF mode in this site is allocated at approximately 300 m depth and account for 90% of the total variance. The first mode of

variability for K2 mooring corresponds to 99% of total variance. The dominant mode of variability for K2, which is located in the NBUC core at this latitude, has the most apparent variances at 14 days, as well as between 30 and 60 days.

Besides currentmeter measurements at 11°S, wind stress along the western boundary of South Atlantic, have revealed 10-14 and 14-30 days oscillations (Figure 4.6 in the Chapter 4), suggesting thus, that currents signals are a response to wind stress forcing. The spectral analysis of the Principal Components for different depths in the moorings K1 to K4 shows a dominant mode of variability for 14 and 30 days. Hence, the results discussed, in the Chapter 3 and Chapter 4, indicate that the CTW are a good candidate to explain the connection between these signals.

7.3. Cross-correlation analysis between wind stress, sea surface height gauge and currents

Coastal trapped waves typically have a signature at the sea surface height field. Hence, their propagation has been also studied using satellite altimetry data. This is only possible for long periods compared with the periodicity of the satellite orbit, which is not the case of the propagation of biweekly waves. Several studies analyzed intraseasonal oscillations in the East Pacific using local measurements of sea levels (Enfield, 1987; Spillane et al., 1987; Camayo and Campos, 2006). In this chapter daily sea level measurements of local stations along the Brazil coast are used to investigate its signal variability once it could be an indicator of the existence of CTW. The variance preserving spectrum of sea level, from Ponta da Armação Station, located in Rio de Janeiro (22°53'S and 43°08'W) shows peaks at 14 and 30 days (Figure 7.1). The variance preserving spectrum of a sea level, obtained from the Cananéia Station, São Paulo (25°01'S and 47°55.5'W), shows peaks at 11-14 and at 20 days. Therefore, intraseasonal fluctuations exist in the sea level time series, in time with the corresponding fluctuations of the wind stress and also with the currents oscillations.

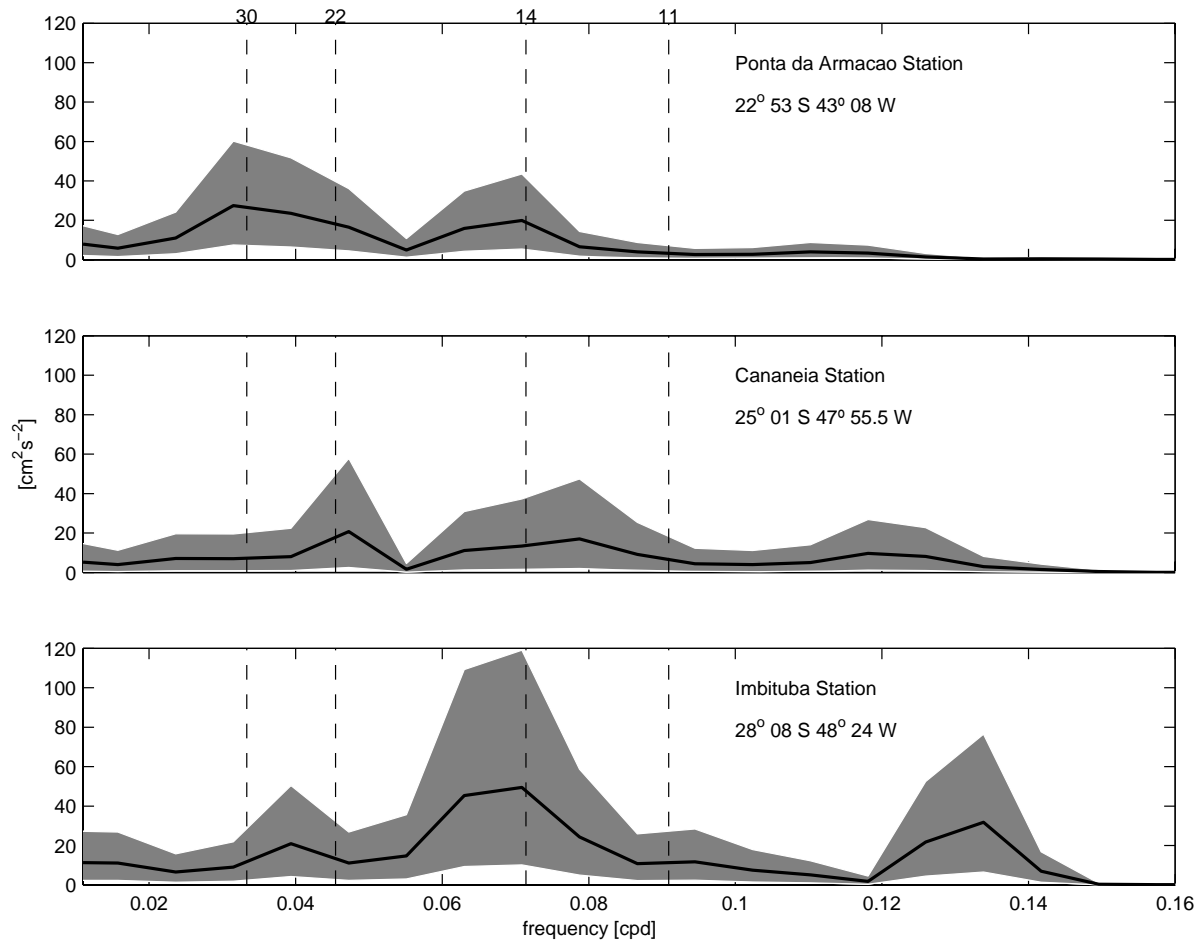


Figure 7.1. The variance preserving spectra of sea level data [$\text{cm}^2 \text{s}^{-2}$] for Ponta da Armação, Cananéia, and Imbituba Stations. The 95% confidence interval is shaded.

At Ponta da Armação Station, the results indicate that during the austral winter (JJA) a higher variability exists. The connection between the sea level and meridional wind stress is more noticeable for July to December of 2002 and July to November in 2003 and 2004 (Figure 7.2). A higher variability is also observed in austral winter for Cananéia Station. Good coupling between both time series is present during almost whole time. The zero lag cross-correlation between local meridional wind stresses with the sea level data is 0.30 for Ponta da Armação and 0.50 for Cananéia (Figure 7.2). For the Imbituba Station, the sea level signals show a good agreement with the meridional wind stress, particularly in May and July of the three analyzed years. The zero lag cross-correlation value for this site is 0.55.

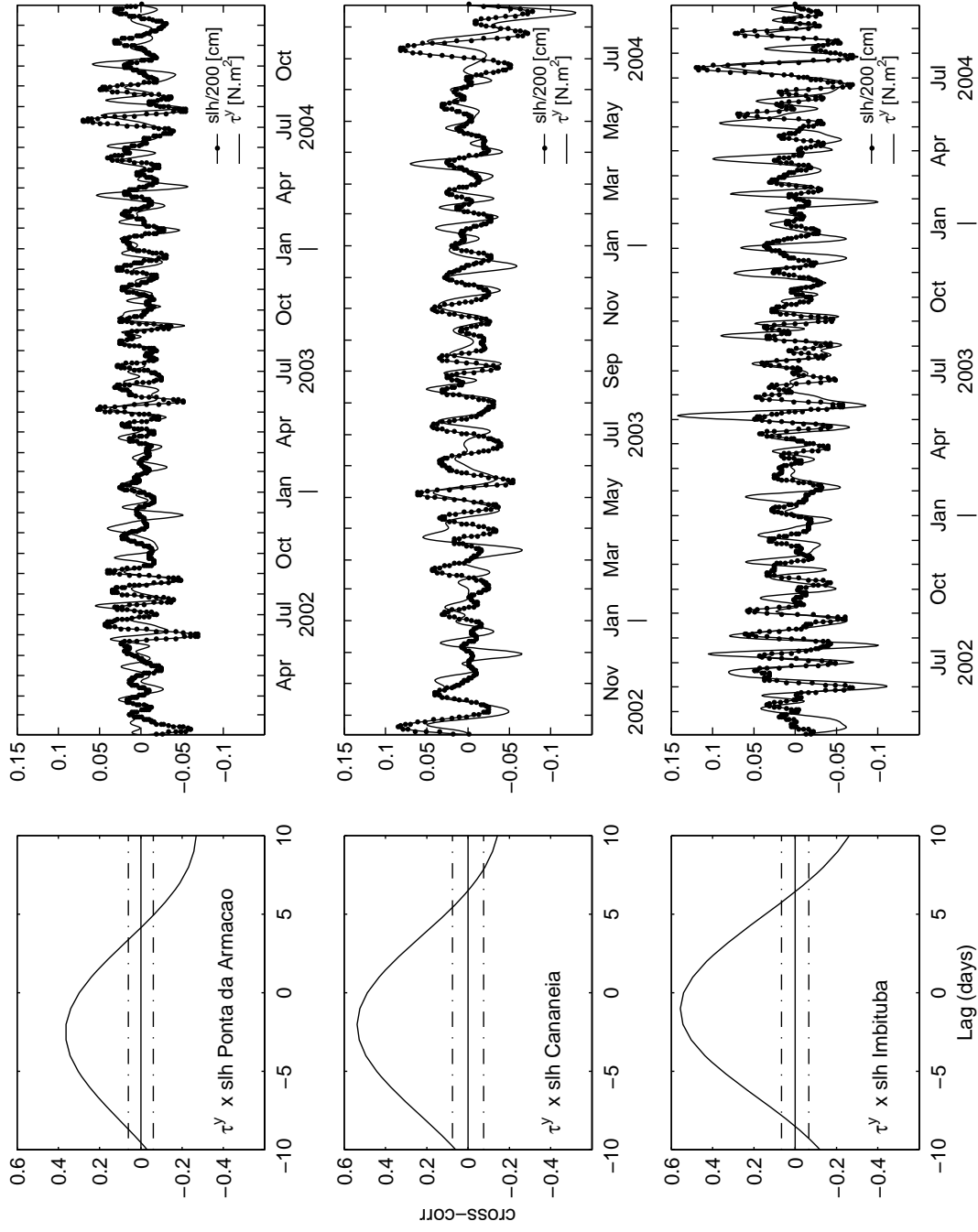


Figure 7.2. Cross-correlation between local meridional wind stress and sea level. The 95% confidence level is ± 0.0604 for Ponta da Armacao, ± 0.0750 for Cananeia, and ± 0.0662 for Imbituba Station.

Alongshore component of currents in the K2 mooring are correlated with the three sea level stations in Figure 7.3. The K2 mooring is located along the main core of the NBUC and for this site there are longer data time series among near shore moorings. The signals have a good lagged correlation of 10 days. As in Figure 7.2, stronger signals occur during austral winter (JJA).

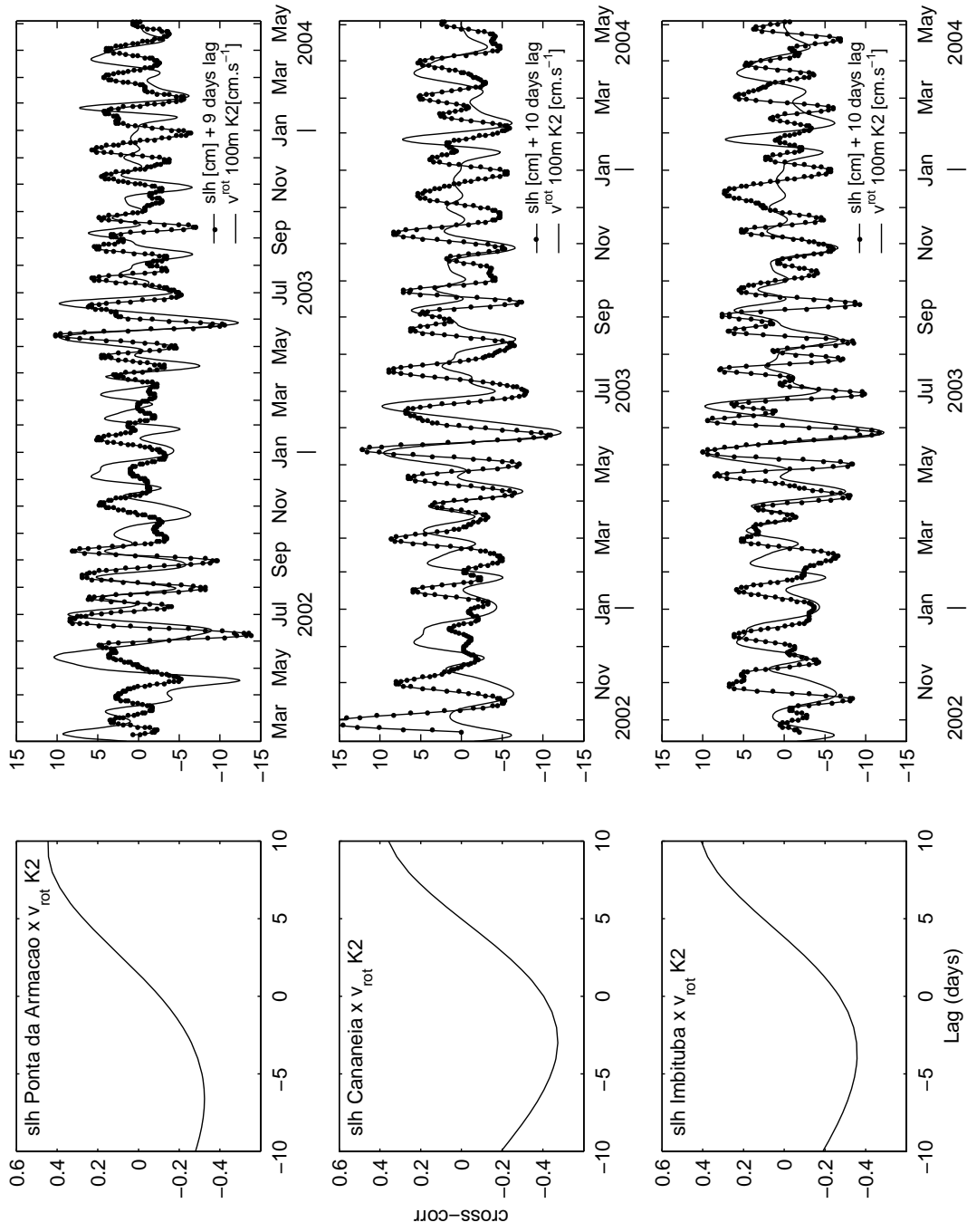


Figure 7.3. Cross-correlation for sea level and alongshore current at 100m depth in K2 mooring. The 95% confidence level is ± 0.0604 for Ponta da Armacão, ± 0.0750 for Cananeia, and ± 0.0662 for Imbituba Station.

7.4. Cross-correlation between wind stress and currents

The basin scale zonal and meridional components of wind stress are cross-correlated with alongshore currents in 100 m depth at 11°S for moorings K1 to K4 (Figures 7.4 to 7.8). For the K1 mooring two separated periods are showed, due to a gap between available measurements. Since the interest here is in the intraseasonal signals on the band of 10-30 days, a 10-30 days bandpass filter was applied to both the atmospheric and oceanic data to be compared. For each cross-correlation field a lag map is showed and the variance preserving spectra are constructed for each area with relative higher cross-correlation. The spectral analysis points out the signal periodicity of both data. In addition, the time evolution of the zonal and meridional wind stress and alongshore currents are also plotted to the regions where higher cross-correlation was found.

For the first period of available data in the K1 mooring, the maximum cross-correlation between meridional wind and alongshore current is found between 22° and 36°S, that is approximately 1500-2000 km from the 11°S moorings (Figure 7.4). According to lag map in Figure 7.4, the zonal wind stress lag the alongshore current in 6 days, while the meridional wind stress lag the alongshore current in about 6.5 days. The spectral analysis show a dominant signal at approximately 20 days period for the zonal and meridional components of the wind stress (green and red lines, respectively) and also for alongshore current (blue line). Other significant signal is present at 11-14 days. In the plot of the time evolution of the zonal and meridional wind stress component, 6 and 6.5 days respectively lagged and the alongshore current at K1 a good data coupling exists, mainly during the austral winter months (JJAS) of 2002.

During 2003-2004 (Figure 7.5), more prominent wind stress signals are verified in 20 days, as well as in 11-14 days (red line), which agree with the variance spectrum of the alongshore current (blue line). The 10 days lagged meridional wind stress plus alongshore current plot indicate a good coupling during JJAS 2003 and MJ 2004. A good coupling also appear during late

summer-early austral fall (JFM) of 2004. The alongshore current was relatively good correlated with local zonal wind stress. The 5 days lagged local zonal wind stress plus alongshore current plot indicate also good coupling during austral winter in 2003.

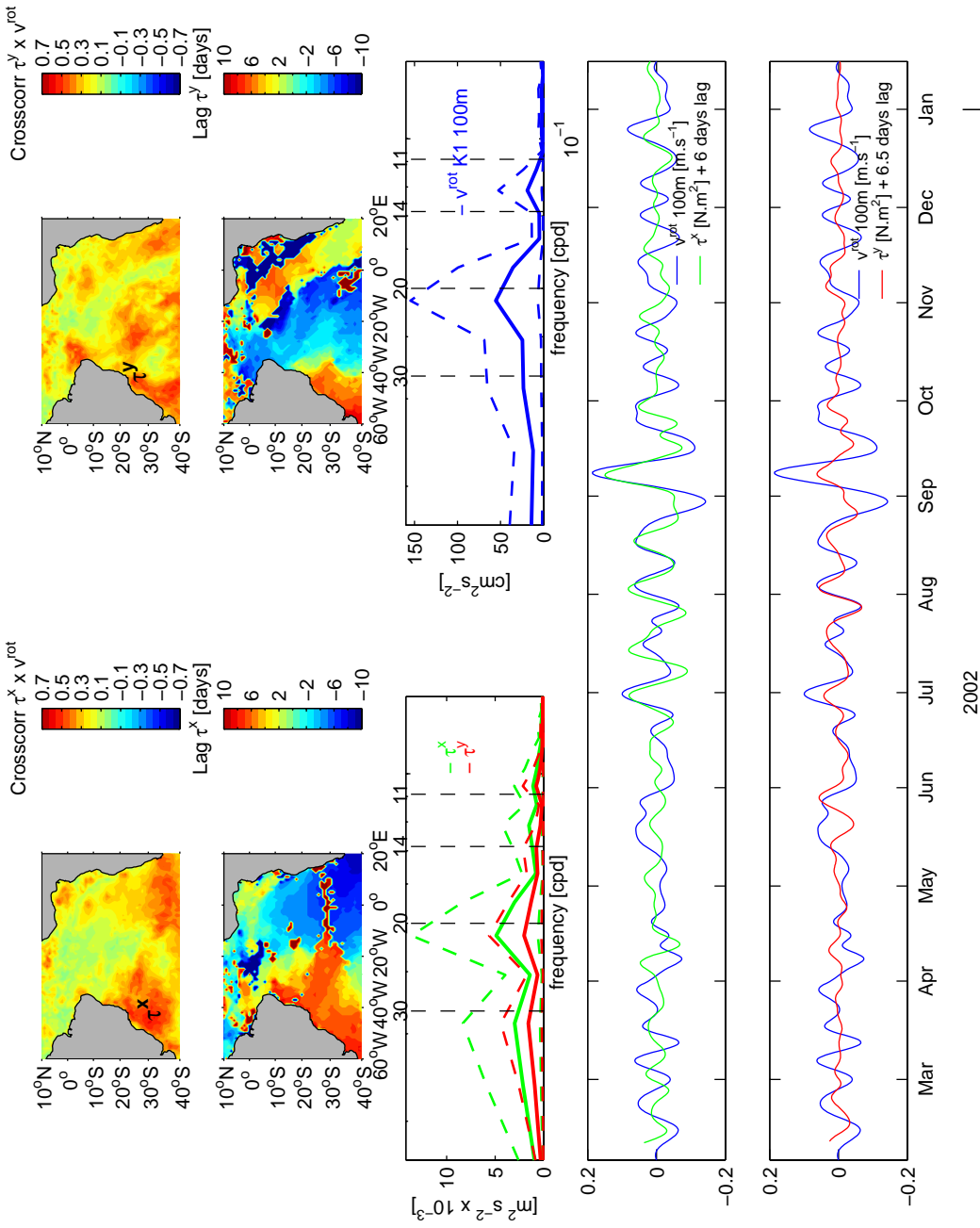


Figure 7.4. Cross-correlation between wind stress and currents at 100 m depth in K1 mooring, March/2002 to January/2003. The upper left panel shows cross-correlation between zonal wind stress and alongshore current; the upper right panel shows cross-correlation between meridional wind stress and alongshore current. Just below are the lags for zonal and meridional wind stress, respectively. At center, the variance spectra for both wind stress components (left) and alongshore current (right). The 95% confidence interval is ± 0.076 (dashed lines). At lower 2 panels, the 10-30 days bandpass filter data for zonal wind stress lagged 6 days with the alongshore current and, the 10-30 days bandpass filter data for meridional wind stress lagged 6.5 days with alongshore current.

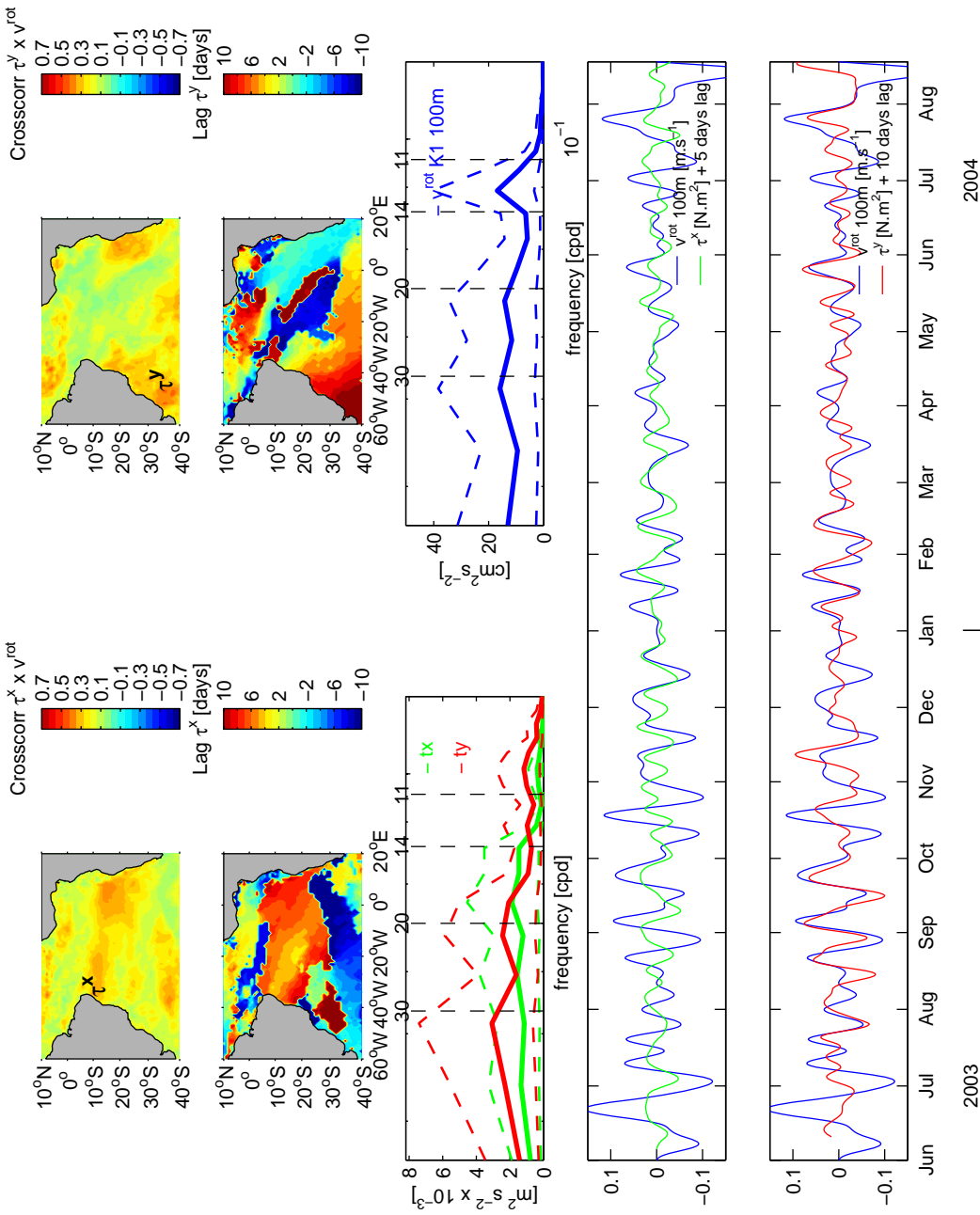


Figure 7.5. Cross-correlation between wind stress and currents at 100 m depth in K1 mooring, June/2003 to August/2004. The upper left panel shows cross-correlation between zonal wind stress and alongshore current; the upper right panel cross-correlation between meridional wind stress and alongshore current. Just below are the lags for zonal and meridional wind stress, respectively. At center, the variance spectrums for both wind stress components (left) and alongshore current (right). The 95% confidence interval is ± 0.067 (dashed lines). At lower 2 panels, the 10-30 days bandpass filter data for zonal wind stress lagged 6 days with the alongshore current and, the 10-30 days bandpass filter data for meridional wind stress lagged 10 days with alongshore current.

In the K2 position (Figure 7.6), the maximum cross-correlation between zonal and meridional wind stress and alongshore current have lags of 10 and 9 days, respectively. Dominant signals are found for the variance spectrum of wind stress at 14-20 days, 20-30 days as well as at 11-14 days, in correspondence with dominant signal of the alongshore current. The 9 days lagged meridional wind stress plotted together with the alongshore current in K2 confirms that these signals are synchronized during the second half (JJASON) of 2002 and 2003.

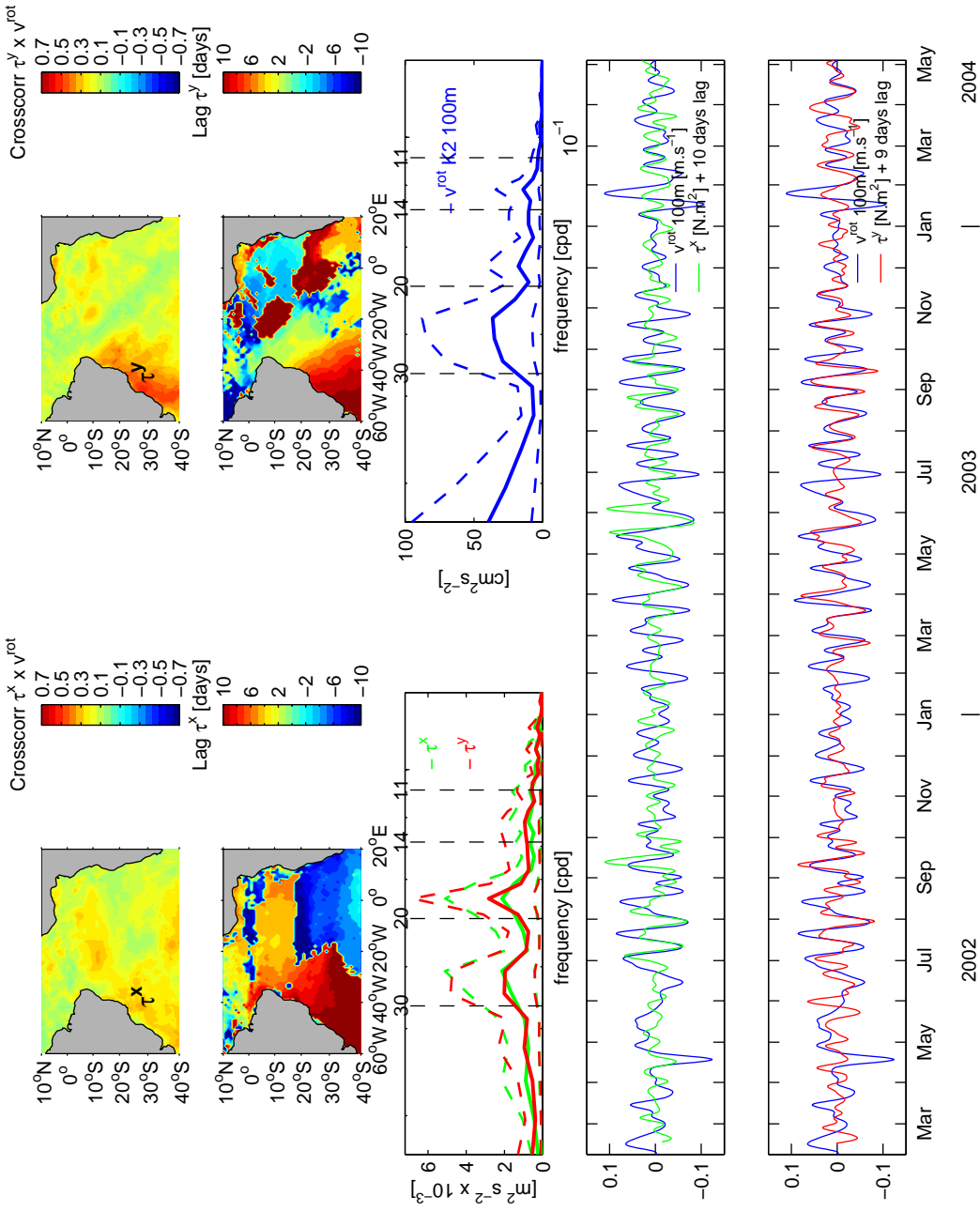


Figure 7.6. Cross-correlation between wind stress and currents at 100 m depth in K2 mooring, March/ 2002 to May/ 2004. The upper left panel shows cross-correlation between zonal wind stress and alongshore current; the upper right panel cross-correlation between meridional wind stress and alongshore current. Just below are the lags for zonal and meridional wind stress, respectively. At center, the variance spectrums for both wind stress components (left) and alongshore current (right). The 95% confidence interval is ± 0.05 (dashed lines). At lower 2 panels, the 10-30 days bandpass filter data for zonal wind stress lagged 10 days with the alongshore current and, the 10-30 days bandpass filter data for meridional wind stress lagged 9 days with alongshore current.

In the mooring K3 the maximum cross-correlation values between meridional wind stress and the alongshore current have lag of 7 days (Figure 7.7). Major signals are found for the variance spectrum of wind stress at 14-20 days, in correspondence with the signals found for the alongshore current. For the meridional wind stress the variance spectrum peaks about 11 and 18 days in connection with the alongshore current. The 7 days lagged meridional wind stress is plotted with alongshore current and a coupling is present during June 2003 to February 2004. From April to August 2004 synchronization also exists. The 5.5 days lagged local zonal wind stress plus alongshore current plot indicate also good coupling during austral winter and spring in 2003 and January to March 2004.

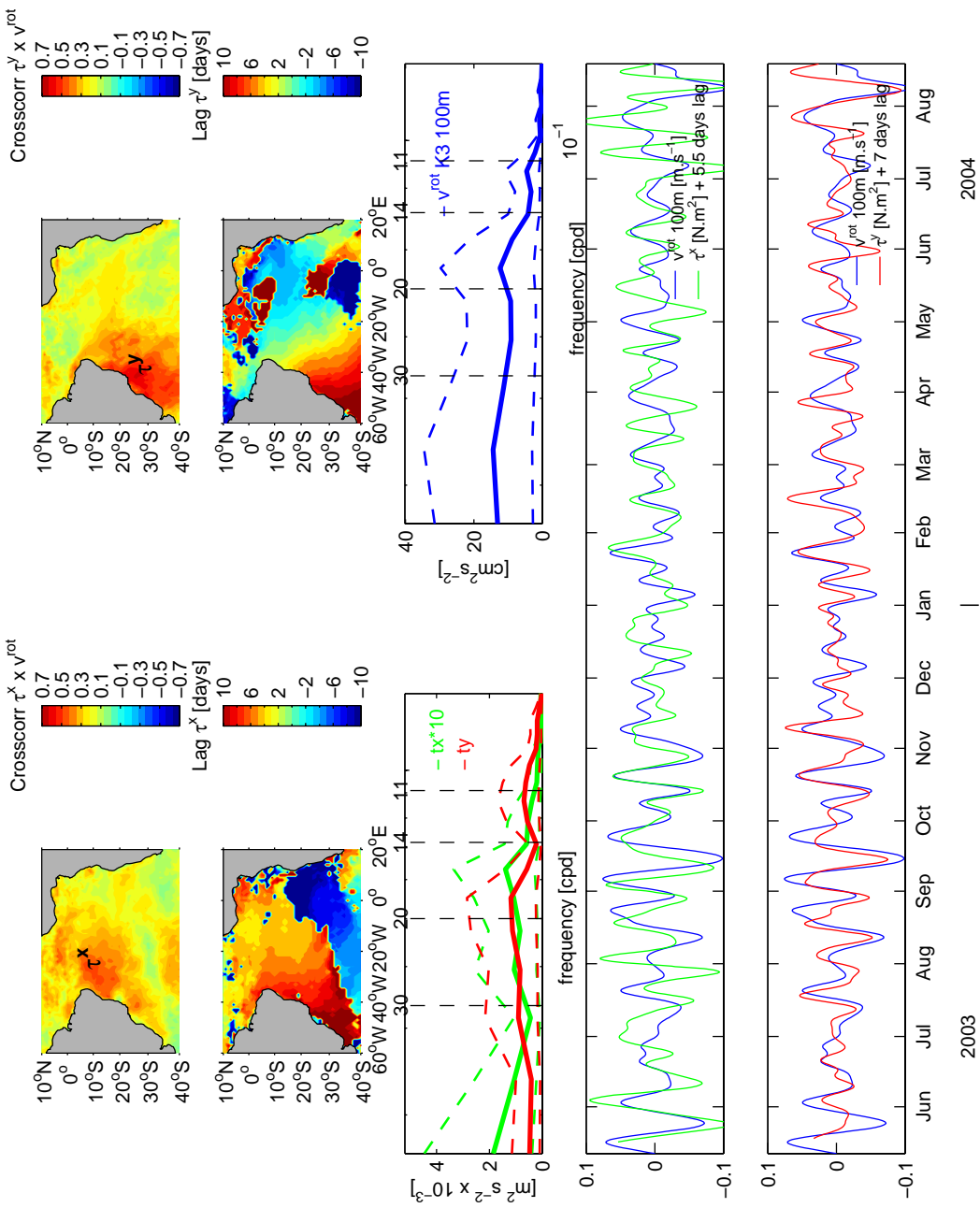


Figure 7.7. Cross-correlation between wind stress and currents at 100 m depth in K3 mooring, June/2003 to August/2004. The upper left panel shows cross-correlation between zonal wind stress and alongshore current; the upper right panel cross-correlation between meridional wind stress and alongshore current. Just below are the lags for zonal and meridional wind stress, respectively. At center, the variance spectrums for both wind stress components (left) and alongshore current (right). At lower 2 panels, the 10-30 days bandpass filter data for zonal wind stress lagged 5.5 days with the alongshore current and at last the meridional wind stress lagged 7 days with alongshore current. The 95% confidence interval is ± 0.065 .

The mooring K4 presents higher cross-correlation values for zonal and meridional wind stress and the alongshore current at about 36°S, with lag of 9.5 days (Figure 7.8). The variance spectrum indicates 11-14 days and a second signal is about 18 days for meridional wind stress as well as in the variance spectrum of alongshore current. The coupling is manifested between wind stress components and the alongshore current, for June to November 2002 and for September 2003 to April 2004.

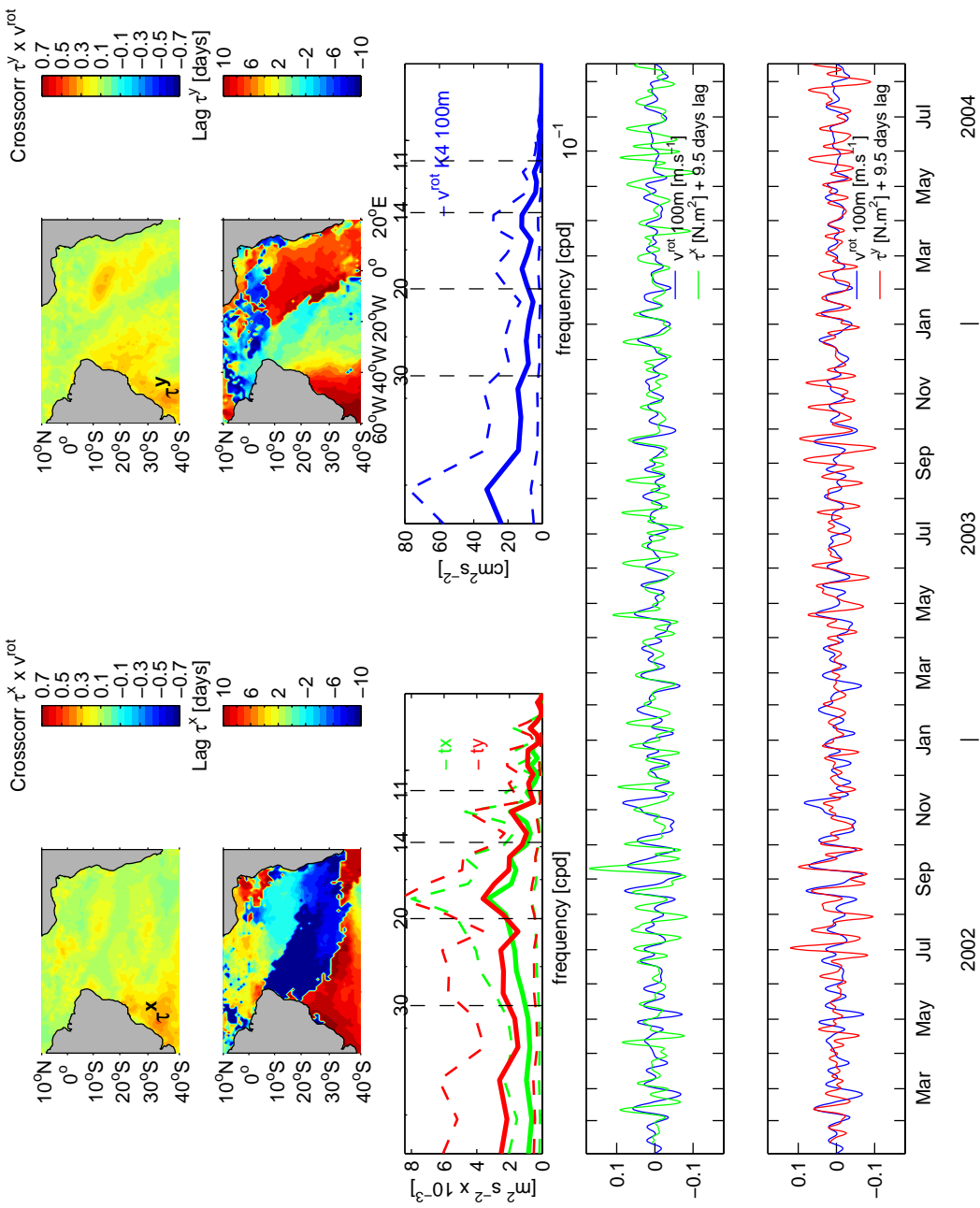


Figure 7.8. Cross-correlation between wind stress and currents at 100 m depth in K4 mooring, March/2002 to August/2004. The upper left panel shows cross-correlation between zonal wind stress and alongshore current; the upper right panel cross-correlation between meridional wind stress and alongshore current. Just below are the lags for zonal and meridional wind stress, respectively. At center, the variance spectra for both wind stress components (left) and alongshore current (right). The 95% confidence interval is ± 0.046 (dashed lines). At lower 2 panels, the 10-30 days bandpass filter data for zonal wind stress lagged 9.5 days with the alongshore current and at last the meridional wind stress lagged 9.5 days with alongshore current.

Table 7.1 summarize the cross-correlation results between meridional wind stress and alongshore current at 11°S. The coordinates of the maxima of the cross-correlation of the two data sets are indicated in Table 7.1. Also in Table 7.1 are displayed the distance to the mooring sites and lag periods. The values appearing in this table are clearly indicating a strong relation between the alongshore current signal at 11°S and a remote atmospheric forcing situated at about 23°S to 36°S.

Table 7.1. Cross-correlation between meridional wind stress and alongshore currents for moorings K1 to K4. The coordinates of the oceanic regions where the maxima cross-correlations occur are shown, as well as the corresponding distances (in km) and lag periods (in days) between these regions to 11°S and the respective wind and current signals.

<i>Mooring</i>	<i>Max. cross-correlation.</i>	<i>Position</i>	<i>Distance (km)</i>	<i>Lag period (days)</i>
<i>K1_I</i>	<i>0.55</i>	<i>25°S - 44°W</i>	<i>1554</i>	<i>6.5</i>
<i>K1_II</i>	<i>0.44</i>	<i>34°S - 47°W</i>	<i>2553</i>	<i>10</i>
<i>K2</i>	<i>0.52</i>	<i>28°S - 45°W</i>	<i>1887</i>	<i>8.5</i>
<i>K3</i>	<i>0.64</i>	<i>33°S - 48°W</i>	<i>2442</i>	<i>7</i>
<i>K4</i>	<i>0.39</i>	<i>36°S - 50°W</i>	<i>2775</i>	<i>9.5</i>

7.5. Cross-correlation between wind stress curl and crossshore and alongshore currents

In this section is analyzed the spatial and temporal coupling of the alongshore intraseasonal signals and wind stress curl forcing. The Figure 7.9 shows the spatial pattern of the cross-correlation between the wind stress curl with the crossshore and alongshore components of currents.

The upper panel at left shows the cross-correlation between the wind stress curl and crossshore component of currents. The upper panel at right shows the cross-correlation between the wind stress curl and alongshore component of currents. Just below are the lag maps for respective cross-

correlations. At center are the spectrums of wind stress curl for the position 1 (p1) and position 2 (p2), and at right the energy spectrum of the currents. In the two lower panels are plotted the time series.

The cross-correlation fields between wind stress curl and currents do not have a good coupling. The cross-correlation was calculated for moorings K1 to K4 (not showed here) but the results were not in synchronization relative to the alongshore component of wind stress, described in the last section. The next Figure is an example of correlation between wind stress curl and crossshore and alongshore component of the K1 mooring. The best correlation was found between wind stress curl and the currents at mooring K1. The others mooring measurements were weaker and sparse coupling.

For mooring K1, from June 2003 to August 2004, the maximum cross-correlation is positioned close to coast, south of 20°S (Figure 7.9). The wind stress curl lag the crossshore current in 6.5 days and the alongshore current in 2 days. The wind stress curls positions 1 and 2, where maximum cross-correlation was found, shows a spectrum which peaks at band of 11 and 20 days. These energy maxima are similar with the energy spectrum of currents in K1.

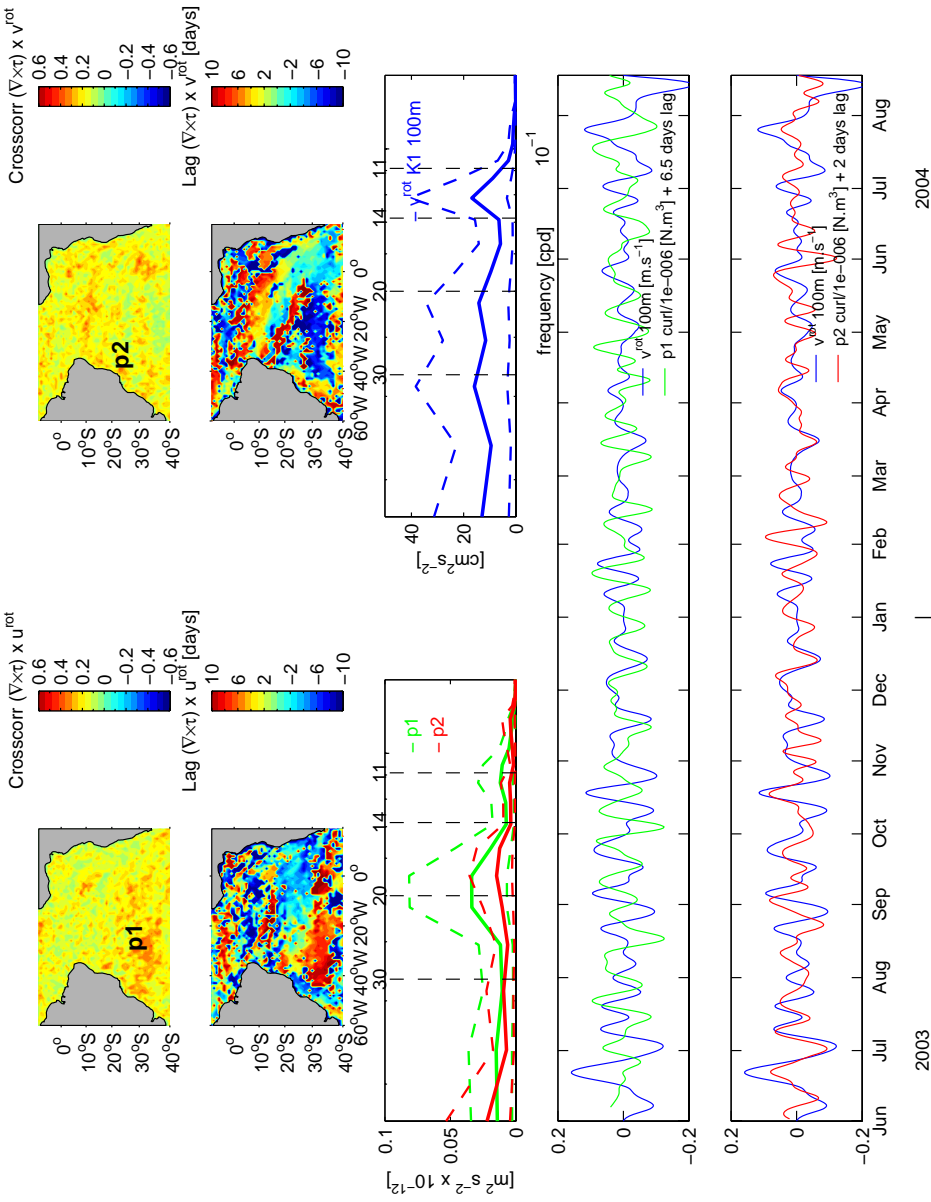


Figure 7.9. Cross-correlation between wind stress curl and currents at 100 m depth in K1 mooring, June/2003 to August/2004. The upper left panel shows cross-correlation between wind stress curl and crossshore current; the upper right panel is the cross-correlation between wind stress curl and alongshore current. Just below are the lags between curl and the crossshore and alongshore currents, respectively. At center, the variance spectra for wind stress curl (left) and alongshore current (right). The 95% confidence interval is ± 0.067 (dashed lines). At lower 2 panels, the 10-30 days bandpass filter data for wind stress curl lagged 6.5 days with the crossshore current and the wind stress curl lagged 2 days with alongshore current.

7.6. Cross-correlation between wind stress curl and Chlorophyll concentration

Many works use physical data such as sea level anomaly (SLA), temperature, and wind and surface currents, to examine plausible physical processes responsible for surface chlorophyll changes in regions where the seasonal variability is significant. For example, Messié and Radenac (2006) related the seasonal chlorophyll signal to the seasonal physical forcing. They found that the chlorophyll maximum coincides with the maximum North Equatorial Counter Current velocity and occurs during the upwelling favorable phase of the wind stress curl. The purpose here is use the chlorophyll data to examine if its variability corresponds to those from wind stress, wind stress curl and currents.

Daily chlorophyll concentration was averaged for the area comprehended from 22°S to 26°S and 43°W to 48°W. The gaps were identify and interpolated to obtain a time series comparable to wind stress and curl data. The area was chosen based where higher cross-correlation between the wind stress and current measurements (Figures 7.4-7.8) was found. For the same area the local wind stress curl data are averaged. The time series of chlorophyll concentration are showed (Figure 7.11 a) with a 40 hours filter to compare with wind stress curl. The variance spectrum for wind stress curl presents a dominant peak at 14 days. For the chlorophyll concentration the variance spectrum shows a dominant signal at 18 days with a second peak at 14 days. Both time series are best correlated (negative) with 9 days lag. A cross-correlation between meridional wind stress and the chlorophyll concentration was found weaker. The time series of meridional wind stress and wind stress curl with the chlorophyll data are plotted with a 10-30 days bandpass (Figures 7.11 d, e). It is expected that the chlorophyll concentration presents positive peaks when wind stress curl is negative. It is more evident in time series from April to December of 2004.

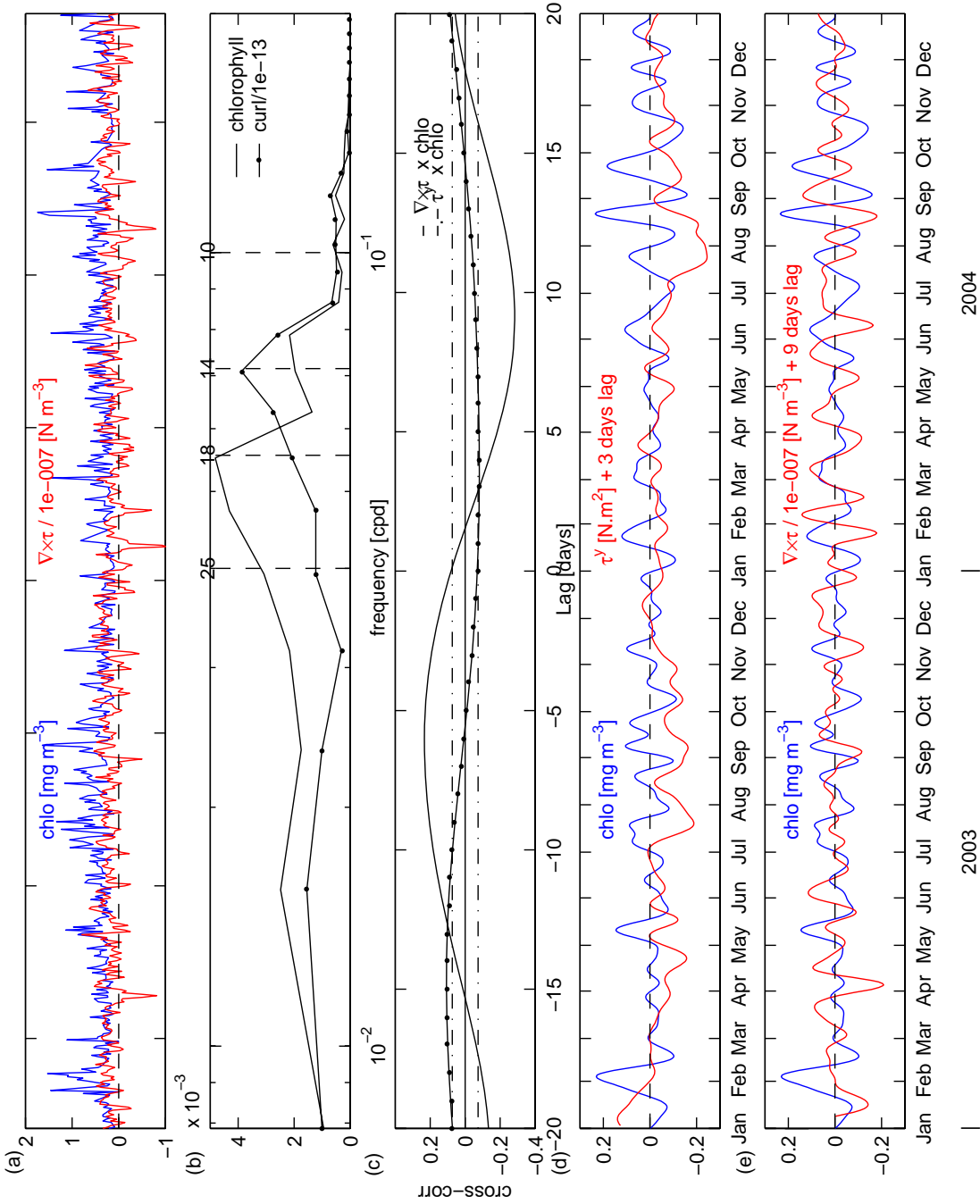


Figure 7.1.1. a) Time series of chlorophyll (mg m⁻³) and wind stress curl (N m⁻³) for 2003-2004; b) variance preserving spectrum of chlorophyll and wind stress curl; c) cross-correlations for wind stress curl and chlorophyll (full line) and for alongshore wind stress and chlorophyll (point line); d) 10-30 days bandpass for alongshore wind stress and chlorophyll; e) 10-30 days bandpass for wind stress curl and chlorophyll.

The cross-correlations between alongshore wind stress and also the wind stress curl with the Chlorophyll concentration were weak. The satellite period is about 2 days and an interpolation was necessary. Perhaps better results could be found for shorter time with quasi-continuous data measurements. In our case the correlation about 0.2 for the wind stress curl was not a good coupling. Besides these results, the behavior of the wind stress curl with chlorophyll concentration for 2004 appears to be reasonable.

In the same way as the variability in the currents at 11°S and the remote wind stress were related, the goal is now, to relate the chlorophyll concentration with either of those signals. Both currents and wind stress signals have variability within a range of 14-30 days and the variance preserving spectrum for the chlorophyll concentration presents a maximum at 18 days.

7.7. Discussion

The results obtained in this chapter support that the propagation of Coastal Trapped Waves along the Brazilian coast is a suitable mechanism for explaining the correlation between the meridional wind stress at the latitudes range 22°S-36°S and the alongshore currents at 11°S.

The meridional wind stress component located in the area located between 22°S to 36°S along the Brazilian coast (40°W to 50°W), where higher cross-correlation was found, are averaged and cross-correlated here with the section of currents at 11°S (K1-K4 moorings) in Figure 7.9. The higher correlations are confined to NBUC core, reaching about 250 m depth and decreasing gradually towards the open ocean (Figure 7.12). These higher cross-correlation, found at the NBUC axis, show lags of 8 to 10 days.

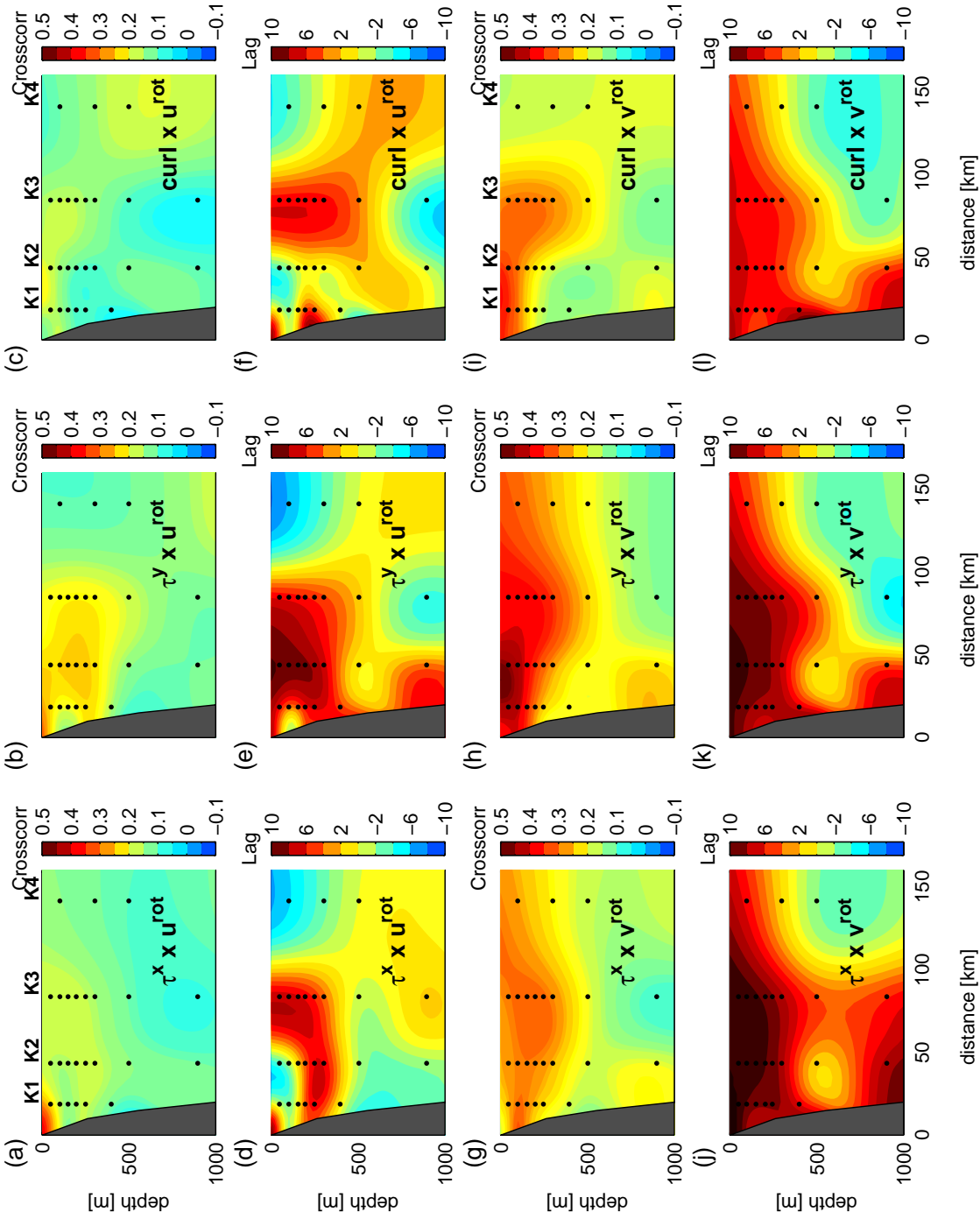


Figure 7.12. Cross-correlation at 11° S between: a) zonal wind stress and crossshore current, b) meridional wind stress and crossshore current, c) curl and crossshore current, g) zonal wind stress and crossshore current, h) meridional wind stress and alongshore current, i) curl and alongshore current. Lag (days) between: d) zonal wind stress and crossshore current, e) meridional wind stress and crossshore current, j) zonal wind stress and alongshore current, k) meridional wind stress and alongshore current, l) curl and alongshore current.

According to EOF analysis, more than 90% of the variability is verified between 50 and 300 m depth in K1 and K2 moorings, within the 14-60 days periods. For K3 mooring, the dominant mode of variability corresponds to 63% of the variability at 100m depth, with a first variance mode of 14-30 days period (see Table 4.1, Chapter 4). The second mode in K3 is also significant with 34% of the total variability and its maximum variance is at 14 days between 300 and 500m depth. The thermocline at 11°S is located at about 65m depth (Schott et al., 2005; von Schuckmann, 2006), which means that the main variability modes at this latitude are positioned just underneath in a zone with strong gradients of density and temperature, which is potentially favorable to internal Kelvin waves propagation.

There are three main types of topographically trapped waves, the Kelvin waves, the shelf waves and edge waves (Mysak, 1980). A Kelvin wave is a low-frequency gravity wave. Kelvin waves occur where the deflection caused by the Coriolis force is either constrained by coastlines or zero at the equator. The amplitudes of these waves are several tens of meters along the thermocline region, and their lengths are thousands of kilometers.

The internal coastal trapped Kelvin wave can be generated by an abrupt change in the winds and depend on the existence of a coast against which they can lean. For all correlation results shown here, the maximum cross-correlations are found for the near shore wind data between 22°S and 36°S, a region along the Brazilian coast usually referred in the literature as the Southeast Brazil Bight - SBB (Castro Filho, 1985; Stech and Lorenzzetti, 1992; Campos et al., 1995; Campos et al., 1999; Cirano and Campos, 1996). The northernmost boundary of this area corresponds to a relatively narrow shelf close to Cabo Frio (22°S), where an abrupt change in coastline direction is observed (see Figure 3.1). The change in the coastline orientation at Cabo Frio induces a meandering pattern.

As already discussed in the Chapter 2, the Brazilian coast, mostly its southern portion, is often under the influence of synoptic and mesoscale meteorological systems, which induce significant disturbances in the ocean,

such as mean sea level changes, generations of surface waves and drive currents. Frontal systems propagate typically of southwest to northeast along the coast of Brazilian and they are more frequent between 20°S and 35°S, with frequencies of 3-4 times a month (Rodrigues et al., 2004). These frontal systems propagate from SW to NE at an average speed of 500 km day⁻¹, crossing the region in 2 days (Stech and Lorenzetti, 1992). Furthermore, this drastic change in the wind direction is the main forcing for CTWs. We propose here that the combination between local wind stress variability and the abrupt change in coastline direction reveal the SBB as a privileged locus for CTW generation along the Brazilian shore. In this work, the distance between the currents at 11°S and the area where high cross-correlation was found is about 1600-2700 km. The ratio between these distances to their correspondent lags periods give us equatorward propagation wave speeds of 285±63 km.day⁻¹ along the Brazilian shore.

7.8. Summary

In this chapter cross-correlation and EOF analysis was applied to currents, wind stress and sea level time series data, along the Brazilian shore in order to investigate the relation between the intraseasonal oceanic variability observed at 11°S, and remote atmospheric forcing.

The high-frequency variability is a dominant mode at the western flank of the NBUC. Significant signals at periods between 10-14 and 14-30 days have been detected in the spectral analysis of current meters at surface as well as at deeper measurements, mainly at the western flank of the NBUC. The high-frequency signals are evident mostly close to coast, at mooring K1, which means that these fluctuations are confined to the near boundary region.

Theoretical models propose that CTW are generated by the alongshore component of the wind stress (Allen, 1980; Brink, 2006). These studies indicate that the wind is generally more effective for generating the first wave mode, and that this mode has normally the largest coastal sea-level signal.

Higher order modes are preferentially damped by bottom friction, so most of the studies of CTWs have assumed that the first mode is dominant (Church and Freeland, 1987).

Daily sea level measurements of local stations along the Brazil coast were also used to investigate its signal variability, since it indicates the existence of coastal waves. Intraseasonal fluctuations exist in the sea level time series, consistent with those of the corresponding wind stress and currents oscillations. Good coupling is also found between the sea level data meridional wind stress, mainly in austral winter and spring.

The higher values of correlation are mainly found in austral winter and spring, where the 10-30 days band pass filter for both meridional wind stress and alongshore currents reveal signals with lags about 8 to 10 days and with an alongshore propagation speed of $285 \pm 63 \text{ km.day}^{-1}$.

Besides, several features of the alongshore currents with wind stress oscillations suggest that the signals found propagate equatorward as a coastal wave forced by remote meteorological influences. The features are: The wind stress field between 22° - 36° S, close to Brazilian coast, produces an energy input into the ocean and origins a response of the alongshore current at 11° S. The wind stress at these latitudes presents high variability of wind direction, caused by a route of atmospheric frontal systems.

The wind stress, alongshore currents and sea level pointed out signals with the same periods, which are more restricted at bands of 11-14 days and 14-30 days. A well defined lagged correlation structure of the alongshore currents exists, suggesting an equatorward propagation of events located between 22° - 36° S. These signals propagate equatorward, with the coastline at left, and have an alongshore propagation speed consistent with predictions of wave propagation processes found in Enfield and Allen (1980). The spectral analysis of the first mode for K1 mooring, obtained by an EOF analysis, shows a dominant mode of variability at 14 and 30 days. This first mode represents 90% of the variability in K1 and the maximum of variability is located at 300 m depth. The second mode EOF in K3 identified a signal at 300 to 500m depth and the cross-correlation between the wind stress at 20° -

36°S and the section at 11°S evidence a good correlation in K3 at these depths. Additionally, the main correlations are found at the core of the NBUC and at K3 position, from the surface to about 300 m depth. Furthermore, the system BC/IWBC velocity field between 22°-23°S, where the forcing for the intraseasonal signals of the currents were found, is dominated (75-80%) by the first baroclinic mode over the continental slope (Silveira et al., 2004). Additionally, this area has stronger density stratification in austral winter (Campos et al., 2000), which can support baroclinic internal Kelvin waves.

Chapter 8

8. Summary and perspectives

The South Equatorial Current is the major pathway by which water of South Atlantic origin is imported into the tropical Atlantic Ocean (Stramma et al., 2005), transporting climatic signals toward the western boundary of the South Tropical Atlantic. This current gives origin to the North Brazil Undercurrent, which is an important crossroads of inter-hemispheric transfer of warm and cold water masses (Bourlès et al., 1999; Schott et al., 2005). The North Brazil Undercurrent is the upper limb of the MOC transporting warm surface waters northward to close the thermohaline overturning cell.

The main goal of this thesis was to investigate the seasonal and intraseasonal variability of the western boundary regime of the South Atlantic. In order to achieve the proposed goal several strategies were developed:

- a. The analysis of the structure of the currents at 11°S close to Brazilian coast, linking with the seasonal and intraseasonal variability of the North Brazil Undercurrent;

- b. The use of a climatologic oceanic modeling and an ocean reanalysis database as tools to confirm the theories about the dynamic of the western boundary regime in the South Atlantic. As suggested by recent literature, the seasonal variability of the bifurcation of the NBUC is coupled to large scale mechanism such as the seasonal migration of the sSEC along the eastern Brazilian edge;
- c. The investigation of the wind stress variability as an important forcing for the intraseasonal variability of the western boundary regime at 11°S. The higher frequencies are studied and linked to its main forcing, the wind stress, aiming to explain coastal wave theories.

The mooring section at 11°S shows dominant fluctuation with a period about two to three months in the NBUC core, about 50 km from the coastline. At the western flank of the NBUC biweekly signals are the dominant modes of variability, but those amplitudes scale down with increasing distance from the NBUC current core. The dominant variability at NADW (EOF of 99% in K3 and 98% in K4) is 2 months. The PCA shows weak coupling between currents and temperature at K4 mooring (PCA = 34%, Table 4.1). On the other hand, the temperature is strongly coupled to the velocity current at the core of the DWBC for the first year of K3 mooring data, which reveals that these two fields are in the same phase each two months. The intensity of coupling between alongshore currents and temperature at K3 mooring position is 60% at 2000 m depth. It means that the currents at the core of the NADW are responsible for 60% of the interhemispheric heat transport along this level. This coupling can be linked to the bowl-shaped temperature anomaly found in eddies at the DWBC core (as also indicated in ROMS simulations).

In the Chapter 6 a climatological regional ocean model with 1/12° horizontal resolution was used to identify the main velocities and transport structures close to Brazilian coast. Numerical transports and currents results were compared to ocean measurements at 11°S. The ROMS was able to reproduce the main features of the circulation observed from CLIVAR

measurements. For example, the model was used to study the seasonal variability of the sSEC bifurcation. An important characteristic found in the simulated sSEC divergence is that it shifts southward as ocean depth increases: it varies from 8°S at 100 m depth to about 20°S at the 500 m depth. At 200 m depth the ROMS model results indicate that the sSEC bifurcates at 13°S from September to January and at 19°S in May-July. The sSEC at 200 m depth shows a meander characteristic in austral summer and is stronger than in austral winter. In austral summer, south of sSEC bifurcation an anticyclonic eddy attached to coast between 12° and 15°S exists. Furthermore, monthly averages of 47 years of SODA reanalysis also indicated the seasonal variability of the sSEC found in ROMS climatology. The results from SODA reanalysis confirm the seasonal migration of the sSEC, with northernmost position in austral summer and southernmost position in austral winter. Comparing results of wind stress curl (Chapters 4 and 5), ROMS model results and SODA reanalysis results (Chapter 6), a synchronized meridional variability was found. The zero line of wind stress curl, such as the ROMS simulation and the climatology from SODA, indicated the same meridional excursion with the southernmost position of the sSEC in austral winter.

The model simulations also reproduced the intensification of the NBUC and the southernmost position of the sSEC bifurcation in austral winter. During austral summer the NBUC is weaker while the sSEC bifurcation has its northernmost position. Associated to the weakness of the NBUC was identified an anticyclonic eddy attached to Brazilian coast, between 12°-15°S at 200 m depth, which reduces the northward transport of the NBUC in austral summer. The sSEC bifurcation at 500 m depth is at 20°S around the Vitória-Trindade Ridge. Eddies structures along the Brazilian coast are stronger than in austral winter, such as at 200 m depth. The sSEC bifurcates in two branches separated by cyclonic and anticyclonic eddies attached to coast at 20°S.

The NBUC and the DWBC represent the main path to interhemispheric exchange of the MOC. The outputs from ROMS model evidenced that higher

temperature anomalies are concentrated into eddies at the DWBC level. The results show a strong coupling between high velocities from eddies and a high temperature into these mesoscale structures. According to simulations, the upstream DWBC between 7°S and 10°S is reinforced during austral winter (August), enhancing eddies generation. The ROMS simulations indicate that the DWBC breaks up into eddies reproducing anticyclonic structures with the same order of magnitude of the average eddy scales estimated from moorings data (Dengler et al., 2004). On the other hand, the simulated upstream DWBC flow is clearly reduced during the austral summer (February), when less well defined eddies are present.

Another issue from numerical modeling is the indication of a well formed NBUC counterflow just offshore of the NBUC at 11°S, with more intense flow in November and less intense in July, when no retroflection of the NBUC was found. The SODA reanalysis data analyzed in a horizontal section at 500 m depth indicated a retroflection in the NBUC from January to March, which reaches at 10°S such as in Schott et al. (2005). In May to September there is another contribution for the counterflow. It would be an explanation that the westward flow from the deep cSEC could shift southward and feed this NBUC counterflow.

The intraseasonal variability at higher frequencies found in the upper South Atlantic western boundary (Chapter 4) was studied altogether with wind stress data (Chapter 5). The signals detected at periods between 10-14 and 14-30 days in both time series of alongshore currents and wind stress were correlated (Chapter 7). Additionally three daily sea level gauges were also correlated as well as chlorophyll concentration data. The higher values of correlation were in austral winter and spring, where the 10-30 days band pass filter for both meridional wind stress and alongshore currents at 11°S reveal signals with lags about 8 to 9 days and with an alongshore speed varying of $285 \pm 63 \text{ km.day}^{-1}$, propagating equatorward as a coastal wave.

All these results are very encouraging. For example, this is the first time that a high-resolution ($1/12^\circ$) regional modeling approach is used for investigating the western tropical south Atlantic boundary and in particular

the sSEC divergence area off Brazil. The ROMS reproduces the main features of the mean NBUC and DWBC transports at different seasons near Brazilian edge. Numerical results were confirmed by moorings measurements and Principal Component Analysis, giving confidence in the simulated seasonal migration of the sSEC, which appears as a powerful justification to explain the seasonal cycle of the NBUC at 11°S. So, the verified model adjustment to offshore field data is promising. These results can be extensively used in the future as boundary conditions for smaller-scale shelf sea modeling as a way to evaluate the remote influences of the open ocean forcing over the dynamics of the still little studied coastal seas neighboring the northeastern Brazilian region.

Concerning the intraseasonal variability, results herein indicated that the currents signals at 11°S section are forced by remote winds between 22°-36°S acting close to Brazilian coast, where the higher variability of wind stress kinetic energy are found. Furthermore, the BC/IWBC cinematic field between 22°-23°S is dominated (75-80%) by the first baroclinic mode over the continental slope (Silveira et al., 2004), where strong density stratifications are present in austral winter (Campos et al., 2000). These findings can support the Southeast Brazil Bight as a cradle to internal Kelvin waves. Complementary, the results found in this thesis point out to Coastal Trapped Waves (CTW) as a suitable mechanism for explaining the lagged correlation between the meridional wind stress at the latitudes range 22°-36°S and the alongshore currents at 11°S. We suggest here the CTW as a key mechanism in the dynamics of the western boundary regime of the South Atlantic. A full description, however, would require a considerable effort on the characterization of the stratification and bottom topography. One fruitful direction can be the wavelet correlation analysis between current and wind stress data. Another privileged way can be an extensive use of CTW numerical modeling approaches.

References

- Allen, J. S., 1980. Models of wind-driven currents on the continental shelf. *Annual Review of Fluid Mechanics* 12, 389 - 433.
- Battisti, D. S., Hickey, B. M., 1984. Application of remote wind-forced coastal trapped wave theory to the Oregon and Washington coasts. *Journal of Physical Oceanography* 14, 887 - 903.
- Bourlès, B., Molinari, R.L., Jonhs, E., Wilson, W.D., Leaman, K.D., 1999. Upper layer currents in the western tropical North Atlantic. *Journal of Geophysical Research* 104, 1361-1375.
- Brink, K. H., 1982. A comparison of long coastal trapped wave theory with observations off Peru. *Journal of Physical Oceanography* 12, 897 - 913.
- Brink, K. H., Stuart, D. W., Van Leer, J. C., 1984. Observations of the coastal upwelling region near 34°30'N off California: Spring 1981. *Journal of Physical Oceanography* 14, 378 - 391.
- Brink, K. H., 1989. Evidence for wind-driven current fluctuations in the western North Atlantic. *Journal Geophysical Research* 94, 2029 - 2044.
- Brink, K. H., 1991. Coastal-trapped waves and wind-driven currents over the continental shelf. *Annual Review of Fluid Mechanics* 23, 389 - 412.
- Camayo, R., Campos, E. J. D., 2006. Application of wavelet transform in the study of coastal trapped waves off the west coast of South America. *Geophysical Research Letters* 33, L22601, 1-5.
- Campos, E. J. D., Goncalves, J. E., Ikeda, Y., 1995. Water mass characteristics and geostrophic circulation in the south Brazil Bight - summer of 1991. *Journal of Geophysical Research* 100(9), 18537 - 18550.
- Campos, E. J. D., Piola, A. R., Miller, J. L., 1999. Water mass distribution on the shelf and shelf-break upwelling in the southeast Brazil Bight. *Annals*

References

- of the 10th Symposium on Global Change Studies – American Meteorological Society*, 9 - 12.
- Campos, E. J. D., Velhote, D., da Silveira, I. C. A., 2000. Shelf break upwelling driven by Brazil Current cyclonic meanders. *Geophysical Research Letters* 27, 751 - 754.
- Castelão, R. M., Campos, E. J. D., Miller, J. L., 2004. A modelling study of coastal upwelling driven by wind and meanders of the Brazil Current. *Journal of Coastal Research* 20, No. 3, 662 - 671.
- Castelão, R. M., Barth, J. A., 2006. Upwelling around Cabo Frio, Brazil: The importance of wind stress curl. *Geophysical Research Letters* 33, L03602, 1 - 4.
- Castro Filho, B. M., 1985. Subtidal response to wind forcing in the South Brazil Bight during winter. Ph.D. Thesis. University of Miami, USA, 211pp.
- Castro, B. M., Miranda, L. B., 1998. Physical oceanography of the western Atlantic continental shelf located between 4° N and 34° S. In: Robinson, A. R. and Brink, K. H. *The Sea* 11. John Wiley, New York, 209 - 251.
- Cavalcanti, I. F. A., Kousky, V. E., 2003. Climatology of South American cold fronts. In: VII International Conference on Southern Hemisphere Meteorology and Oceanography, Wellington, New Zealand, 2003.
- Chelton, D. B., Schlax, M. G., Witter, D. L., Richman, J. G., 1990. Geosat altimeter observations of the surface circulation of the Southern Ocean. *Journal of Geophysical Research* 95(C10), 17877 - 17903.
- Church, J. A., Freeland, H. J., 1987. The energy source for the coastal trapped waves in the Australian coastal experiment region. *Journal of Physical Oceanography* 17, 289-300.
- Cirano, M., Campos, E. J. D., 1996. Numerical diagnostic of the circulation in the Santos Bight with COROAS hydrographic data. *Brazilian Journal of Oceanography* 44(2), 105-121.
- Cirano, M., Mata, M. M., Campos, E. J. D., Deiró, N. F. R., 2006. A circulação oceânica de larga-escala na região oeste do Atlântico Sul com base no modelo de circulação global OCCAM. *Brazilian Journal of Geophysics* 24(2), 209 – 230.

References

- Da Silva, A. M., Young, C. C., Levitus, S., 1994. Atlas of surface marine data 1994, vol. 1, algorithms and procedures, NOAA Atlas Nesdis 6. US Department of Commerce, NOAA, Nesdis, Usa, 74pp.
- Defant, A., 1941. Die absolute Topographie des physikalischen Meeresniveaus und der Druckflächen, sowie die Wasserbewegungen im Raum des Atlantischen Ozean. Wissenschaftliche Ergebnisse Deutschen Atlantischen Expedition auf dem Forschungs und Vermessungsschiff. "Meteor" 1925-1927, 6(2), 191-260.
- Dengler, M., Schott, F. A., Eden C., Brandt, P., Fischer, J., Zantopp, R., 2004. Break-up of the Atlantic deep western boundary current into eddies at 8°S. *Nature* 432, 1018–1020.
- Enfield, D. B. and Allen, J. S., 1980. On the structure and dynamics of monthly mean sea level anomalies along the Pacific Coast of North and South America. *Journal of Physical Oceanography* 10, 557 - 578.
- Enfield, D. B., 1987. The Intraseasonal oscillation in eastern Pacific sea levels: How is it forced? *Journal of Physical Oceanography* 17, 1860 - 1876.
- Fennel, W., Lass, H. U., 2007. On the impact of wind curls on coastal currents. *Journal of Marine Systems* 68, 128 - 142.
- Fischer, J., Schott, F.A., 1997. Seasonal transport variability of the deep western boundary current in the Atlantic. *Journal of Geophysical Research* 102, 27751-27769.
- Gordon, A. L., 1986. Inter-ocean exchange of thermocline water. *Journal of Geophysical Research* 91, 5013-5046.
- Gordon, A. L., Greengrove, C. L., 1986. Geostrophic circulation of the Brazil-Falklands confluence. *Deep Sea Research I* 33, 573-585.
- Grodsky, S. A., Carton, J. A., 2003. The intertropical convergence zone in the South Atlantic and the equatorial cold tongue. *Journal of Climate* 16, 723-733.
- Haidvogel, D. B., Arango, H. G., Hedstrom, K., Beckmann, A., Malanotte-Rizzoli, P., Shchepetkin, A. F., 2000. Model evaluation experiments in the North Atlantic basin: simulations in nonlinear terrain-following coordinates. *Dynamics of the Atmosphere and Oceans* 32, 239-281.

References

- Harrison, D. E., 1989. On climatological monthly mean wind stress and wind stress curl fields over the world ocean. *Journal of Climate* 2, 57-70.
- Jolliffe, I. T., 2002. Principal component analysis. Springer. New York.
- Kayano, M. T., Rao, V. B., Andreoli, R. V., 2005. A review of short-term climate variability mechanisms. *Advances in Space Research* 35, 843-851.
- Large, W. G., McWilliams, J. C., Doney, S. C., 1994. Oceanic vertical mixing: a review and a model with a nonlocal boundary layer parametrization. *Reviews in Geophysics* 32, 363-403.
- Lemos, C. F., Calbete, N. O., 1996. Sistemas que atuaram no Brasil de 1987 a 1995. Climanálise Especial, Edição comemorativa de 10 anos. MCT/INPE-CPTEC.
- Lumpkin, R., Garzoli, S. L., 2005. Near-surface circulation in the tropical Atlantic Ocean. *Deep-Sea Research I* 52, 495-518.
- Lutjeharms, J. R. E., Penven, P., Roy, C., 2003. Modelling the shear edge eddies of the southern Agulhas Current. *Continental Shelf Research* 23, 1099-1115.
- MacCready, P., Geyer, G. R., 2001. Estuarine salt flux through an isohaline surface. *Journal of Geophysical Research* 106, 11629-11637.
- Malanotte-Rizzoli, P., Hedstrom, K., Arango, H. G., Haidvogel, D. B., 2000. Water mass pathways between the subtropical and tropical ocean in a climatological simulation of the North Atlantic. *Dynamics of the Atmosphere and Oceans* 32, 331-371.
- Marchesiello, P., McWilliams, J.C., Shchepetkin, A., 2001. Open boundary conditions for long-term integration of regional oceanic models. *Ocean Modelling* 3, 1-20.
- Meacham, S. P., 2000. Low-frequency variability in the wind-driven circulation. *Journal of Physical Oceanography* 30, 269-293.
- Messié, M., Radenac, M-H., 2006. Seasonal variability of the surface chlorophyll in the western tropical Pacific from SeaWiFS data. *Deep-Sea Research I* 53, 1581-1600.
- Miranda, L. B., 1985. Forma de correlação T-S de massa de água das regiões costeira e oceânica entre o Cabo de São Tomé (RJ) e a Ilha de São

References

- Sebastião (SP), Brasil. Boletim Mensal do Instituto Oceanográfico, São Paulo, 33(2), 105-119.
- Miyama, T., McCreary Jr., J. P., Sengupta, D., Senan, R., 2006. Dynamics of biweekly oscillations in the equatorial Indian Ocean. *Journal of Physical Oceanography* 36, 827-846.
- Molinari R. L., 1983. Observations of near-surface currents and temperature in the central and western tropical Atlantic Ocean. *Journal of Geophysical Research* 88, 4433-4138.
- Münchow, A., 2000. Wind stress curl forcing of the coastal ocean near Point Conception, California. *Journal of Physical Oceanography* 30, 1265-1280.
- Mysak, 1980. Topographically trapped waves. *Annual Review of Fluid Mechanics* 12, 45-76.
- Oliveira, A. S., 1986. Interações entre sistemas frontais na América do Sul e convecção na Amazônia. Dissertação de mestrado, São José dos Campos INPE – 4008 – TDL/239.
- Penven, P., Roy, C., Colin De Valdiere, A., Largier, J., 2000. Simulation and quantification of a coastal jet retention process using a barotropic model. *Oceanologica Acta* 23, 615-634.
- Penven, P., Roy, C., Lutjeharms, J. R. E., Colin De Valdiere, A., Johnson, A., Shillington, F., Freon, P., Brundrit, G., 2001a. A regional hydrodynamic model of the southern Benguela. *South African Journal of Science* 97, 472-476.
- Penven, P., Lutjeharms, J. R. E., Marchesiello, P., Roy, C., Weeks, S. J., 2001b. Generation of cyclonic eddies by the Agulhas Current in the lee of the Agulhas bank. *Geophysical Research Letters* 27, 1055-1058.
- Peterson, R. G., Stramma, L., 1991. Upper-level circulation in the South Atlantic Ocean. *Progress in Oceanography* 26, 1-73.
- Preisendorfer, R. W., 1988. Principal component analysis in meteorology and oceanography. Elsevier. Amsterdam.
- Rhein, M., Stramma, L., Send. U., 1995. The Atlantic Deep Western Boundary Current. Water masses and transports near the equator. *Journal of Geophysical Research* 100, 2441-2451.

References

- Rodrigues, R. R., Lorenzzetti, J. A., 2001. A numerical study of the effects of bottom topography and coastline geometry on the Southeast Brazilian coastal upwelling. *Continental Shelf Research* 21, 371-394.
- Rodrigues, M. L. G., Franco, D., Sugahara, S., 2004. Climatologia de frentes frias no litoral de Santa Catarina. *Brazilian Journal of Geophysics* 22(2), 135-151.
- Rodrigues, R. R., Rothstein, L. M., Wimbush, M., 2007. Seasonal variability of the South Equatorial Current bifurcation in the Atlantic Ocean: A numerical study. *Journal of Physical Oceanography* 37, 16-30.
- Satyamurty, P., Nobre, C. A., Silva Dias, P. L., 1998. South America, In: Karoly, D. J., Vincent, D. G. ed. *Meteorology of the Southern Hemisphere*. American Meteorological Society, Meteorological Monographs 27(49), 119-139.
- Savtchenko, A., Ouzounov, D., Ahmad, S., Acker, J., Leptoukh, G., Koziana, J., Nickless, D., 2004. Terra and Aqua MODIS products available from NASA GES DAAC. *Advances in Space Research* 34(4), 710-714.
- Schmid, C., Schäfer, H., Podestá, G., Zenk, W., 1995. The Vitória Eddy and its relation to the Brazil Current. *Journal of Physical Oceanography* 25, 2532-2546.
- Schmitz Jr., W. J., 1995. On the interbasin-scale thermohaline circulation. *Reviews in Geophysics* 33, 151-173.
- Schott F., Boning, C. W., 1991. The WOCE model in the western equatorial Atlantic: upper-layer circulation. *Journal of Geophysical Research* 96, 6993-7004.
- Schott, F., Fischer, J., Reppin, J., Send, U., 1993. On mean and seasonal currents and transports at the western boundary of the equatorial Atlantic. *Journal of Geophysical Research* 98, 14353-14368.
- Schott, F., Fischer, J., Stramma, L., 1998. Transports and pathways of the upper-layer circulation in the western tropical Atlantic. *Journal of Physical Oceanography* 28, 1904-1928.
- Schott, F., Brandt, P., Hamann, M., Fisher, J., Stramma, L., 2002. On the boundary flow off Brazil at 5-10° S and its connection to the interior tropical Atlantic. *Geophysical Research Letters* 29(17), 21.1 – 21.4, 1840,

References

- doi:10.1029/2002GL014786.
- Schott, F. A., Dengler, M., Zantopp, R., Stramma, L., Fischer, J., Brandt, P., 2005. The shallow and deep western boundary circulation of the South Atlantic at 5°–11°S. *American Meteorological Society* 35, 2031-2053.
- Shchepetkin, A. F., McWilliams, J. C., 1998. Quasi-monotone advection schemes based on explicit locally adaptive dissipation. *Monthly Weather Review* 126, 1541–1580.
- Shchepetkin, A. F., McWilliams J. C., 2003. A method for computing horizontal pressure-gradient force in an ocean model with a non-aligned vertical coordinate. *Journal of Geophysical Research* 108, 35.1-35.34.
- Shchepetkin, A. F., McWilliams, J. C., 2005. The regional ocean modeling system (ROMS): A split-explicit, free surface, topography-following-coordinate oceanic model. *Ocean Modelling* 9, 347-404.
- Silva, M., Araújo, M., Servain, J., Peven, P., Lentini, C., 2007. High-resolution regional ocean dynamics simulation in the South-Western Tropical Atlantic. *Ocean Modelling* 1, 1-42.
- Silveira, I. C. A., Miranda, L. B., Brown, W. S., 1994. On the origins of the North Brazil Current. *Journal of Geophysical Research* 99, 22501-22512.
- Silveira, I. C. A., Schmidt, A. C. K., Campos, E. J. D., Godoi, S. S., Ikeda, Y., 2000. The Brasil Current off the eastern Brazilian coast. *Brazilian Journal of Oceanography* 48(2), 171-183.
- Silveira, I. C. A., Calado, L., Castro, B. M., Cirano, M., Lima, J. A. M., Mascarenhas, A. S., 2004. On the baroclinic structure of the Brazil Current-Intermediate Western Boundary Current system at 22° - 23° S. *Geophysical Research Letters* 31, L14308: 1-5.
- Silveira, I. C. A., Oliveira, E. R., Mattos, R. A., Fernandes, F. P. A., Lima, J. A. M., 2006. Mesoscale patterns of the Brazil Current between 20°S and 25.5°S. Ocean Sciences Meeting 2006, AGU/ASLO/IAPSO/TOS, Honolulu, OS45N-12.
- Smith, R. L., 1978. Poleward propagating perturbations in currents and sea levels along the Peru coast. *Journal of Geophysical Research* 83, 6083-6092.
- Smith, W. H. F., Sandwell, D. T., 1997. Global seafloor topography from

References

- satellite altimetry and ship depth soundings. *Science* 277, 1957-1962.
- Soutelino, R. G., 2008. A origem da Corrente do Brasil. Dissertação de Mestrado. Instituto Oceanográfico da Universidade de São Paulo - IO/USP, São Paulo.
- Spillane, M. C., Enfield, D. B., Allen, J. S., 1987. Intraseasonal oscillations in sea level along the west coast of the Americas. *American Meteorological Society* 17, 313-325.
- Stech, J. L., Lorenzzetti, J. A., 1992. The response of the South Brazil Bight to the passage of wintertime cold fronts. *Journal of Geophysical Research* 97 (C6), 9507-9520.
- Stramma, L., Ikeda, Y., Peterson, R. G., 1990. Geostrophic transport in the Brazil Current region north of 20° S. *Deep-Sea Research* 37, 1875-1886.
- Stramma, L., 1991. Geostrophic transport of the South Equatorial Current in the Atlantic. *Journal of Marine Research* 49, 281-284.
- Stramma, L., Fischer, J., Reppin, J., 1995. The North Brazil Undercurrent. *Deep-Sea Research I* 42, 773-795.
- Stramma, L., England, M., 1999. On the water masses and mean circulation of the South Atlantic Ocean. *Journal of Geophysical Research* 104(C9), 20,863–20,883.
- Stramma, L., Schott, F., 1999. The mean flow field of the tropical Atlantic Ocean. *Deep-Sea Research*, 46B, 279–303.
- Stramma, L., Fischer, J., Brandt, P., Schott, F., 2003. Circulation, variability and near-equatorial meridional flow in the central tropical Atlantic. In G. J. Goni, P. Malanotte-Rizzoli, Interhemispheric water exchanges in the Atlantic Ocean, P.1-22, Elsevier B.V.
- Stramma, L., Rhein, M., Brandt, P., Dengler, M., Böning, C., Walter, M., 2005. Upper ocean circulation in the western tropical Atlantic in boreal fall 2000. *Deep-Sea Research* 52, 221–240.
- Trenberth, K. E., Large, W. G., Olson, J. G., 1990. The mean annual cycle in global ocean wind stress. *Journal of Physical Oceanography* 20, 1742-1760.
- Truccolo, E. C., Franco D., 2000. Characterization and prediction of the meteorological tides at São Francisco do Sul, SC. Anais do XI Congresso

References

- Brasileiro de Meteorologia, Rio de Janeiro, 2752–2757.
- Vautard R., Yiou P., Ghil M., 1992. Singular spectrum analysis: a toolkit for short, noisy chaotic signals. *Physical D* 58, 95–126.
- von Schuckmann, K., 2006. Intraseasonal variability in the southwestern and central tropical Atlantic Ocean. Ph.D. Thesis, 140 pp. Christian-Albrechts-Universität. Kiel, Germany.
- Wüst, G., 1935. Schichtung und zirkulation des Atlantischen Ozeans. Die Stratosphäre des Atlantischen Ozeans. Wissenschaftliche Ergebnisse Deutschen Atlantischen Expedition auf dem Forschungs und Vermessungsschiff. “Meteor” 1925-1927, 6, 109-228.
- Zhang, H. M., Bates, J. J., Reynolds, R. W., 2006. Assessment of composite global sampling: sea surface wind speed. *Geophysical Research Letters* 33, L17714: 1-5.